Mechanistic Insights into Homotypic Fusion of ER Membranes by the Atlastin GTPase

by

Simran G. Saini

A thesis submitted in partial fulfillment of the requirements for the degree of

Doctor of Philosophy in the field of Biological Sciences

Department of Biological Sciences
Carnegie Mellon University
Pittsburgh, Pennsylvania

December 16th, 2014

Thesis Advisor: Dr. Tina H. Lee, Ph.D.

For my brothers Paul and Jas

ACKNOWLEDGEMENTS

I would like to acknowledge Dr. Tina H. Lee for her outstanding mentorship throughout my graduate career; her steady guidance, unwavering support and generous tutelage have been instrumental in my development as a scientific researcher. While it is impossible to convey the numerous lessons I have learned from Tina, there are several that stand out. Tina has taught me how to recover from failure; that there are good moments, even when there are bad moments; to work smarter, not necessarily harder; to always give back by helping others and most importantly, to never give up. As I continue on in my career and in life, I will never forget these valuable lessons. Thank you Tina for fostering a supportive lab environment that influenced my growth on both a professional and personal level.

I would also like to thank my committee members, Dr. Adam D. Linstedt, Dr. Manojkumar A. Puthenveedu, Dr. David D. Hackney and Dr. Peijun Zhang. Your advice and feedback were essential throughout my graduate studies and I am truly grateful for the time each of you afforded me.

I would also like to thank current and former members of the Lee Lab—Dr. Jeanne Morin-Leisk, Dr. Kaitlyn Dykstra, Idil Ulengin, John Park and James Winsor, as well as members of the Linstedt Lab and the Puthenveedu Lab for their constant support and insightful discussions.

Most of all, I would like to thank my family for their unconditional love and support. Despite being so far away, my parents and my brother Jas were integral to the completion of my graduate studies. Not only did they share in my struggles and accomplishments at every stage, but they also remained steadfast in their belief that I would make it through, even when I did not believe it myself.

Lastly, I would like to thank my brother Paul for encouraging me to pursue my dreams and for reminding me that I should always strive to be happy in the pursuit, as well as in the achievement, of these dreams. While you are no longer with us, the memories of your kind, thoughtful and compassionate nature remains close to my heart—one love, always and forever.

ABSTRACT

A variety of diseases, including Hereditary Spastic Parapalegia (HSP), are associated with defects in Endoplasmic Reticulum (ER) morphogenesis, highlighting the significance of forming and maintaining proper ER structure in the context of human health. While the overall shape and structure adopted by the ER is mainly influenced by the lipid and protein composition of its membrane, fusion plays an equally important role. Recent studies have implicated a conserved family of proteins called atlastin/Sey1 as the fusion machinery responsible for generating three-way junctions within the peripheral ER; however, the actual mechanism used by atlastin (ATL) to catalyze homotypic membrane fusion remains to be clarified. Structural and biochemical studies performed largely with the soluble domain of ATL, suggested that GTP binding facilitated membrane tethering between ATLs anchored in opposing membranes (pre-fusion), followed by GTP hydrolysis catalyzing a crossover conformational change that pulled opposing membranes together for fusion (post-fusion). Through structure-function analysis, I identified key residues that are required for stabilizing the post-fusion conformation, which assisted in elucidating the energy requirements for achieving the post-fusion conformational state of the ATL soluble domain. Using various nucleotides and analogs, I discovered that the soluble domain of ATL was capable of adopting the post-fusion dimer in the absence of GTP hydrolysis, suggesting that GTP hydrolysis may be required for another discrete step within the ATL fusion cycle, such as disassembly. However, this result appeared to be inconsistent with the requirement for GTP hydrolysis in the ATL-mediated fusion of synthetic liposomes and may perhaps be attributed to the different behaviors exhibited by the soluble domain verses membrane-anchored ATL molecules. Therefore, I extended our initial analysis of the ATL soluble domain to membrane-anchored ATL, specifically focusing on identifying the energetic and conformational requirements for ATL-mediated tethering. My investigation revealed that membrane tethering depended on GTP hydrolysis; but, unlike fusion, it did not depend on crossover.

TABLE OF CONTENTS

LIST OF FIGURES

CHAPTER 1

INTRODUCTION

Biological Membranes

Regardless of their functional and structural differences, all cells possess biological membranes that define and control the composition of the cell (Martens and McMahon, 2008). These biological membranes are largely comprised of amphipathic phospholipids, which possess a hydrophilic polar head group and hydrophobic fatty-acid chains that spontaneously form into an energetically favorable lipid bilayer structure that surrounds the entire cell and serves as a barrier between the cell and the external environment. This particular arrangement of lipids is energetically favorable because it ensures that the hydrophobic fatty-acid chains are shielded from the aqueous environment, while the hydrophilic polar head groups are exposed to the aqueous environment. In addition to the outer cell membrane, often referred to as the plasma membrane, cells also possess intracellular membrane-enclosed organelles that include: the nucleus, endoplasmic reticulum (ER), Golgi apparatus, lysosomes, endosomes and mitochondria (Heald and Cohen-Fix, 2014). Whether external or internal, biological membranes serve two main functions. First, they serve as physical barriers, allowing them to define the shape and structure of the space they enclose, while also regulating the entry and exit of molecules (Heald and Cohen-Fix, 2014). Second, they permit intracellular compartmentalization, which allows for diverse cellular processes to occur simultaneously and with high fidelity under optimal environmental conditions (Shibata et al., 2006). The continuous, interconnected membrane network of the ER exemplifies the role of membranes in defining an organelle's structure and for isolating organelle-specific processes.

ER Structure and Functions

The ER is composed of relatively flat cisternal sheets and highly curved tubules that extend throughout the cell (Shibata et al., 2010). While both membrane and luminal continuity are maintained, the general partitioning of cisternal sheets near the nuclear

envelope and highly curved tubules towards the cell periphery ensures that the ER is able to carry out numerous cellular processes effectively within discrete sub-domains. These processes include: secretory and membrane protein biosynthesis, lipid synthesis, drug detoxification and the regulation of intracellular calcium (Baumann and Walz, 2001). The expansive reach of the peripheral ER is especially important for establishing contacts between the ER and other intracellular organelles, including: mitochondria, peroxisomes, chloroplasts, Golgi and the plasma membrane (Daniele and Schiaffino, 2014). These diverse associations are implicated in a variety of functional roles, such as non-vesicular transport of ER-synthesized lipids and calcium homeostasis (Toulmay and Prinz, 2011). Furthermore, a variety of diseases, including Hereditary Spastic Parapalegia (HSP), are associated with defects in ER morphogenesis (Blackstone, 2012), highlighting the significance of forming and maintaining proper ER structure in the context of human health.

ER Structuring Determinants

The overall shape and structure adopted by the ER is mainly influenced by the lipid and protein composition of its membrane (Shibata et al., 2009). ER membranes are largely composed of phospholipids, including glycerophospholipids and sphingolipids that are symmetrically distributed between both leaflets, which results in the loose packing of ER membrane lipids (Meer et al., 2008). This particular lipid arrangement is necessary for proper insertion and transport of newly synthesized lipids and proteins via the secretory pathway (Fagone and Jackowski, 2009). In addition to lipid composition, membrane-shaping proteins are important for establishing and maintaining the overall structure of the ER. For instance, the integral membrane protein Climp-63 is responsible for conferring the characteristic flat morphology of ER cisternal sheets. It has been proposed that Climp-63 causes cisternal sheets to adopt a more flattened morphology because it serves as a scaffold, linking two separate membrane regions through the lumen, resulting in a characteristic sheet thickness of 50nm in mammalian cells (Shibata et al., 2006). Unlike ER cisternal sheets, peripheral ER membrane tubules are enriched with integral membrane proteins belonging to the reticulon and DP1 families (Heald et al., 2014). Reticulons and DP1 have an unusual topology in that they do not fully

penetrate the bilayer, causing the formation of hairpin-like structures in the membrane that induce positive membrane curvature (Voeltz et al., 2006). Initial deletion studies of RTN1 and RTN2 in *S. cerevisiae* had no discernable effect on the ER network; however, simultaneous deletion of DP1, RTN1 and RTN2 in *S. cerevisiae* resulted in a loss of cortical ER tubules (Voeltz et al., 2006). Furthermore, reconstitution of purified reticulon and DP1 proteins into synthetic liposomes was sufficient to generate highly curved membrane tubules (Hu et al., 2009).

In addition to membrane shaping proteins, the formation, maintenance and movement of the highly dynamic peripheral ER network is also partially dependent upon microtubules (Terasaki et al., 1986; Lee and Chen, 1988), with new ER tubules frequently extending outwards along preformed microtubule tracks (Terasaki et al., 1986; Lee and Chen, 1988), likely via kinesin-1 motor proteins (Shibata et al., 2009). ER tubules were also found to be associated with the growing ends of microtubules via the tip attachment complex (TAC) (Shibata et al., 2009; Lee and Chen, 1988; Waterman-Storer and Salmon, 1998). Upon extension, the majority of ER tubules proceed to fuse with pre-existing ER tubules, generating new three-way junctions within the network (Baumann and Walz, 2001). However, these three-way junctions are frequently lost through sliding movements (Shibata et al., 2009; Friedman et al., 2010). Therefore, maintenance of the peripheral ER tubular network requires that homotypic ER fusion events offset sliding events (Lee and Chen, 1988). Recent studies have revealed that a conserved family of proteins called atlastin/Sey1 (Orso et al, 2009; Anwar et al., 2012) generates three-way junctions in the ER by homotypic membrane fusion; however the actual mechanism used by atlastin (ATL) to fuse membranes remains to be clarified.

Membrane Fusion

As described above, while lipid composition, membrane-shaping proteins and the cytoskeleton greatly influences the shape and structure of the ER, homotypic membrane fusion is equally important. Membrane fusion is defined as the merging of two separate lipid bilayers, followed by the mixing of their respective aqueous contents (Martens and McMahon, 2008). In cells, membrane fusion is not a spontaneous process because it requires a substantial amount of energy to draw two separate membranes, with repulsive

membrane charges, in close apposition while also minimizing the exposure of the hydrophobic portion of the bilayer to the aqueous environment during lipid mixing en route to fusion (Jahn et al., 2003). Although highly curved membranes can overcome some of these energy barriers, it is largely accepted that fusion proteins provide the remaining energy necessary for productive fusion events within the cell (Martens and McMahon, 2008). As mentioned, while studies have identified ATL/Sey1 (Orso et al., 2009; Anwar et al., 2012) as the fusion machinery required for homotypic membrane fusion at the ER, the actual mechanism used by ATL to fuse membranes remains to be clarified. Insights into how ATL might fuse membranes can be gained from other characterized membrane fusion mechanisms, which include: (1) cell-cell fusion, (2) viral fusion and (3) intracellular fusion, allowing for the formulation of testable ATL-mediated fusion models.

Cell-Cell Fusion

The process of cell-cell fusion has been observed in many fundamental cellular processes, including: mating, epithelial development, fertilization, myogensis and osteoclast/giant cell formation (Chen et al., 2007). Although the fusion machinery and the molecular mechanisms involved in each of these cell-cell fusion events remain poorly characterized, it is evident that cell-cell fusion events share some common features. For the most part, cells fated to fuse will initially send out signals that allow them to enter into a pre-fusion state, followed by the formation of adhesive interactions, usually mediated by specialized transmembrane proteins, between the plasma membranes of the two cells. These interactions can either directly catalyze fusion or they can stabilize opposing membranes en route to fusion (Chen et al., 2007). Similarly to cell-cell fusion, it is possible that ATL fuses membranes by adopting a pre-fusion state initiated by an external cue, followed by a stable interaction between opposing membranes, perhaps in combination with ATL-interacting partners, that either directly or indirectly permits fusion.

Viral Fusion

Although viruses utilize different mechanisms to gain entry and infect host cells,

the entry of the influenza virus via hemagglutinin (HA) employs arguably the most well characterized viral fusion mechanism to date (Podbilewicz, 2014). In the context of the viral fusion mechanism, HA serves two distinct roles. First, it facilitates attachment of the virus to the host cell and second, it promotes fusion of the viral membrane with the host cell membrane, ensuring that the viral genome enters the host cell (Skehel and Wiley, 2000). For attachment, the viral HA protein recognizes and binds sialic acid containing receptors located within the host cells plasma membrane (Skehel and Wiley, 2000). Upon attachment, the virus enters the cell via receptor-mediated endocytosis and is enclosed within an endosome that proceeds to acidify in order to effectively degrade the contents of the endosomal compartment; however, once the pH within the endosome reaches 6.0, the overall structure of the HA protein changes dramatically. Structurally, the HA protein transitions from its originally folded structure to a partially unfolded one that results in the release of a hydrophobic peptide and leads to the alignment of three alpha helices, predicted to form a trimeric coiled-coil (Bullough et al., 1994). While the hydrophobic peptide inserts itself into the endosomal membrane, thereby tethering the viral and host cell membranes together, the three alpha helices assemble into a coiled-coil pulling the viral membrane and endosomal membrane together, resulting in fusion (Carr and Kim, 1993). Once fusion has occurred, the genomic content of the virus is deposited within the host-cell cytoplasm and additional viral particles are synthesized using the host-cell's cellular machinery (Samji, 2009). Similarly to the viral fusion mechanism, it is possible that ATL undergoes a large conformational change triggered by either an external or internal cue that provides enough energy to draw opposing membranes together, thereby permitting fusion.

Soluble NSF attachment protein receptor (SNARE) - Mediated Fusion

Although evolutionarily distinct, the mechanism of viral fusion and SNARE-mediated fusion are remarkably similar in that a protein folding reaction, involving coiled-coil forming transmembrane proteins, provides the necessary energy required to drive membrane fusion (Mozdy and Shaw, 2003). Traditionally, SNARE proteins were classified as v-SNAREs or t-SNAREs depending on whether they were present on vesicle or target membranes respectively. More recently they have been re-classified based on

sequence and structural analysis as either Q-SNAREs or R-SNAREs depending upon the identity of the amino acid located at the center of the SNARE motif; Q-SNAREs have a glutamine (Q) located at the center of the SNARE motif, whereas R-SNAREs have an arginine (R) (Fasshauer et al., 1998). The SNARE motif consists of homologous coiled-coil regions of approximately 60 residues in length that is located adjacent to their respective C-terminal membrane anchors (Jahn and Sudhof, 1999). Most SNARE complexes are composed of three Q-SNAREs and one R-SNARE. It is generally accepted that SNAREs fuse membranes through a "zippering" mechanism, where partially unfolded Q-SNAREs located on one membrane and the cognate R-SNARE, located on another membrane come into contact and once paired, the alpha helices "zipper" together to form a stable, fully folded coiled-coil (Chen and Scheller, 2001). It is the formation of this stable SNARE complex that provides the energy to pull opposing membranes together for fusion. While recent reports have suggested that SNAREs are the minimal machinery required for SNARE-mediated membrane fusion *in vitro* (Shi et al., 2012), it appears that additional proteins, including Rabs and Sec1/Munc18 are necessary for vesicle docking and fusion *in vivo* (Rizo and Sudhof, 2002). Regardless, once fusion has occurred, the stable SNARE complex must be disassembled and recycled for further rounds of fusion. Using energy derived from ATP hydrolysis, N-ethylmaleimide sensitive fusion protein (NSF) and its co-factor alpha-SNAP, disassembles the SNARE complex, thereby re-priming SNAREs for further rounds of fusion (Mayer, 2001). While most intracellular fusion events are SNARE-mediated, including a recent report of SNARE-mediated ER-ER fusion at the nuclear envelope in yeast cells (Rogers et al., 2014), there is little evidence to suggest that homotypic fusion of peripheral ER membranes is SNARE-mediated. Instead, recent studies suggest that ATL is the primary fusion machinery at the ER and is required for establishment and maintenance of the peripheral ER network. Nevertheless, it is feasible that the ATL fusion mechanism shares some features with the SNARE fusion mechanism either with regards to drawing opposing membranes together via the formation of a stable complex through a conformational rearrangement and/or possibly in the context of hydrolysis-driven disassembly for re-priming the fusogenic proteins for further rounds of fusion.

ATL GTPase

ATLs are large GTPases that belong to the dynamin superfamily (Praefcke and McMahon, 2004). Humans express three isoforms of ATL (ATL1, ATL2 and ATL3). ATL2 and ATL3 are expressed ubiquitously and are generally ER localized; whereas, ATL1 is mainly found in the central nervous system, predominantly in neurons of the corticospinal tract as well as the cerebral cortex and hippocampus and is localized to the cis-Golgi and to a lesser extent in the ER (Zhu et al., 2006; Rismanchi et al., 2008). Various mutations within ATL1 have been identified in patients suffering from hereditary spastic paraplegia (HSP), a neurodegenerative disorder affecting motor neuron function in the lower extremities (Fink, 2006).

ATLs potential role in ER network formation was initially identified in expression studies performed across different cells lines. In HeLa cells, knock down of endogenous ATL2/3 expression resulted in long unbranched ER tubules (Hu et al., 2009). It should be noted that Golgi apparatus fragmentation was also observed, but this fragmentation was not functionally significant, as VSVG trafficking was not impaired in cells knocked down for both ATL2/3 (Rismanchi et al., 2008). Overexpression of various ATL2/3 mutants also caused severe perturbations in ER morphology (Rismanchi et al., 2008). Separate depletion studies of ATL by RNAi in *Drosophila*, which possess a single, highly conserved ATL orthologue (D-ATL), resulted in ER fragmentation, inconsistent with the finding of Hu *et al.* (Orso et al., 2009). Furthermore, overexpression of D-ATL in flies caused enlargement of the ER, possibly due to excessive fusion of ER membranes (Orso et al., 2009), but the observed phenotype could also be attributed to aggregation. Collectively, these studies suggested that ATL could be involved in ER network formation either in the context of tubule formation/extension, membrane curvature, tethering, and/or fusion (Shibata et al., 2006). However, the remarkable finding that D-ATL was capable of fusing synthetic liposomes *in vitro* when hydrolysable GTP was present in the reaction solidified its role as the fusion machinery of the peripheral ER (Orso et al., 2009). Interestingly, unlike the D-ATL orthologue and the more distantly related yeast SEY1 and Arabidopsis RHD3 orthologues, the three human ATL isoforms have not been shown to fuse synthetic liposomes *in vitro* (Anwar et al., 2012; Zhang et al., 2013).

Despite the identification of ATL, the molecular mechanism of ATL-mediated ER fusion still remains unclear. To understand how ATL might fuse membranes, two key questions needed to be addressed: (1) how does ATL molecules in opposing membranes interact to draw two separate membranes together for fusion and (2) what is the role of GTP hydrolysis in the ATL fusion cycle. Fortunately, the recently solved ATL1 crystal structures of the soluble domain provided some insight into how the molecules might interact to draw membranes together for fusion. Two striking features of the solved structures were that (1) the structures were dimeric, with the globular GTPase head domains interacting in a head-to-head fashion with bound nucleotides near the dimer interface and that (2) there were two different dimer forms. In the first form, designated as the pre-fusion dimer, a head-to-head dimer, with each transmembrane (TMB) segment expected to reside in separate and opposing membranes was observed; whereas, the second form, designated as the post-fusion dimer, a head-to head dimer, with TMB segments expected to reside within the same membrane due to rotation about a linker region between the GTPase head domain and the middle domain was observed (Bian et al., 2011; Brynes and Sondermann, 2011). The two distinct dimer structures suggested the following sequence of events as outlined in Figure 1-1, where: (1) ATL monomers, within opposing membranes (Figure 1-1A) would form a nucleotide-dependent dimer in trans for membrane tethering (pre-fusion dimer) (Figure 1-1B), followed by a (2) conformational change that resulted in the monomers crossing over (Figure 1-1C), allowing for the (3) two membranes to be drawn together for fusion (post-fusion dimer) (Figure 1-1D) (Bian et al., 2011; Byrnes and Sondermann, 2011). While the crystal structures revealed how ATL molecules might interact to draw membranes together for fusion, they failed to account for the role of the TMB domains and the tail in the fusion reaction.

Subsequent studies showed that both the TMB domains and the tail were required for fusion (Liu et al., 2012). Deletion of either of the two TMB domains or replacement with the Sec61beta TMB domain inhibited fusion (Liu et al., 2012), suggesting that the ATL TMB domains played an important role in the fusion reaction cycle. Similarly, deletion of the tail inhibited fusion (Moss et al., 2011; Liu et al, 2012) and this requirement was attributed to an amphipathic helix within the tail located adjacent to the

second TMB domain. A synthetic peptide corresponding to this amphipathic helix was shown to insert into membranes and when added in trans to the tail-delete variant, restored fusion (Liu et al., 2012). Accordingly, it was proposed that the amphipathic helix within the tail plays an important role in destabilizing the membranes for fusion. Separately, the crystal structures also failed to address the role of GTP hydrolysis in the fusion cycle, since both the pre-fusion and post-fusion crystal structures only possessed GDP in their respective nucleotide binding pockets, despite crystallization with various nucleotides and analogs (Bian et al., 2011; Byrnes and Sondermann, 2011).

Figure 1-1. Structure based model for Atlastin mediated fusion.

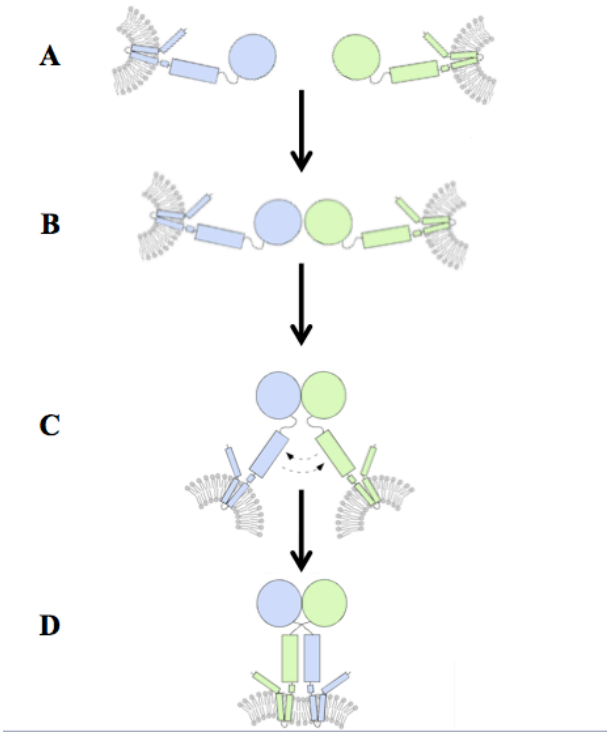

(A) ATL monomers present within opposing membranes (B) ATL monomers form a nucleotide-dependent dimer in trans to tether opposing membranes (pre-fusion dimer), followed by a (C) conformational change that resulted in the monomers crossing over, allowing for the (D) two membranes to be drawn together for fusion (post-fusion dimer).

Therefore, I investigated the role of GTP hydrolysis in the ATL-mediated fusion mechanism, specifically focusing on the coupling of the GTP hydrolysis cycle to the different conformational states of ATL. Chapter 1 describes the energetic and structural requirements for achieving the post-fusion conformation for the soluble domain of ATL. In this study, I identified key residues required for stabilization of the post-fusion conformation and also determined that the post-fusion conformation could be achieved in the absence of GTP hydrolysis, suggesting that GTP hydrolysis may not be required for fusion, but rather for another discrete step within the ATL fusion cycle, such as disassembly of ATL trans dimers after fusion for ATL subunit recycling. However, due to the requirement of GTP hydrolysis in ATL-mediated fusion of synthetic liposomes (Orso et al., 2009), it was difficult to reconcile that the post-fusion conformation could be achieved in the absence of GTP hydrolysis. One possible explanation was that the soluble domain exhibited behaviors that did not necessarily reflect that of the membrane anchored full-length molecule. Therefore, I set out to resolve this discrepancy, as outlined in chapter 2, by extending our initial studies to membrane-anchored ATL. This investigation resulted in the identification of a putative ATL tethering intermediate, which I characterized in collaboration with Peijun Zhang's lab (University of Pittsburgh). Our analysis revealed that GTP hydrolysis was required for trans dimer formation of membrane-anchored ATL, revealing that the constraints of membrane anchoring increased the energy input required to bring two opposing ATL molecules together in trans. Furthermore, we found that trans dimer formation was not strictly dependent on crossover. Collectively, my work has revealed that membrane tethering of opposing ATL molecules in trans requires GTP hydrolysis; whereas, formation of the post-fusion dimer conformation appears to be more closely associated with lipid mixing en route to full fusion.

REFERENCES

Anwar, K., R.W. Klemm, A. Condon, K.N. Severin, M. Zhang, R. Ghirlando, J. Hu, T.A. Rapoport, and W.A. Prinz. 2012. The dynamin-like GTPase Sey1p mediates homotypic ER fusion in S. cerevisiae. J Cell Biol. 197:209-217.

Baumann, O. and B. Walz. 2001. Endoplasmic reticulum of animal cells and its organization into structural and functional domains. Int Rev Cytol. 205: 149-214.

Bian, X., R.W. Klemm, T.Y. Liu, M. Zhang, S. Sun, X. Sui, X. Liu, T.A. Rapoport, and J. Hu. 2011. Structures of the atlastin GTPase provide insight into homotypic fusion of endoplasmic reticulum membranes. Proc Natl Acad Sci U S A. 108:3976-3981.

Blackstone, C. 2012. Cellular pathways of hereditary spastic paraplegia. Annu Rev Neurosci. 35:25-47.

Bullough P.A., F. Hughson, J. Skehel, D.C. Wiley. 1994. Structure of influenza haemagglutinin at the pH of membrane fusion. Nature. 371:37–43

Byrnes, L.J., and H. Sondermann. 2011. Structural basis for the nucleotide-dependent dimerization of the large G protein atlastin-1/SPG3A. Proc Natl Acad Sci U S A. 108:2216-2221.

Carr C.M. and P.S. Kim. 1993. A spring-loaded mechanism for the conformational change of influenza hemagglutinin. Cell. 73:823–32.

Chen, E.H., E. Grote, W. Mohler, and A. Vignery. 2007. Cell-cell fusion. FEBS Letters. 581:2181-2193.

Chen, Y.A. and R. H. Scheller. 2001. SNARE-mediated membrane fusion. Nat Rev Mol Cell Bio. 2:98-106.

Daniele, T. and M. V. Schiaffino. 2014. Organelle biogenesis and interorganelle connections: Better in contact than in isolation. Commun Integr Biol. 7:e29587. doi: 10.4161/cib.29587

Fagone, P.. and S. Jackowski. 2009. Membrane Phospholipid synthesis and endoplasmic reticulum function. J. Lipid Res. 50:(Supplement) S311-S316.

Fasshauer, D., R.B. Sutton, A.T, Brunger, and R. Jahn. 1998. Conserved structural features of the synaptic fusion complex: SNARE proteins reclassified as Q-and R-SNAREs. Proc Natl Acad Sci U.S.A. 95: 15781-15786.

Fink, J.K. 2006. Hereditary spastic paraplegia. Curr Neurol Neurosci Rep. 6:65-76.

Friedman, J.R., B.M. Webster, D.N. Mastronarde, K.J. Verhey, and G.K. Voeltz. 2010. ER sliding dynamics and ER-mitochondrial contacts occur on acetylated microtubules. J Cell Biol. 190:363-375.

Heald R., and O. Cohen-Fix. 2014. Morphology and function of membrane-bound organelles. Curr Opin Cell Biol. 26:79-86

Hu, J., Y. Shibata, P.P. Zhu, C. Voss, N. Rismanchi, W.A. Prinz, T.A. Rapoport, and C. Blackstone. 2009. A class of dynamin-like GTPases involved in the generation of the tubular ER network. Cell. 138:549-561.

Jahn, R., T. Lang, and T.C. Sudhof. 2003. Membrane Fusion. Cell. 112: 519-533.

Jahn, R., T.C. Sudhof. 1999. Membrane fusion and exocytosis. Annu Rev Biochem. 68: 863-911.

Lee, C., and L.B. Chen. 1988. Dynamic behavior of endoplasmic reticulum in living cells. Cell. 54:37-46.

Liu, T.Y., X. Bian, S. Sun, X. Hu, R.W. Klemm, W.A. Prinz, T.A. Rapoport, and J. Hu. 2012. Lipid interaction of the C terminus and association of the transmembrane segments facilitate atlastin-mediated homotypic endoplasmic reticulum fusion. Proc Natl Acad Sci U S A. 109:E2146-2154.

Martens, S., and H. T. McMahon. 2008. Mechanisms of membrane fusion: disparate players and common principles. Nat Rev Mol Cell Bio. 9:543-556.

Mayer A. 2001. What drives membrane fusion in eukaryotes. Trends Biochem Sci. 26:717-723.

Meer, G.V., D. R. Voelker, and G. W. Feigenson. 2008. Membrane lipids: where they are and how they behave. Nat Rev Mol Cell Biol. 9:112-124.

Moss, T.J., C. Andreazza, A. Verma, A. Daga, and J.A. McNew. 2011. Membrane fusion by the GTPase atlastin requires a conserved C-terminal cytoplasmic tail and dimerization through the middle domain. Proc Natl Acad Sci U S A. 108:11133-11138.

Mozdy, A.D. and J.M. Shaw. 2003. A Fuzzy Mitochondrial Fusion Apparatus Comes into Focus. Nat Rev Mol Cell Biol. 4: 468-478.

Orso, G., D. Pendin, S. Liu, J. Tosetto, T.J. Moss, J.E. Faust, M. Micaroni, A. Egorova, A. Martinuzzi, J.A. McNew, and A. Daga. 2009. Homotypic fusion of ER membranes requires the dynamin-like GTPase atlastin. Nature. 460:978-983.

Podbilewicz B. 2014. Virus and cell fusion mechanisms. Annu Rev Cell Dev Biol. 30:111-139.

Praefcke, G.J., and H.T. McMahon. 2004. The dynamin superfamily: universal membrane tubulation and fission molecules? Nat Rev Mol Cell Biol. 5:133-147.

Rismanchi, N., C. Soderblom, J. Stadler, P.P. Zhu, and C. Blackstone. 2008. Atlastin GTPases are required for Golgi apparatus and ER morphogenesis. Hum Mol Genet. 17:1591-1604.

Rizo J., and T. C. Sudhof. 2002. Snares and Mun18 in synaptic vesicle fusion. Nat Rev Neurosci. 3:641-653.

Rogers, J.V., C. McMahon, A. Baryshnikova, F.M. Hughson and M.D. Rose. 2014. ER-associated retrograde SNAREs and the Dsl1 complex mediate an alternative, Sey1p-independent homotypic ER fusion pathway. Mol Biol Cell. 25: 3401-3412.

Samji T., 2009. Influenza A: understanding the viral life cycle. Yale J Biol Med. 82:153-159.

Shi L., Q.T. Shen, A. Kiel, J. Wang, H.W. Wang, T.J. Melia, J.E. Rothman and F. Pincet. 2012. SNARE proteins: one to fuse and three to keep the nascent furion pore open. Science. 335:1355-1359.

Shibata Y, G. K. Voeltz, T.A. Rapoport. 2006. Rough sheets and smooth tubules. Cell. 126:435-439.

Shibata Y., H. Junjie., M.M. Kozlov, and T.A. Rapoport. 2009. Mechanisms Shaping the Membranes of Cellular Organelles. Annu Rev Cell Dev Biol. 25: 329-354.

Shibata, Y., T. Shemesh, W.A. Prinz, A.F. Palazzo, M.M. Kozlov, and T.A. Rapoport. 2010. Mechanisms determining the morphology of the peripheral ER. Cell. 143:774-788.

Skehel, J. J. and D. C. Wiley. 2000. Receptor binding and membrane fusion in virus entry: the influenza hemagglutinin. Annu Rev Biochem. 69: 531-569.

Terasaki, M., L.B. Chen, and K. Fujiwara. 1986. Microtubules and the endoplasmic reticulum are highly interdependent structures. J Cell Biol. 103:1557-1568.

Toulmay A. and W.A. Prinz. 2011. Lipid transfer and signaling at organelle contact sites: the tip of the iceberg. Curr Opin Cell Bio. 23: 458-463.

Voeltz G.K., M.M. Rolls, T.A. Rapport. 2002. Structural organization of the endoplasmic reticulum. EMBO Rep. 3:944-950.

Voeltz GK, W.A. Prinz, Y. Shibata, J.M. Rist, and T.A. Rapport. 2006. A class of membrane proteins shaping the tubular endoplasmic reticulum. Cell. 124:573-586

Voeltz GK and W.A. Prinz. 2007. Sheets, ribbons and tubules—how organelles get their shape. Nat Rev Mol Cell Biol., 3:258-264.

Waterman-Storer, C.M. and E.D. Salmon. 1998. Endoplasmic reticulum membrane tubules are distributed by microtubules in living cells using three distinct mechanisms. Curr. Biol. 8:798-806.

Zhang, M., F. Wu, J. Shi, Y. Zhu, Z. Zhu, Q. Gong, and J. Hu. 2013. ROOT HAIR DEFECTIVE3 family of dynamin-like GTPases mediates homotypic endoplasmic reticulum fusion and is essential for Arabidopsis development. Plant Physiol. 163:713-720.

Zhu, P.P., C. Soderblom, J.H. Tao-Cheng, J. Stadler, and C. Blackstone. 2006. SPG3A protein atlastin-1 is enriched in growth cones and promotes axon elongation during neuronal development. Hum Mol Genet. 15:1343-1353.

CHAPTER 2

An Intramolecular Salt Bridge Drives the Soluble Domain of GTP-bound Atlastin Into the Post-fusion Conformation*

ABSTRACT

Endoplasmic reticulum (ER) network branching requires homotypic tethering and fusion of tubules mediated by the atlastin (ATL) guanosine triphosphatase (GTPase). Recent structural studies on the ATL soluble domain reveal two dimeric conformers proposed to correspond to a tethered pre-fusion state and a post-fusion state. How the pre-fusion conformer transitions to the post-fusion conformer is unknown. In this paper, we identify an intramolecular salt bridge mediated by two residues outside the GTPase domain near the point of rotation that converts the pre-fusion dimer to the post-fusion state. Charge reversal of either residue blocked ER network branching, whereas a compensatory charge reversal to reestablish electrostatic attraction restored function. In vitro assays using the soluble domain revealed that the salt bridge was dispensable for GTP binding and hydrolysis but was required for forming the post-fusion dimer. Unexpectedly, the post-fusion conformation of the soluble domain was achieved when bound to the nonhydrolyzable GTP analogue guanosine 5′-[β, γ-imido]triphosphate, suggesting that nucleotide hydrolysis might not be required for the pre-fusion to post-fusion conformational change.

* This manuscript appeared as an article in the Journal of Cell Biology, and is reprinted here.
Morin-Leisk J, **Saini SG**, Meng X, Makhov AM, Zhang P, and Lee TH. JCB. 2011. 195(4): 605-615.

Saini SG's contribution to this work involved designing a post-fusion ATL dimer crosslinking assay, which enabled the elucidation of the energy requirements for achieving the post-fusion conformational state of the ATL soluble domain (Figure 2-6). Additionally, Saini SG performed extensive mutational analysis on residues predicted to stabilize the post-fusion conformation, which led to the identification of a key salt-bridge required for adopting the post-fusion conformation (Figures: 2-1, 2-3 and S2-2).

INTRODUCTION

The membrane-anchored atlastin (ATL) proteins belong to the dynamin superfamily of large GTPases (Zhu et al., 2003; Praefcke and McMahon, 2004). In humans, the neuron-specific isoform ATL1/SPG3A is enriched in the cis-Golgi apparatus, and mutations in it are linked to motor neurological deficits associated with hereditary spastic paraplegia (Zhu et al., 2003). ATL2 and ATL3, 62 and 60% identical to ATL1, respectively, are expressed in most, if not all, tissues and primarily ER localized (Rismanchi et al., 2008). siRNA-mediated depletion of isoforms 2 and 3 from HeLa cells, expressing little, if any, isoform 1 (Rismanchi et al., 2008), leads to an unbranched ER morphology, implying a function for ATL2/3 in ER network branching (Hu et al., 2009). This requirement could reflect a role for the molecule in tubule formation, extension, tethering, and/or fusion (Lee et al., 1989; Baumann and Walz, 2001). Though, based on the remarkable finding that the single *Drosophila melanogaster* orthologue of ATL, purified and incorporated into artificial liposomes, is sufficient to drive membrane tethering and fusion, ATLs have been proposed to mediate the homotypic tethering and fusion of membranes that underlies the branched ER network (Orso et al., 2009). Recently, two groups have solved the x-ray crystal structure of the soluble domain of human ATL1 (Bian et al., 2011; Byrnes and Sondermann, 2011). The structures reveal a globular GTPase head connected through an eight–amino acid linker to a middle domain comprised of a three-helix bundle. As expected, the GTPase domain has an overall fold similar to that of GBP1 (Prakash et al., 2000), the closest relative of ATL1–3 in the dynamin superfamily (14, 14, and 16% identical to ATL1, ATL2, and ATL3, respectively). Dynamin superfamily members undergo conformational changes in a manner dependent on their nucleotide-bound state (Ghosh et al., 2006; Chappie et al., 2010). Accordingly, ATL1 crystallization by both groups was performed in the presence of a variety of GTP analogues. Both groups observed two strikingly distinct ATL1 conformers, indicating that, like GBP1 and dynamin, ATL1 indeed undergoes discrete conformational changes during its reaction cycle. Moreover, both structures showed ATL1 as a head to head dimer, reminiscent of the head to head dimers observed in crystal structures of the GTPase domains of dynamin bound to the transition state analogue GDP

+ AlFx (Chappie et al., 2010), and GBP1 bound to either guanosine 5′-[β,γ-imido]triphosphate (GMPPNP) or GDP + AlFx (Ghosh et al., 2006). Curiously, only GDP was observed in the nucleotide-binding pocket of the structures obtained, possibly because of either slow hydrolysis or increased mobility of the terminal phosphate of GMPPNP and other analogues (Bian et al., 2011; Byrnes and Sondermann, 2011). Therefore, how changes in the nucleotide-bound state of ATL1 relate to changes in its conformation remains to be clarified.

In the first of the two ATL1 dimer conformers (form 2), the monomers interact in a head to head fashion with an interfacial area of 756 $Å^2$ because of contacts solely between the GTPase domains. The α-helical bundles of the respective middle domains point away from the dimer interface, and although not present in the crystal structures, the trans-membrane segments would be expected to anchor the interacting subunits in opposing membranes. In the second conformer (form 1), a similar head to head configuration is observed as in the form 2 dimer, though additional contacts increase the interfacial area between the GTPase domains to 1,226 $Å^2$. In addition, the α-helical bundles of the middle domains are crossed over with respect to the head domains caused by a 90° rotation about a central conserved proline residue in the linker. In this crossed dimer configuration (form 1), a new set of contacts are made between the middle domains and the opposing heads. As a consequence of the crossover, the C termini of the two subunits of the form 1 dimer are within 14 Å of one another, necessarily placing the transmembrane segments of the interacting subunits in the same membrane. Based on the orientation of the molecules relative to the presumed orientation of the lipid bilayer, the form 2 and form 1 dimers have been designated pre- and post-fusion states, respectively (Bian et al., 2011; Byrnes and Sondermann, 2011;Daumke and Praefcke, 2011).

The dimer pairs suggest a compelling model for membrane tethering and fusion. First, head to head dimerization of ATL in trans (form 2) would initiate membrane tethering. Once tethered, crossover of the middle domains would catalyze membrane fusion, presumably by bringing opposing lipid bilayers into tight apposition and deforming them, consequently reducing the activation barrier for membrane fusion (Bian et al., 2011; Daumke and Praefcke, 2011). In part because dimerization of ATL1 in solution is nucleotide dependent (Bian et al., 2011; Byrnes and Sondermann, 2011), GTP

binding has been suggested to form the pre-fusion dimer for the membrane-tethering step, whereas GTP hydrolysis and Pi release has been hypothesized to trigger the 90° rotation and crossover of the middle domains to achieve the fused state (Bian et al., 2011). According to this scenario, a cycle of GTP binding and hydrolysis would drive both membrane tethering and fusion, though how the post-fusion complex is disassembled for further rounds of fusion remains to be clarified.

If the crossed dimer conformation indeed represents the post-fusion state, contacts unique to this conformer should be important for driving membrane fusion. Conversely, inhibiting such contacts should block the conversion of pre-fusion dimers to the post-fusion state. Here, we report a functional analysis of residues within the middle domain of ATL2 in search of ones that might be involved in the pre-fusion to post-fusion transition. We then focus on a pair of residues that appear to mediate a post-fusion conformer-specific salt bridge. We show that the salt bridge is not required for either GTP binding or hydrolysis but is necessary for transitioning to the post-fusion dimer conformation. Furthermore, although GTP hydrolysis has been suggested to be required for formation of the post-fusion conformation of the soluble domain, our results indicate that hydrolysis is not required, at least in the context of the soluble domain. The potential implications of this finding with regard to the ATL fusion mechanism are discussed.

MATERIALS AND METHODS

Cells, constructs, antibodies, and reagents

All experiments were conducted on HeLa cells maintained at 37°C in a 5% CO2 incubator in MEM (Sigma-Aldrich) and 10% FBS (Atlanta Biologicals) with 1% penicillin/streptomycin (Thermo Fisher Scientific). The N-terminally HA-tagged ATL2 isoform 2 construct was contributed by C. Blackstone (National Institutes of Health, Bethesda, MD). All ATL2 variant constructs were generated by PCR-mediated site-directed mutagenesis (QuikChange; Agilent Technologies). The siRNA-immune HA-ATL2 construct was generated using QuikChange to replace the 21 nucleotides targeted by the ATL2 siRNA 5′-GGAGCTATCCTTATGAACATTCATA-3′ with 5 ′-GGAGCTATCCGTACGAACACTCATA-3′. N-terminally Myc-tagged PRA2 and DP1 constructs were generated by PCR amplification of a HeLa cDNA library and cloning into the pCS2 Myc vector at the EcoRI and XbaI sites and the XbaI site, respectively. All constructs used herein were fully verified by sequencing (Genewiz). An mAb used to detect protein disulfide isomerase (Abcam) and the HA epitope (Sigma-Aldrich) were purchased, and the 9E10 mAb was used to detect the Myc epitope. The rhodamine anti–mouse secondary antibody was also purchased (Invitrogen). GTP, GDP, and GMPPNP were purchased (Sigma-Aldrich), reconstituted to 100 mM stocks in 10 mM Tris, pH 8.0, and 1 mM EDTA, and stored at -80°C.

Knockdown replacement assay

Cells plated on 60-mm culture dishes were transfected with ~5μg of the indicated HA-ATL2 replacement constructs using transfection reagent (jet-PEI; VWR). Myc-tagged PRA2 and Myctagged DP1, both ER-localized proteins, served as negative controls. Neither affected either the percentage of cells showing the unbranched ER phenotype or the extent of loss of network branching relative to siRNA treatment alone. 24 h after DNA transfection, cells were trypsinized and replated onto 12-mm glass coverslips in a 24-well plate. siRNA treatment targeting both ATL2 and ATL3 was performed the next day using transfection reagent (Oligofectamine; Invitrogen) according to manufacturer's recommendations. The ATL2 (#1) and ATL3 (#2) siRNAs were

identical in sequence to those previously published (Rismanchi et al., 2008). 72 h after knockdown, cells were fixed in ice-cold methanol and processed for immunofluorescence. In brief, primary (1h at RT) and secondary (30 min at RT) antibody incubations were performed in a blocking solution consisting of PBS + 2.5% calf serum + 0.1% Triton X-100, and washes were with 5x 1ml PBS. All images were obtained using a spinning-disk confocal scanhead (Yokagawa; PerkinElmer) mounted on a microscope (Axiovert 200; Carl Zeiss) with a 100x 1.4 NA objective (Carl Zeiss) and acquired using a 12-bit camera (ORCA-ER; Hamamatsu Photonics). Maximal value projections of sections at 0.2-μm spacing (approximately six per cell) were acquired using Imaging Suite software (PerkinElmer) and imported as 8-bit images into Photoshop (Adobe). Quantification of functional replacement was performed manually on a wide-field fluorescence microscope (Axioplan; Carl Zeiss) with a 40x 1.4 NA objective. Images were acquired using a 12-bit camera (ORCA-ER) and QED software (Media Cybernetics). For quantification of functional replacement, the fraction of cells expressing the indicated HA-ATL2 that showed a loss of ER network branching (among ≥100 cells per experiment) was counted. Some of the HA-ATL2 variants, when expressed at high levels, exhibited a dominant-negative ER phenotype (even without ATL knockdown). For these variants, a threshold level of HA-ATL2 immunofluorescence below which expression of the replacement construct alone did not confer an ER phenotype was determined. Quantification of functional replacement was then restricted to those cells expressing the HA-ATL2 variant below the predetermined threshold.

Protein expression and purification

The 6His-tagged cytoplasmic domain of ATL2 was generated using PCR amplification of nucleotides encoding amino acids 1–467 from HA-ATL2 and cloned into the pRSETB vector at NheI and EcoRI sites. Variants were generated using QuikChange mutagenesis and sequence verified. Protein expression was induced with 0.5 mM IPTG in BL21(DE3)pLysS cells at 23°C for 16 h, and purification used standard protocols for purification of 6His-tagged proteins on Ni^{+2} agarose beads (QIAGEN). Proteins, eluted in 50 mM Tris, pH 8.0, 250 mM imidazole, 100mM NaCl, 5 mM $MgCl_2$,

and 10% glycerol, were typically 8–24 mg/ml, >95% pure, flash frozen in liquid N 2 , and stored at -80°C.

GTPase assay

Purified 6His-ATL2 variant proteins, dialyzed into SEC and precleared by centrifugation in a rotor (TLA-100; Beckman Coulter) at 100,000 rpm for 15 min, were diluted to various concentrations in the same buffer. GTP at the indicated concentrations was added to the protein and incubated at 37°C for varying times. After quenching with 5 mM EDTA, 160 µl of each reaction was then added to 40 µl malachite green phosphate assay reagent (Accurate Chemical & Scientific Corp.) in a 96-well transparent flat-bottomed dish (Costar; Thermo Fisher Scientific) and developed for 10 min at 25°C before measuring the absorbance at 650 nm. Phosphate release was calculated using a standard curve according to the manufacturer's instructions.

K_M and k_{obs} determinations

1 µM dialyzed and precleared 6His-ATL2 variant proteins were incubated with 5, 10, or 20 µM GTP at 37°C for varying times, quenched, and assayed for phosphate release (see previous paragraph). Initial velocities for each ATL2 variant were plotted against substrate concentration on a double reciprocal scatter plot, and the K_M for each ATL2 variant was extracted from the x intercept of its best-fit line ($R^2 = 0.99 - 1$; x intercept = $-1/K_M$). For k_{obs} determinations at differing protein concentrations, varying concentrations of 6His-ATL2 variants were incubated with 0.2 mM GTP (determined to be saturating for ≤2 µM ATL2) for 5 min at 37°C. During this time, product formation was predetermined to be linear with time. Samples were quenched and assayed for phosphate release (see previous paragraph). When assaying GTPase activity at high concentrations (3 and 30 µM ATL2), GTP was added at 1 mM in the reaction and incubated for 1 min at 37°C. Thereafter, samples were diluted 10-fold before assaying for phosphate release.

SEC

Purified 6His-ATL2 variant proteins, dialyzed into SEC buffer + 0.5 mM DTT

and precleared by centrifugation in a rotor (TLA-100) at 100,000 rpm for 15 min, were diluted to 10 or 30 μM and incubated with or without 2 mM GMPPNP for 30 min at RT. 100 μl of each sample was then injected onto a fast protein liquid chromatography column (Superdex 200; GE Healthcare) preequilibrated in SEC buffer + 0.5 mM DTT and separated at a flow rate of 0.5 ml/min at 4°C. 0.5-ml fractions within the included volume of 24 ml were collected, precipitated with TCA using 0.5% Triton X-100 as a carrier, resuspended in reducing sample buffer, resolved by SDS-PAGE, and stained using Coomassie blue. Where indicated, wild-type ATL2 was incubated with 5 mM GDP for 30 min at RT and resolved on the same column, except that 1 mM GDP was also included in the column buffer.

Cross-linking

Purified 6His-ATL2 variant proteins were dialyzed into SEC buffer, pH 7.0, at 4°C and precleared by centrifugation in a rotor (TLA-100) at 100,000 rpm for 15 min. 20 μM of each protein was incubated at RT in SEC buffer, pH 7.0, in the absence or presence of 2 mM GMPPNP, GDP, or GTP. After 30 min at RT, the reaction was diluted fivefold into SEC (to 4 μM ATL2) in the absence or presence of 12 μM BMOE (Thermo Fisher Scientific) and incubated for 1 h at RT. Samples were then quenched with 20 mM DTT for 15 min, mixed with reducing sample buffer, and resolved by SDS-PAGE.

EM

20 μM purified 6His-ATL2 in buffer containing 25 mM Tris-HCl, pH 7.5. 100 mM NaCl, 5 mM $MgCl_2$, 2 mM EGTA, 5% glycerol, and 0.5 mM DTT was diluted twofold in the same buffer without glycerol in the presence of 1 mM GMPPNP. After 30 min at RT, the reaction mixture was further diluted 30-fold into the same buffer and immediately applied onto glow-charged thin carbon foil grids, blotted with a filter paper, and stained with a 2% solution of uranyl acetate in water. The grids were examined at 120 kV with an electron microscope (Tecnai 12; FEI). Images were recorded with a 2,000 × 2,000 charge-coupled device camera (UltraScanT 1000; Gatan, Inc.) at a nominal magnification of 52,000.

Image processing and model docking

EM images were processed using the EMAN image analysis software (National Center for Macromolecular Imaging; Ludtke et al., 1999; Tang et al., 2007). Individual particles were boxed manually with 80 × 80 pixels (2.17 Å/pixel), normalized, and combined to yield one raw image stack file. A total of 571 individual particle images were collected, band-pass filtered, and aligned with respect to their center of mass. To test the likelihood of the conformations that the ATL GTPase could adopt, two simulated 3D density maps were computed with Chimera (version 3; University of California, San Francisco) from the atomic models of two conformers (shown in Fig. 2-6 A), pre-fusion (Protein Data Bank accession no. 3QOF) and post-fusion (Protein Data Bank accession no. 3QNU). These two density maps were then used as initial references for the reference-based projection matching of the particle images followed by the reconstruction of particle images in EMAN2. The iterative refinement cycles were ended when the calculated Fourier shell correlation between the 3D models generated in two consecutive iterations showed no further improvement. This indicated that the 3D reconstruction was converging to a stable optimum, and the final 3D density maps were calculated. For model docking, the atomic models of pre-fusion and post-fusion were fitted into the reconstructed EM density map using the feature Fit model in map implemented in Chimera. Cross-correlation values between the final density maps and the simulated 3D density maps from two conformers were calculated. The value was 0.293 for the pre-fusion conformer and 0.425 for the post-fusion conformer, with 55% volume included.

RESULTS

Loss of ER network branching upon ATL2/3 knockdown is rescued by wild-type ATL2 expression

To identify ATL residues that participate in the inter-conversion between pre- and post-fusion conformers, we used an RNAi knockdown replacement assay. The assay is based on the previously reported requirement for ATL2/3 in ER network branching in HeLa cells (Hu et al., 2009). As anticipated, treatment of HeLa cells with siRNAs identical to those previously shown to knock down ATL2 and ATL3 (Rismanchi et al., 2008) resulted in an abnormal ER morphology characterized by a notable reduction in network branch points (Fig. S2-1, A–C). In contrast to control knockdown cells with 200–400 ER network branch points per cell, ATL2/3 knockdown cells typically had <100 network branch points per cell (Fig. S2-1, C and D). Also consistent with a previous study, knockdown of both isoforms was required to elicit the unbranched phenotype (Fig. S2-1 A), indicating that either ATL2 or ATL3 is sufficient to maintain normal network morphology (Hu et al., 2009). To assess whether the unbranched ER phenotype is a specific consequence of ATL2/3 loss, the ATL2/3 siRNA was cotransfected with either a negative control DNA construct or an siRNA-immune HA-tagged ATL2 replacement construct. Whereas ~50% of cells expressing the negative control construct displayed a largely unbranched network (<100 branch points per cell), few, if any, cells expressing wild-type HA-ATL2 displayed the phenotype (Fig. 2-1, A and B). Therefore, the unbranched ER phenotype can be attributed specifically to the loss of ATL2/3.

Specific middle domain residues are required for ATL2 activity

As our analysis was initiated before the recent determination of the ATL1 crystal structure, we started with a computationally derived ATL2 structure model based on its similarity to GBP1 (Prakash et al., 2000; Pieper et al., 2011). Domain boundaries defined by the model were applied to first test the importance of the middle domain. As anticipated, the HA-tagged variant ATL2Δ377–463 (or ATL2Δmiddle), lacking the entire middle domain, was stably expressed but failed to functionally replace endogenous ATL2/3 (Fig. 2-1, A and B). Then, several conserved middle domain residues were

screened. RNAi knockdown replacement using ATL2 variants with either single or double amino acid substitutions to alanine revealed required residues within the middle domain (Fig. 2-1, A and B). Substitutions that blocked ATL2 function include E380A, L384D, K433A, K434A, M435A, F440A, and Y444A. Most of the residues identified by our analysis are located near the GTPase head (Fig. S2-2, A and B). Notably, M435 is equivalent to M408 in ATL1, which, when mutated, is associated with hereditary spastic paraplegia (Zhu et al., 2003), though the mutations have been reported to have only modest effects on the GTPase activity of ATL1 (Bian et al., 2011; Byrnes and Sondermann, 2011). Also, E380 is equivalent to residue E328 in the *Drosophila* homologue, whose charge reversal inhibits the in vitro liposome fusion reaction by 75% (Bian et al., 2011).

ER network morphology after replacement with the various ATL2 proteins appeared somewhat distinct, not only from one another but also from the morphology seen after knockdown. The exception was ATL2Δmiddle, whose network morphology was similar to the knockdown. The significance of these differences is unclear but may reflect a differing ability of each variant to engage in the ATL2 reaction cycle, with ATL2Δmiddle being the least functional. Many of the single alanine substitutions that blocked ER network branching were in highly conserved residues (Fig. S2-2 A), though substitution of at least one conserved residue, E454, had no apparent effect (Fig. 2-1, A and B). Less conserved or nonconserved surface residues, such as Q447 and S431, respectively, could also be substituted (Fig. 2-1, A and B).

Finally, many of the nonfunctional ATL2 variants, when expressed at high levels, exerted a dominant-negative effect on ER morphology that could be observed even in the presence of endogenous ATL2/3 (Fig. S2-2 C). To avoid the potentially complicating effects of such high level expression, only cells expressing each variant below a predetermined threshold level were included for quantification of functional replacement (see Materials and methods).

Middle domain mutations fall into three classes

The two dimer crystal forms of ATL1 (Bian et al., 2011; Byrnes and Sondermann, 2011) allowed us to analyze the positions of our mutations. Because ATL2 is 73%

identical to ATL1 in its cytoplasmic domain, its overall fold is likely very similar to ATL1 with only minor differences in the precise placement of the backbone and side chains. To aid in the analysis, computational models for ATL2 in both the pre- and post-fusion conformation were derived based on the ATL1 structures (Pieper et al., 2011). Inspection revealed that the required residues fall into three categories (Fig. 2-2, A and B). The first category consists of L384, Y444, and F440 (Fig. 2-2, A and B, box 1). These residues pack together near the surface of the middle domain in the pre-fusion conformer, and the packing interactions remain relatively unchanged in the post-fusion conformer. The second category consists of K433 and M435 (Fig. 2-2, A and B, box 2). These residues are in a loop connecting two helices (α8 and α9) of the middle domain. In the pre-fusion conformer, K433 and M435 contact residues within the head domain of the same monomer. In the post-fusion conformer, K433 and M435 alter their contacts to residues in the head domain of the opposing monomer. The third and final category, consisting of E380 and K372, was of particular interest, as it pointed to residues appearing to make substantial contacts only in the post-fusion conformer (Fig. 2-2, A and B, box 3). In the pre-fusion conformer, the nonpolar portion of the E380 side chain may be involved in a set of middle domain packing interactions, and K372 exhibits no obvious contacts. Significantly, K372 is immediately adjacent to the point of 90° rotation that converts the pre-fusion dimer to the post-fusion dimer conformer, and in the post-fusion conformer, it becomes involved in a salt bridge with E380.

A salt bridge specific to the post-fusion dimer is required for ATL2 activity

To test the functional significance of the K372-E380 salt bridge seen in the post-fusion structure, we first examined the effect of charge reversal of either residue on the ER network branching function of ATL2. For this, two new variants, ATL2 K372E and ATL2 E380R, were generated. Each variant was stably expressed, but neither functioned in ER network branching (Fig. 2-3, A and B), confirming the importance of the respective charges at the two positions. Indeed, at high expression levels, both variants exerted a dominant-negative phenotype such that an abnormal network branching pattern was seen even in the presence of endogenous ATL2/3 (Fig. 2-3 C). Notably, although K372 and E380 are each seen to make an additional polar contact in the post-fusion

dimer structure with E275 and Q376, respectively, neither charge reversal of E275 nor alanine substitution of Q376 interfered with ATL2 function (Fig. 2-3, A–C). Thus, the latter contacts appear dispensable. Finally, to test whether the inability of ATL2 E380R and ATL2 K372E to function might indeed be caused by their inability to form a salt bridge, the double mutant variant ATL2 K372E,E380R was constructed. We reasoned that combining the mutations in the same molecule might serve a compensatory function, restoring electrostatic attraction. Remarkably, this variant functioned indistinguishably from wild-type ATL2 in ER network branching (Fig. 2-3, A and B) and exhibited no dominant-negative phenotype (Fig. 2-3 C). Thus, the salt bridge between K372 and E380, specific to the post-fusion conformer, is required for ATL2 function.

The K372-E380 salt bridge is not required for either GTP binding or hydrolysis

Because the K372-E380 contact is specific to the post-fusion dimer conformer, we anticipated that the most upstream steps of the proposed ATL reaction cycle, namely GTP binding, formation of the pre-fusion dimer, and nucleotide hydrolysis, would all be normal in the single charge reversal mutants. To assess the biochemical properties of the mutant proteins, the soluble cytoplasmic domain of the relevant ATL2 variants—wild type, K372E, E380R, and the double mutant as well as the nucleotide binding–deficient K107A—were expressed, purified, and subjected to GTP hydrolysis assays.

Members of the dynamin superfamily of large GTPases possess a core GTPase domain with a globular fold similar to that of Ras and other small GTPases (Prakash et al., 2000; Niemann et al., 2001), but their biochemical properties differ in significant ways. In contrast to Ras superfamily small GTPases that require guanine nucleotide exchange factors for GTP loading because of their high, subnanomolar nucleotide affinity (Neal et al., 1988), dynamin-related GTPases have a relatively low affinity for nucleotides (Song and Schmid, 2003).

To assess nucleotide binding by ATL2 and how the K372-E380 salt bridge might influence it, the ability of each variant to bind and hydrolyze GTP was measured over a range of substrate concentrations (Fig. 2-4 A). When analyzed using a linearized form of the Michaelis–Menton equation (Fig. 2-4 B), wild-type ATL2 had an expected relatively high apparent Michaelis constant (K_M) for GTP of 34 μM, well within the range of the

10–100-μM K_M exhibited by other dynamin-related GTPases (Song and Schmid, 2003; Song et al., 2004). Under these conditions, K372E, E380R, and the double mutant ATL2 each exhibited a K_M for GTP close to that of wild-type ATL2: 38, 35, and 44 μM for K372E, E380R, and the double mutant, respectively (Fig. 2-4, A and B). Therefore, the inability to form the K372-E380 contact appeared to have little impact on nucleotide binding.

Dynamin-related GTPases are also distinguished from Ras superfamily GTPases by their relatively high intrinsic catalytic activity, which renders them independent of an external GTPaseactivating protein (Song and Schmid, 2003). In the case of dynamin, self-assembly into higher order oligomers further stimulates hydrolysis by as much as 100-fold, in a manner dependent on its associated GTPase effector domain (Stowell et al., 1999; Song and Schmid, 2003). Other dynamin-related GTPases, such as GBP1, have intrinsic GTPase activity but do not undergo higher order assembly (Prakash et al., 2000). Consequently, these GTPases do not exhibit the dramatic assembly stimulated increase in activity that is observed for dynamin. Nevertheless, the basal GTPase activity of full-length GBP1 is stimulated three- to fivefold upon dimer formation, with a dimerization constant of 0.4 μM (Prakash et al., 2000; Ghosh et al., 2006). Notably, dimerinduced stimulation of GBP1 catalytic activity is observed even for truncated molecules retaining only the GTPase head domain, implying that stimulation by dimer formation requires only the head to head binding interface (Ghosh et al., 2006).

To assess the extent to which the ATL2 GTPase is stimulated by dimer formation, the ability of the wild-type ATL2 soluble domain to hydrolyze GTP was measured at saturated GTP concentrations under initial velocity conditions (Fig. S2-3 A) over a range of protein concentrations. As anticipated, the catalytic rate constant, k_{obs}, was stimulated approximately twofold with an apparent dimerization constant of ~0.2 μM (Fig. 2-4 C), presumably caused by enhancement of GTP binding by formation of the head to head dimer. k_{obs} began to level off at 0.3–0.5 μM ATL2, suggesting that ATL2 was largely dimeric above this concentration. No further stimulation of the GTPase activity was observed, even at concentrations as high as 30 μM ATL2 (Fig. S2-3 B), consistent with a lack of higher order assembly under these conditions. Next, to determine the impact of the K372-E380 salt bridge on catalytic activity, the ability of both wild-type and mutant

variants to hydrolyze GTP was measured over a range of protein concentrations at which the wild-type protein was expected to be dimeric. k_{obs} for wild-type ATL2 was ~6 min^{-1}, consistent with previous measurements for ATL1 (Bian et al., 2011; Byrnes and Sondermann, 2011), and it did not vary significantly between 0.3 and 1.25 μM ATL2 (Fig. 2-4 D). As expected, the nucleotide binding–deficient K107A ATL2 exhibited only low activity, with a k_{obs} of ~0.6 min^{-1}. Under these conditions, k_{obs} for K372E and E380R ATL2, as well as the double mutant variant, was indistinguishable from that of the wild type. Therefore, the ability of ATL2 to bind GTP and form a head to head dimer as well as hydrolyze GTP does not appear to depend on the K372-E380 salt bridge.

The K372-E380 ionic contact is required for stable dimer formation

The undiminished ability of K372E ATL2 and E380R ATL2 to bind and hydrolyze GTP suggested that pre-fusion (head to head) dimer formation was normal. Formation of a GMPPNP dependent dimer, as detected by size exclusion chromatography (SEC), has been suggested previously by others to reflect formation of the GTP-bound pre-fusion state (Bian et al., 2011; Byrnes and Sondermann, 2011). Therefore, we next subjected each variant to SEC analysis.

Consistent with previous studies (Bian et al., 2011; Byrnes and Sondermann, 2011), the soluble domain of wildtype ATL2 formed dimers in the presence, but not in the absence, of GMPPNP (Fig. 2-5). No ATL2 dimerization was observed with GDP, consistent with previous studies for ATL1 (Byrnes and Sondermann, 2011; Moss et al., 2011), though contrasting with another (Bian et al., 2011). Also as expected, stable dimer formation was diminished for the nucleotide binding–deficient ATL2 K107 (Fig. S2-4). Under these conditions, both ATL2 K372E and ATL2 E380R were expected to form stable dimers. To our surprise, the level of ATL2 K372E and ATL2 E380R in the dimer fractions was negligible, regardless of whether they had been incubated with GMPPNP (Fig. 2-5). Remarkably, however, the compensatory charge reversal mutation in ATL2 K372E,E380R fully restored GMPPNP-dependent dimer formation. Thus, in contrast to expectations, the K372-E380 salt bridge is required to form a stable GMPPNP dimer.

The soluble domain of ATL2 adopts the post-fusion conformation in the GMPPNP-

bound (GTP bound) state

The inability of ATL2 K372E and ATL2 E380R to form the GMPPNP-dependent solution dimer raised the possibility that the GMPPNP solution dimer actually corresponds to the post-fusion, rather than pre-fusion conformer. The implications of this hypothesis are significant, as it would imply that the ATL2 soluble domain achieves the post-fusion conformation in the GTP-bound state, not requiring nucleotide hydrolysis. To test this possibility, we used two independent means to probe the conformational state of ATL2 in the presence of various nucleotide analogues.

First, we attempted to visualize the GMPPNP-bound ATL2 solution dimer by single-particle EM of negatively stained samples. EM images of GMPPNP-bound ATL2 particles were processed, and a total of 571 individual particle images were boxed manually, band-pass filtered, and aligned with respect to their center of mass. To test whether GMPPNP-bound ATL2 adopts the pre-fusion or post-fusion conformation, two 3D density maps from the same set of particle images were reconstructed using two different initial reference maps calculated from the atomic models of the pre-fusion (Protein Data Bank accession no. 3QOF) and post-fusion (Protein Data Bank accession no. 3QNU) ATL1 conformers (shown in Fig. 2 A). The resulting 3D maps resembled the post-fusion conformation more than the pre-fusion one (Fig. S2-5). Cross-correlation values between the final density maps and their respective initial references were 0.293 for the pre-fusion map and 0.425 for the post-fusion map, indicating that the GMPPNP-bound ATL2 dimer more likely adopts the post-fusion configuration.

The second method was cross-linking. Bismaleimidoethane (BMOE) is a short bifunctional sulfhydryl cross-linker capable of conjugating two cysteine residues to one another if they lie in close enough (~10 Å) proximity. ATL2 has three surface-exposed cysteines. Two are in the head (C59 and C144) and one is in the middle domain (C395). Of these, only the middle domain C395 residue is in a position to mediate cross-linking of one monomer to the other to form a covalently conjugated dimer. Importantly, C395-mediated dimer conjugation is predicted to occur in the post-fusion state but not in the pre-fusion state (Fig. 2-6 A). This is because the C395 residues of the two monomers are <20 Å apart in the post-fusion dimer, but they are >100 Å apart in the pre-fusion dimer. In contrast to C395, the other two cysteines in the head are too far apart, >50 Å, in either

dimer configuration. Nevertheless, they may mediate crosslinking within the monomer, likely leading to the slightly more rapidly migrating species of the monomer seen even in the absence of nucleotide. Significantly, cross-linker–dependent dimer conjugation was observed only in the presence of GMPPNP (Fig. 2-6 B). Dimer formation was not observed in the absence of nucleotide or in the presence of GDP or GTP, indicating that the post-fusion conformation is specific to the GMPPNP-bound (or GTP bound) state. Presumably, post-fusion dimer formation also occurs transiently with bound GTP, but subsequent hydrolysis returns it to the monomer state. As a control to confirm that the GMPPNP dimer is cross-linked through the middle domain C395 residue, an ATL2 variant lacking the C395 sulfhydryl (ATL2 C395N) was tested. As predicted, it failed to form dimers either in the presence or absence of GMPPNP. To further validate our assay for post-fusion dimer formation, ATL2 K372E and ATL2 E380R were each subjected to the same assay. As predicted by their behavior in SEC, neither of the single mutant variants formed the GMPPNP-dependent cross-linked dimer, whereas the compensatory double mutation restored dimer formation (Fig. 2-6 C). These results argue that the soluble domain of ATL2 adopts the post-fusion conformation exclusively in the GMPPNP-bound (or GTP bound) state. Moreover, although nucleotide hydrolysis is dispensable for achieving the post-fusion state, at least for the soluble domain, formation of the K372-E380 salt bridge is not.

FIGURES

Figure 2-1. Identification of ATL2 middle domain residues required for its ER network branching function.

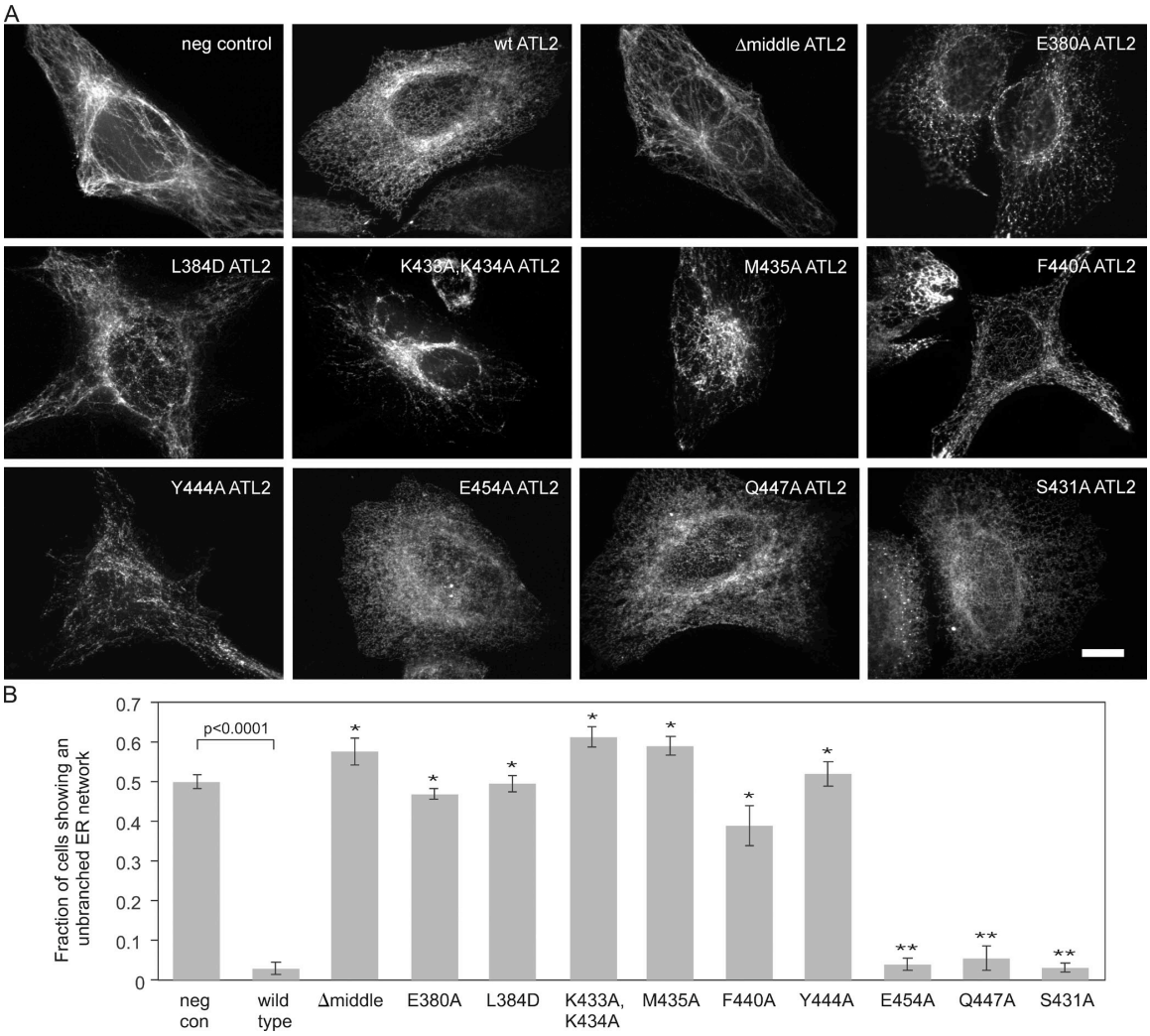

(A) Knockdown replacement assay. 48 h after transfection with a Myc-tagged DP1 negative control (neg con) construct, wild-type HA-ATL2, or each of the indicated HA-tagged ATL2 variants, cells were transfected with siRNAs targeting ATL2 and ATL3. 72 h after knockdown, cells were fixed and stained using an antibody against the Myc or HA epitope and viewed by confocal microscopy. Bar, 10 μm. (B) Quantification of the fraction of cells expressing the indicated proteins that had the unbranched ER phenotype. Values represent the means of three independent experiments ± SD. *, $P < 0.0005$ with respect to wild type; **, $P < 0.0005$ with respect to the Myc-DP1 negative control.

Figure 2-2. View of required ATL2 residues in the pre-fusion and post-fusion conformer.

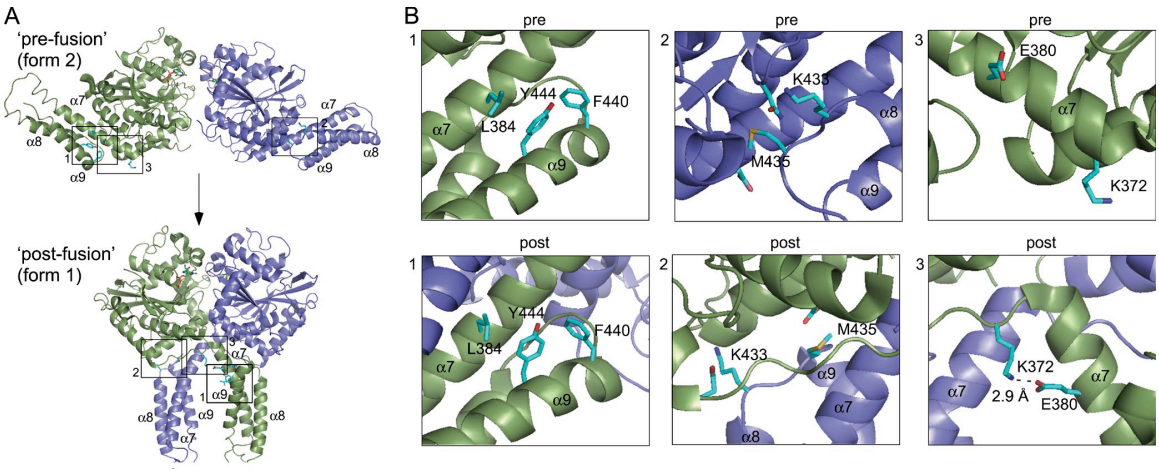

Required residues identified by knockdown replacement (Fig. 1) are shown in cartoon and stick form. The Protein Data Bank coordinates for the pre-fusion (3QOF) and post-fusion (3QNU) ATL1 conformers were downloaded from the RCSB Protein Data Bank database (Bian et al., 2011) and rendered in PyMOL (DeLano Scientific LLC). One subunit is green, and the other is blue. Bound GDP is highlighted in sticks. (A) The location of the three categories of required residues in both pre- and post-fusion dimer conformers are boxed and numbered (1–3). (B) A close-up view of the required residues boxed (1–3) in A. Key residues are numbered by their position in the ATL2 sequence and shown in stick form. See the Results under Middle domain mutations fall into three classes for details.

Figure 2-3. The K372-E380 salt bridge is required for ATL2 function.

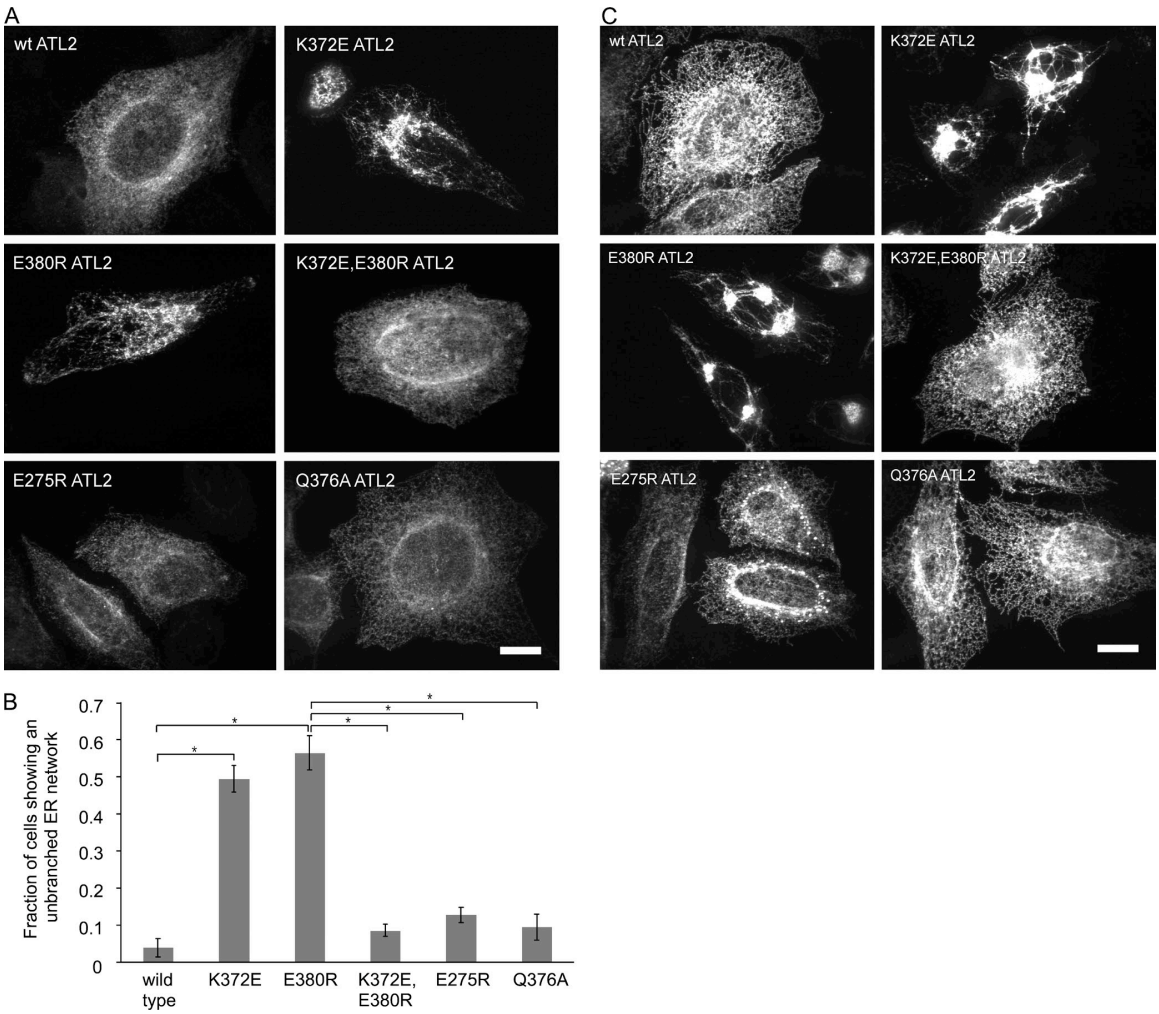

(A) Cells transfected with the indicated HA-ATL2 variants were treated 48 h later with siRNAs against ATL2 and ATL3. 72 h after knockdown, cells were fixed and stained with antibodies against the HA epitope and viewed by confocal microscopy. (B) Quantification of the fraction of cells expressing the indicated proteins that had the unbranched ER phenotype. Values represent the means of three independent experiments ± SD. *, $P < 0.0005$. (C) High level expression of the indicated nonfunctional HA-ATL2 variants also confers a dominantnegative ER phenotype seen here even without ATL2/3 knockdown. Bars, 10 μm.

Figure 2-4. The K372-E380 salt bridge is not required for either nucleotide binding or hydrolysis.

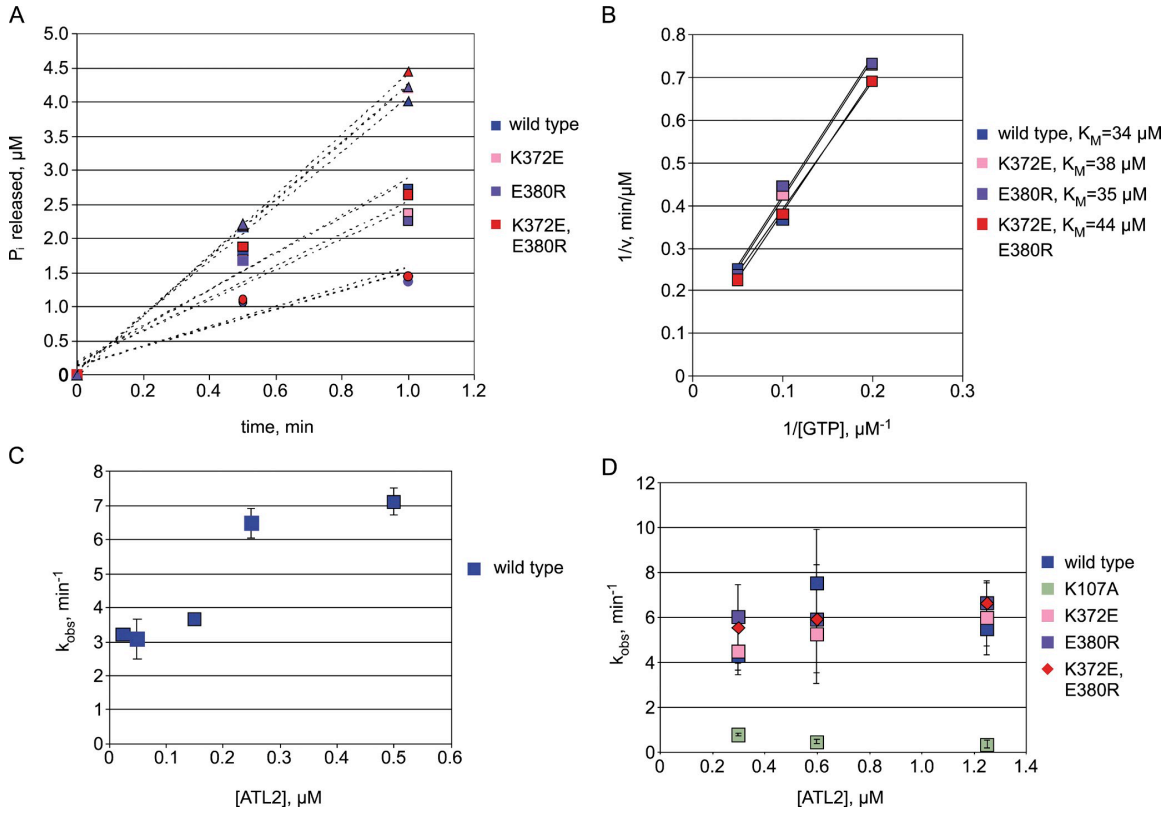

(A) 1 µM of the purified cytoplasmic domains (ATL2 1–467) of the indicated proteins were incubated with 5 µM (circles), 10 µM (squares), or 20 µM (triangles) GTP and assayed for phosphate release at the indicated times. Each point represents the means of two independent measurements. (B) A Lineweaver–Burk plot based on initial velocities from A was used to extract the K_M of the indicated ATL2 proteins for GTP. (C) The indicated concentrations of wild-type ATL2 were incubated with 0.2 mM GTP followed by assaying for phosphate release. (D) 0.3, 0.6, or 1.25 µM of the indicated ATL2 variants was incubated with 0.2 mM GTP followed by an assay for phosphate release. Values represent the means of three independent measurements ± SD. v, initial velocity.

Figure 2-5. The K372-E380 contact is required for GMPPNP-dependent stable dimer formation.

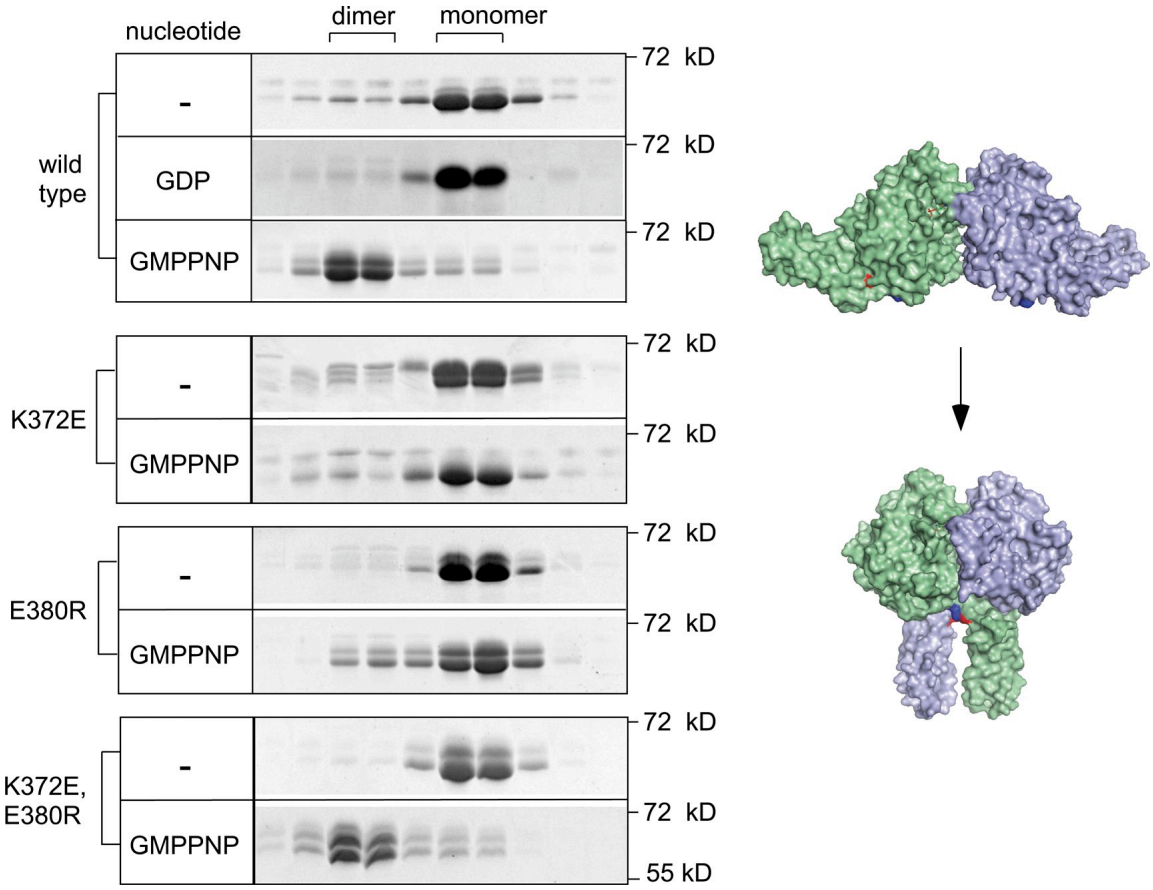

The purified cytoplasmic domains of the indicated ATL2 variants (30 μM) were incubated with no nucleotide (−), 5 mM GDP, or 2 mM GMPPNP for 30 min at RT. Thereafter, samples were resolved on a Superdex 200 column. The Coomassie-stained proteins (~60 kD) present in monomer (~70 kD) and dimer peak (~150 kD) positions from each column run are shown after SDS-PAGE. Also shown is a surface rendering of pre- and post-fusion dimer conformers with K372 and E380 highlighted in blue and red, respectively. Models were drawn in PyMOL from Protein Data Bank no. 3QOF and 3QNU.

Figure 2-6. GTP hydrolysis is not required for the pre-fusion to post-fusion conformational change.

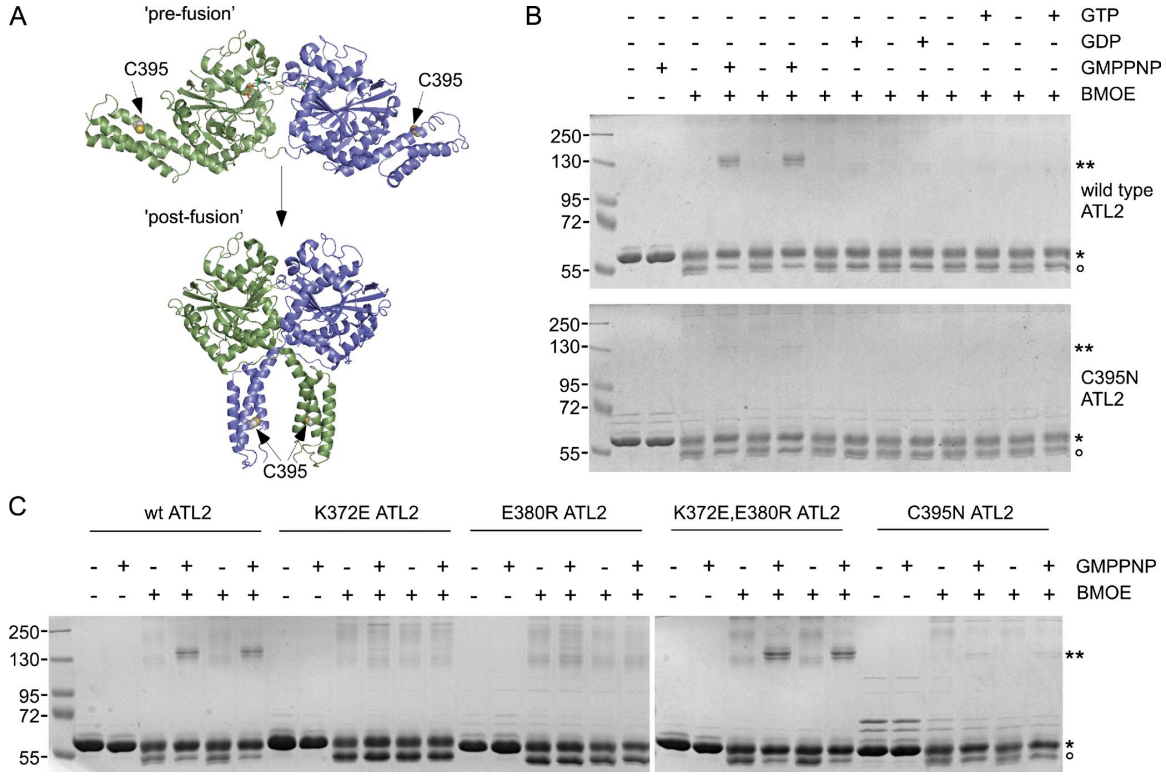

(A) Location of the C395 residue in ATL2 used to report on the post-fusion conformation. The C395 side chain in ATL2 is highlighted as spheres in both pre- and post-fusion ATL1 dimer structures rendered as detailed in Fig. 2. (B) The purified cytoplasmic domain of wild-type or C395N ATL2 (20 μM) was incubated in the presence or absence of the indicated nucleotides for 30 min at RT. Thereafter, samples were diluted, further incubated with or without BMOE for 1 h at RT, resolved by SDS-PAGE, and stained with Coomassie blue. The positions of non–cross-linked monomer and covalently cross-linked dimer ATL2 are indicated by single and double asterisks, respectively. The open circle indicates the position of ATL2 likely to have cysteine modifications not leading to dimer formation. (C) The purified cytoplasmic domains of the indicated ATL2 variants were subjected to the assay as described in B. Molecular masses are given in kilodaltons.

SUPPLEMENTAL FIGURES

Figure S2-1. Depletion of both ATL2 and ATL3 causes a reduction in ER network branch points.

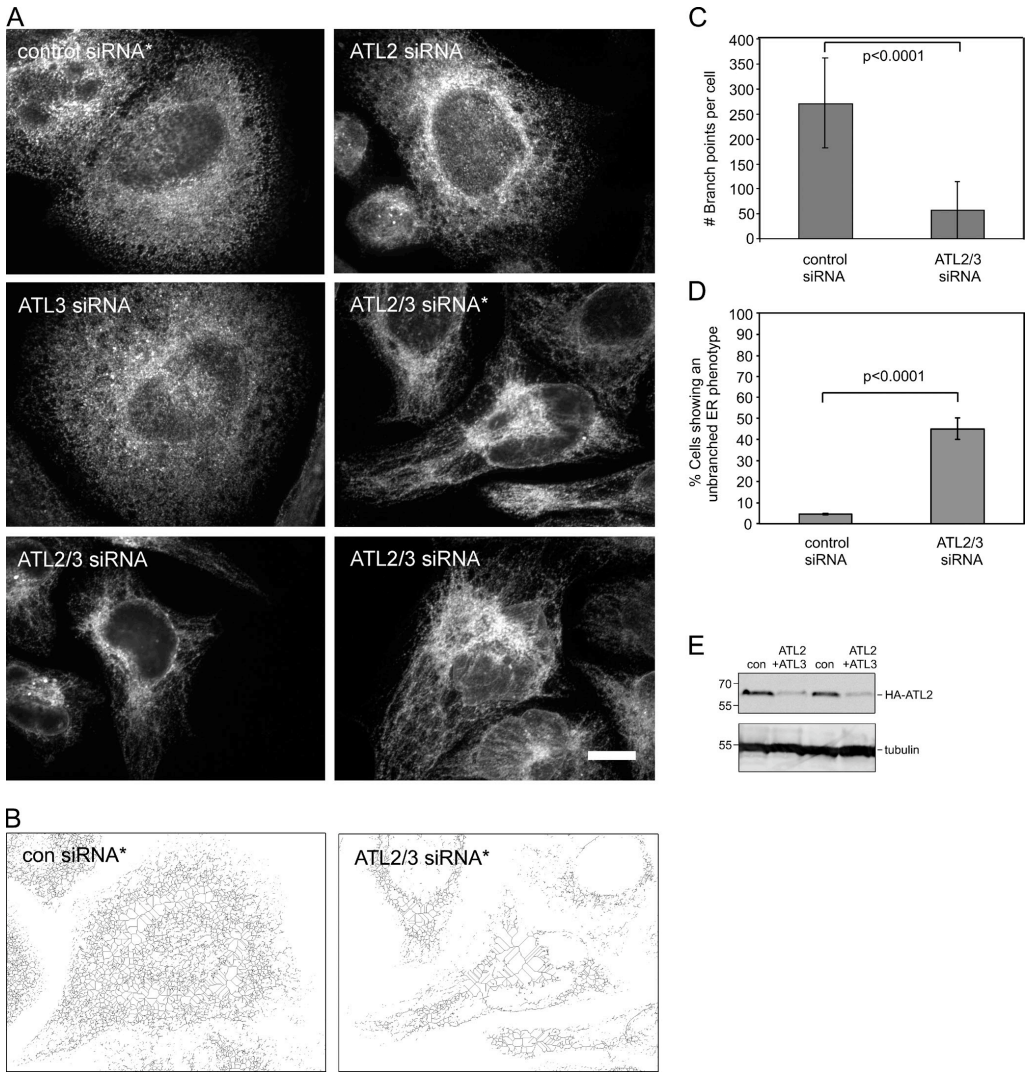

(A) Cells transfected with a PRA2 control (con) siRNA, ATL2 siRNA, ATL3 siRNA, or ATL2/3 siRNA were fixed, stained using an antibody against the ER marker protein disulfide isomerase, and viewed by confocal microscopy. Bar, 10 μm. (B) Maximal z projections of confocal images from A were thresholded and skeletonized in ImageJ (National Institutes of Health). Asterisks indicate corresponding images in A. (C) Quantification of the mean number of three-way junctions in 10 skeletonized images from PRA2 control and ATL2/3 siRNA–treated cells. (D) Quantification of the percentage of cells transfected with a control siRNA or ATL2/ATL3 siRNA showing the unbranched ER phenotype, defined as having <100 branch points per cell. Values represent the means of three independent experiments ± SD. (E) Immunoblot showing ATL2 knockdown. Cells transfected with an siRNA-sensitive HA-ATL2 construct were subsequently treated with a PRA2 control siRNA or ATL2/3 siRNA and processed for immunoblotting using antibodies against the HA epitope. Molecular masses are given in kilodaltons.

Figure S2-2. Middle domain ATL2 residues required for function lie near the GTPase head.

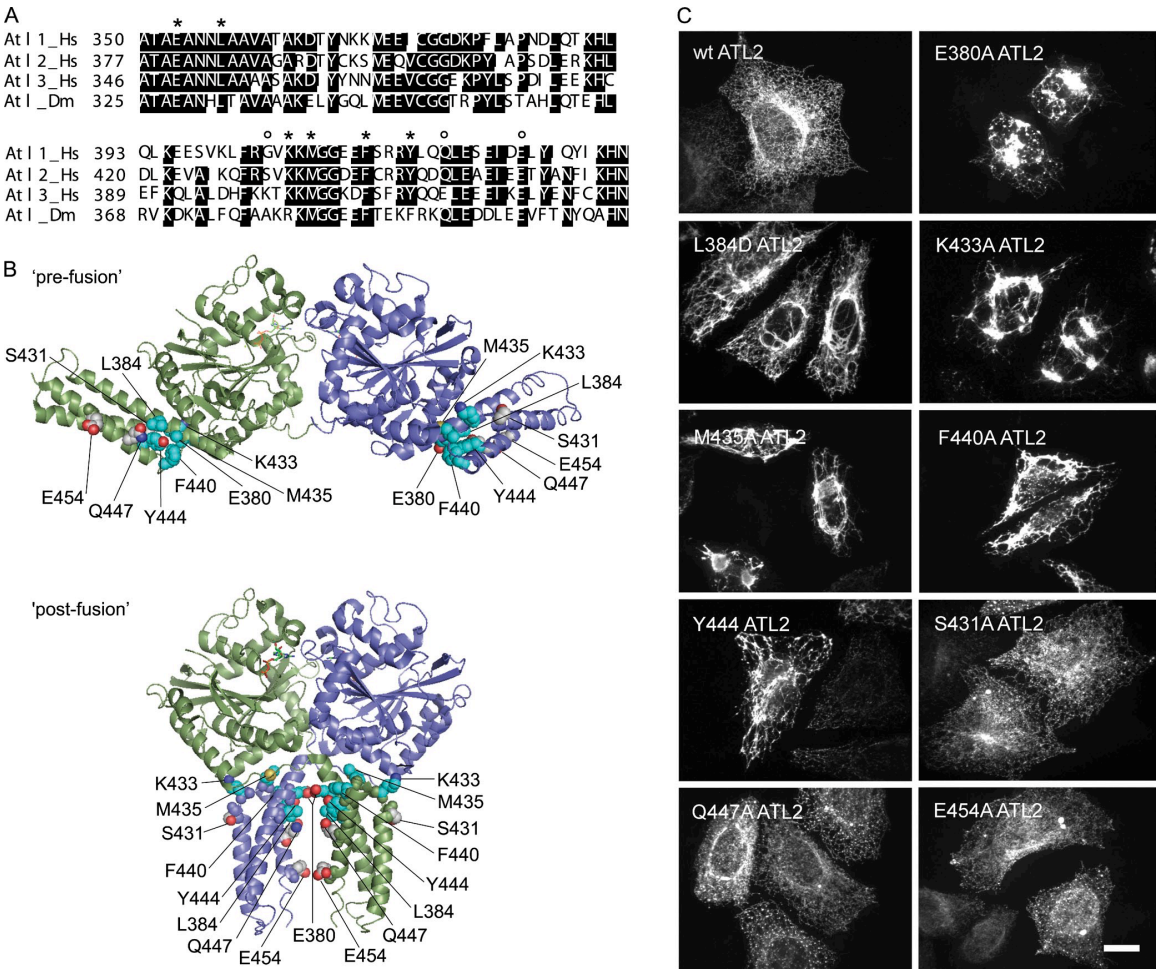

(A) Alignment of middle domain amino acids of human ATL1–3 and Drosophila ATL, with conserved residues shaded. Residues shown to be functionally required are labeled with asterisks, and residues shown to be nonessential are labeled with open circles. (B) Residues marked in A are labeled and highlighted as spheres in both pre-fusion and post-fusion ATL1 dimer structures (L384 was an exception as it was replaced by D384). Functionally required side chains are labeled with carbon in cyan, and nonessential side chains with carbon are in gray. The numbering is according to the ATL2 sequence. The Protein Data Bank coordinates for the pre-fusion (3QOF) and post-fusion (3QNU) ATL1 conformers were downloaded from the RCSB Protein Data Bank database (Bian et al., 2011) and rendered in cartoon form in PyMOL. One subunit is green, and the other is blue. GDP is highlighted in sticks. (C) High level expression of certain ATL2 variants with an alanine substitution in a functionally required residue results in a dominant-negative effect on ER morphology. Cells transfected with wild-type (wt) HA-ATL2 or various point mutant HAtagged ATL2 variants and expressing high levels of the protein were fixed, stained using an antibody against the HA epitope, and viewed by confocal microscopy. Endogenous ATL2/3 is present in these cells, as no knockdown was performed. Bar, 10 μm.

Figure S2-3. Linearity of GTPase assay and ATL2 GTPase activity are not further stimulated at high ATL2 concentrations.

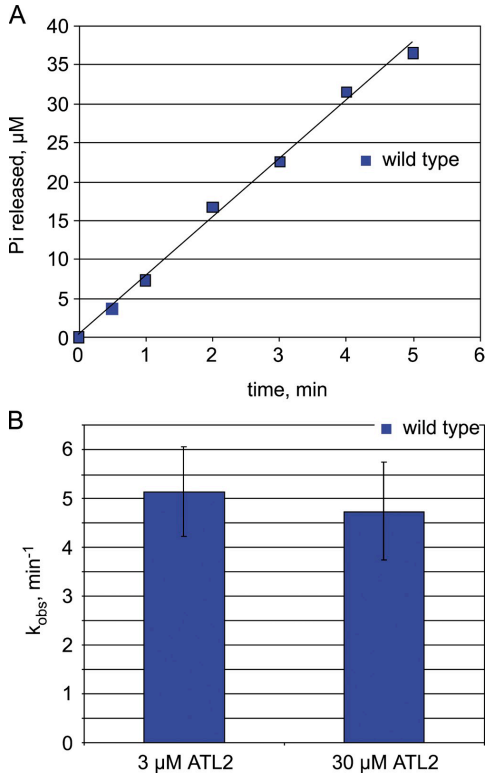

(A) 1 µM ATL2 was incubated with 0.2 mM GTP at 37°C for the indicated times followed by quenching with EDTA and assaying for phosphate release. (B) 3 or 30 µM ATL2 was incubated with 1 mM GTP at 37°C for 1 min, quenched, and diluted 10-fold before assaying for phosphate release. Data represent the means of four independent measurements ± SD. P = 0.57.

Figure S2-4. Stable dimerization of the soluble domain of ATL2 depends on nucleotide binding.

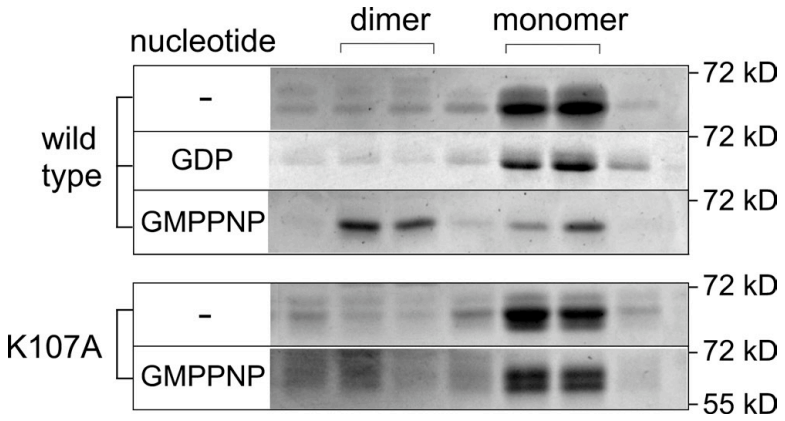

The purified cytoplasmic domain of wild type or the nucleotide binding–deficient K107A ATL2 variant (10 μM) was incubated with no nucleotide (−), 2 mM GMPPNP, or 5 mM GDP for 30 min at RT. Thereafter, samples were resolved on a Superdex 200 column. The Coomassie-stained proteins (60 kD) present in monomer (~70 kD) and dimer peak (~150 kD) positions from each column run are shown after SDS-PAGE.

Figure S2-5. EM of the GMPPNP-bound ATL2 GTPase.

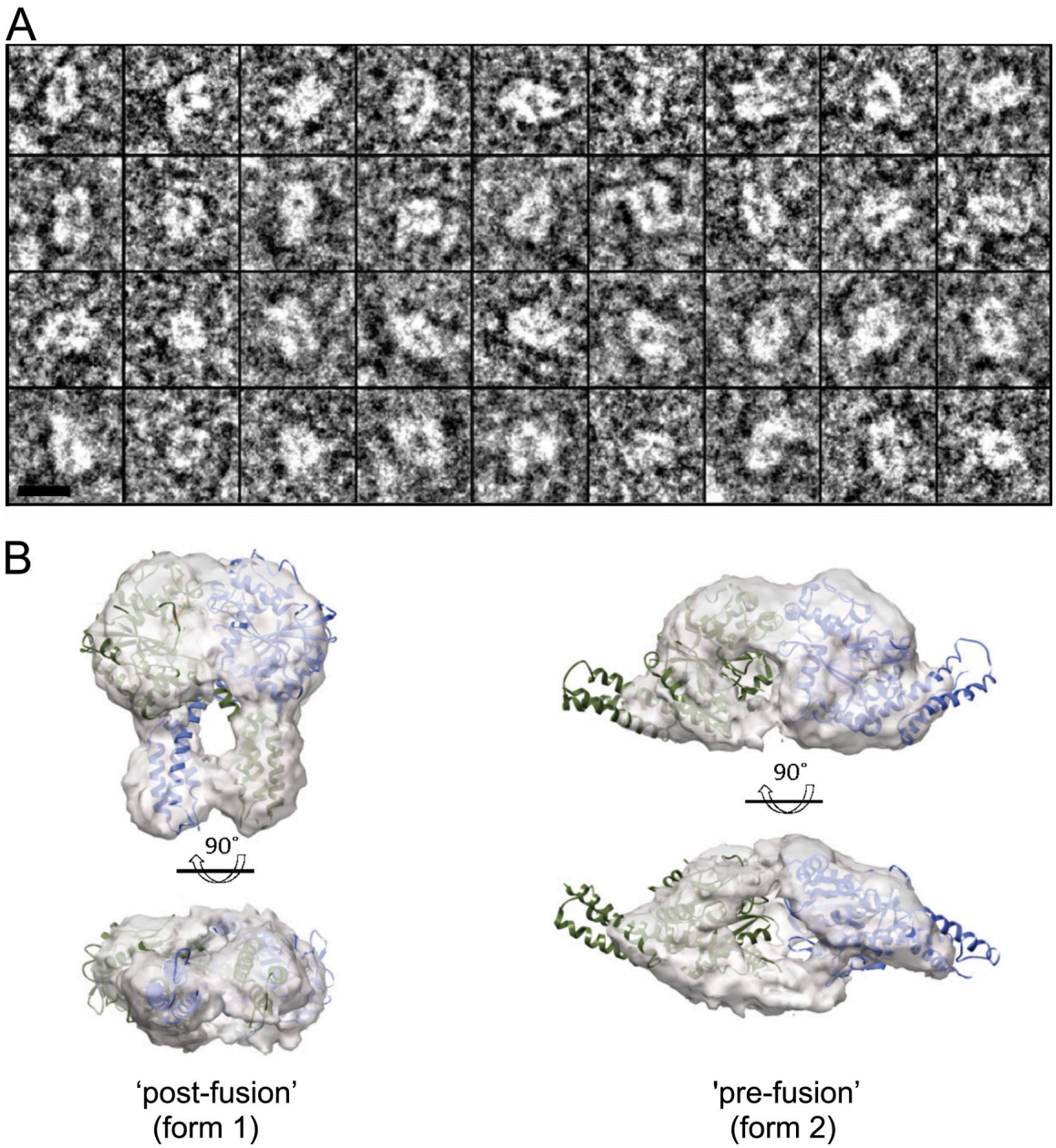

Representative raw particle images of GMPPNP-bound ATL2 boxed out from electron micrographs of negatively stained samples. Bar, 8 nm. (B) 3D reconstruction of dimeric ATL2 density maps using two atomic models representing the two ATL1 conformers, form 1 (Protein Data Bank accession no. 3QNU) and form 2 (Protein Data Bank accession no. 3QOF) as initial references.

DISCUSSION

Our findings reveal an intramolecular salt bridge required for the ER network branching function of ATL2. The importance of the K372-E380 ionic interaction for ATL2 function is likely caused by its stabilization of the post-fusion dimer conformation. This might seem surprising given that the charge interaction occurs intramolecularly, within each monomer subunit of the dimer. Based on the position of the salt bridge in the context of the post-fusion dimer, we speculate that the ionic contact constrains the linker in a kinked conformation relative to the head and middle domains. In so doing, it may serve to position M374 and L375, two intervening nonpolar residues that need to pack extensively against the opposing head, to form the post-fusion conformation. In the absence of the salt bridge, the linker may be rendered too flexible, reducing the ability of M374 and L375 to pack effectively.

Previous observations are consistent with the K372-E380 salt bridge being required for ATL-catalyzed membrane fusion. A *Drosophila* ATL variant bearing a mutation equivalent to E380R is significantly reduced in its ability to catalyze liposome fusion (Bian et al., 2011), though neither its GTPase activity nor its ability to dimerize has been reported. In addition, a *Drosophila* variant with a mutation equivalent to K372E lacks fusion activity (Bian et al., 2011). Thus, the opposing charge carried by the two residues appears functionally important. Whether the salt bridge, per se, is required for fusion activity remains to be determined. But based on the cumulative evidence, it seems likely that the ability of the two residues to engage in a salt bridge will be required for stabilizing the post-fusion dimer and hence for membrane fusion, even in the more distantly related organism.

Our finding that the ATL2 soluble domain can achieve the post-fusion conformation in the GMPPNP (or GTP)-bound state without nucleotide hydrolysis contrasts with the conclusions from an earlier study. In that study, biochemical analyses performed on the ATL1 soluble domain were used to arrive at the opposite conclusion: that ATL1 adopts the pre-fusion conformation in the GTP-bound state and the post-fusion conformation in the GDP-bound state (Bian et al., 2011). This has contributed, at least in part, to the current model for ATL proposing that the pre-fusion to post-fusion conformational change is directly coupled to GTP hydrolysis and Pi release. The reasons

for the conflicting results and conclusions remain unclear, and further work will be needed to resolve the discrepancy. Nevertheless, the results presented herein clearly indicate that GTP binding, in the absence of hydrolysis, is sufficient to induce the pre-fusion to post-fusion conformational change, at least for the ATL2 soluble domain.

As shown previously for GBP1 (Prakash et al., 2000; Ghosh et al., 2006), we observed a modest concentration dependent stimulation of the ATL2 soluble domain GTPase activity in the submicromolar range. By analogy to GBP1, this is likely caused by enhancement of GTP binding by formation of the head to head dimer. As the K372-E380 salt bridge is not present in the crystal structure of the initial nucleotide-bound pre-fusion dimer (Bian et al., 2011; Byrnes and Sondermann, 2011), mutations hindering formation of the salt bridge would not be predicted to impair the initial dimer-induced stimulation of GTP binding and hydrolysis. As expected, neither the K372E nor E380R mutant variants were diminished in their ability to bind or hydrolyze GTP. This result underscores the specificity of the defect in the K372E and E380R mutant ATL2 variants: they are likely able to form the initial head to head contact and bind GTP as well as the wild-type protein, yet they fail to transition to the post-fusion conformation.

Our observation that GTP hydrolysis is neither required for, nor dependent on, formation of the post-fusion conformation is somewhat surprising. It will be important to determine whether this behavior of the soluble domain reflects that of the full-length molecule in membranes. Finally, the interpretation of our findings with respect to the role of GTP hydrolysis in the ATL fusion mechanism also needs to be tempered by the uncertainty of whether the behavior of the ATL2 soluble domain, observed herein, reflects the behavior of the full-length, membrane-anchored protein. A possibility deserving of consideration is that membrane-anchored ATL is more conformationally constrained than its soluble counterpart. That is, whereas the soluble domain is sufficiently flexible to adopt the post-fusion conformation when restricted to the GTP-bound state, membrane-anchored ATL may require an additional input of energy, provided perhaps by the hydrolysis of GTP within the pre-fusion dimer. A requirement for nucleotide hydrolysis for formation of the membrane-anchored post-fusion dimer would serve to explain the requirement for GTP hydrolysis in ATL-catalyzed liposome fusion (Orso et al., 2009). On the other hand, this scenario depends on the membrane-

anchored pre-fusion dimer being compatible with the GTP-bound state and the post-fusion dimer being compatible with the GDP-bound state. This seems counterintuitive, given that the post-fusion conformation of the soluble domain is clearly compatible with the GMPPNP (or GTP)-bound state but most likely not with the GDP-bound state (Fig. 6 B).

An alternative possibility is that the behavior of the soluble domain does indeed reflect the behavior of the membrane-anchored full-length protein. In the latter scenario, we would propose that nucleotide hydrolysis is not directly coupled to the pre-fusion to post-fusion conformational change but rather that the energy released from hydrolysis is harnessed to drive another discrete step in the ATL reaction cycle. Whatever the identity of that hydrolysis-dependent step, it should explain the observed requirement for GTP hydrolysis in the in vitro fusion assay (Orso et al., 2009). Further work to determine the conformational states of GTP- and GDP-bound membrane-anchored ATL2, as well as the impact of the salt bridge identified herein on the catalytic properties of full-length and membrane-anchored ATL2, promises to more clearly delineate the role of nucleotide hydrolysis in the ATL2 mechanism.

REFERENCES

Baumann, O., and B. Walz. 2001. Endoplasmic reticulum of animal cells and its organization into structural and functional domains. Int. Rev. Cytol. 205:149–214.

Bian, X., R.W. Klemm, T.Y. Liu, M. Zhang, S. Sun, X. Sui, X. Liu, T.A. Rapoport, and J. Hu. 2011. Structures of the atlastin GTPase provide insight into homotypic fusion of endoplasmic reticulum membranes. Proc. Natl. Acad. Sci. USA. 108:3976–3981.

Byrnes, L.J., and H. Sondermann. 2011. Structural basis for the nucleotide-dependent dimerization of the large G protein atlastin-1/SPG3A. Proc. Natl. Acad. Sci. USA. 108:2216–2221.

Chappie, J.S., S. Acharya, M. Leonard, S.L. Schmid, and F. Dyda. 2010. G domain dimerization controls dynamin's assembly-stimulated GTPase activity. Nature. 465:435–440.

Daumke, O., and G.J. Praefcke. 2011. Structural insights into membrane fusion at the endoplasmic reticulum. Proc. Natl. Acad. Sci. USA. 108:2175–2176.

Ghosh, A., G.J. Praefcke, L. Renault, A. Wittinghofer, and C. Herrmann. 2006. How guanylate-binding proteins achieve assembly-stimulated processive cleavage of GTP to GMP. Nature. 440:101–104.

Hu, J., Y. Shibata, P.P. Zhu, C. Voss, N. Rismanchi, W.A. Prinz, T.A. Rapoport, and C. Blackstone. 2009. A class of dynamin-like GTPases involved in the generation of the tubular ER network. Cell. 138:549–561.

Lee, C., M. Ferguson, and L.B. Chen. 1989. Construction of the endoplasmic reticulum. J. Cell Biol. 109:2045–2055.

Ludtke, S.J., P.R. Baldwin, and W. Chiu. 1999. EMAN: semiautomated software for high-resolution single-particle reconstructions. J. Struct. Biol. 128:82–97.

Moss, T.J., C. Andreazza, A. Verma, A. Daga, and J.A. McNew. 2011. Membrane fusion by the GTPase atlastin requires a conserved C-terminal cytoplasmic tail and dimerization through the middle domain. Proc. Natl. Acad. Sci. USA. 108:11133–11138.

Neal, S.E., J.F. Eccleston, A. Hall, and M.R. Webb. 1988. Kinetic analysis of the hydrolysis of GTP by p21N-ras. The basal GTPase mechanism. J. Biol. Chem. 263:19718-19722.

Niemann, H.H., M.L. Knetsch, A. Scherer, D.J. Manstein, and F.J. Kull. 2001. Crystal structure of a dynamin GTPase domain in both nucleotide-free and GDP-bound forms. EMBO J. 20:5813–5821.

Orso, G., D. Pendin, S. Liu, J. Tosetto, T.J. Moss, J.E. Faust, M. Micaroni, A. Egorova, A. Martinuzzi, J.A. McNew, and A. Daga. 2009. Homotypic fusion of ER membranes requires the dynamin-like GTPase atlastin. Nature. 460:978–983.

Pieper, U., B.M. Webb, D.T. Barkan, D. Schneidman-Duhovny, A. Schlessinger, H. Braberg, Z. Yang, E.C. Meng, E.F. Pettersen, C.C. Huang, et al. 2011. ModBase, a database of annotated comparative protein structure models, and associated resources. Nucleic Acids Res. 39(Suppl. 1):D465–D474.

Praefcke, G.J., and H.T. McMahon. 2004. The dynamin superfamily: universal membrane tubulation and fission molecules? Nat. Rev. Mol. Cell Biol. 5:133–147.

Prakash, B., G.J. Praefcke, L. Renault, A. Wittinghofer, and C. Herrmann. 2000. Structure of human guanylate-binding protein 1 representing a unique class of GTP-binding proteins. Nature. 403:567–571.

Rismanchi, N., C. Soderblom, J. Stadler, P.P. Zhu, and C. Blackstone. 2008. Atlastin GTPases are required for Golgi apparatus and ER morphogenesis. Hum. Mol. Genet. 17:1591–1604.

Song, B.D., and S.L. Schmid. 2003. A molecular motor or a regulator? Dynamin's in a class of its own. Biochemistry. 42:1369–1376.

Song, B.D., M. Leonard, and S.L. Schmid. 2004. Dynamin GTPase domain mutants that differentially affect GTP binding, GTP hydrolysis, and clathrin-mediated endocytosis. J. Biol. Chem. 279:40431–40436.

Stowell, M.H., B. Marks, P. Wigge, and H.T. McMahon. 1999. Nucleotide dependent conformational changes in dynamin: evidence for a mechanochemical molecular spring. Nat. Cell Biol. 1:27–32.

Tang, G., L. Peng, P.R. Baldwin, D.S. Mann, W. Jiang, I. Rees, and S.J. Ludtke. 2007. EMAN2: an extensible image processing suite for electron microscopy. J. Struct. Biol. 157:38–46.

Zhu, P.P., A. Patterson, B. Lavoie, J. Stadler, M. Shoeb, R. Patel, and C. Blackstone. 2003. Cellular localization, oligomerization, and membrane association of the hereditary spastic paraplegia 3A (SPG3A) protein atlastin. J. Biol. Chem. 278:49063–49071.

CHAPTER 3

Membrane Tethering by the Atlastin GTPase Depends on GTP Hydrolysis but Not on Forming the Crossover Configuration*

ABSTRACT

The membrane-anchored atlastin GTPase couples nucleotide hydrolysis to the catalysis of homotypic membrane fusion to form a branched endoplasmic reticulum network. Trans dimerization between atlastins anchored in opposing membranes, accompanied by a crossover conformational change, is thought to draw the membranes together for fusion. Previous studies on the conformational coupling of atlastin to its GTP hydrolysis cycle have been carried out largely on atlastins lacking a membrane anchor. Consequently, whether fusion involves a discrete tethering step and, if so, the potential role of GTP hydrolysis and crossover in tethering remain unknown. In this study, we used membrane-anchored atlastins in assays that separate tethering from fusion to dissect the requirements for each. We found that tethering depended on GTP hydrolysis, but, unlike fusion, it did not depend on crossover. Thus GTP hydrolysis initiates stable head-domain contact in *trans* to tether opposing membranes, whereas crossover formation plays a more pivotal role in powering the lipid rearrangements for fusion.

* This manuscript appeared as an article in the Molecular Biology of the Cell, and is reprinted here.
Saini SG, Liu C, Zhang P, and Lee TH. MBoC. 2014. 25 (24): 3942-3953

All experiments were performed by Saini, SG and analyzed by Saini, SG and Lee, TH, with the exception of the CryoEM experiments, which were performed and analyzed by Liu C and Zhang P. The manuscript was written by Saini, SG, Lee, TH and Zhang P.

INTRODUCTION

Atlastin (ATL) is a large membrane-anchored GTPase required to form the branched endoplasmic reticulum (ER) network in organisms ranging from yeast to human (Park and Blackstone, 2010; McNew *et al*., 2013). The requirement for ATL in ER network formation may reflect its role in one or more membrane-shaping processes, including membrane curvature, tubule extension, and/or membrane fusion (Lee and Chen, 1988; Lee *et al*., 1989; Allan, 1991; Waterman-Storer, 1998; Friedman *et al*., 2010; Shibata *et al*., 2010). However, the remarkable finding that *Drosophila melanogaster* ATL (D-ATL), as well as the distantly related yeast SEY1 and *Arabidopsis* RHD3 orthologues, can catalyze GTP-dependent fusion when purified and inserted into synthetic liposomes is most consistent with a direct role for ATL in homotypic membrane fusion (Orso *et al*., 2009; Anwar *et al*., 2012; Zhang *et al*., 2013).

Current models for the ATL fusion mechanism are based on several key findings. First, fusion depends strictly on GTP hydrolysis. The nonhydrolyzable GTP analogue guanosine 5-*O*-[gamma-thio]triphosphate (GTPγS) failed to substitute for GTP (Orso *et al*., 2009; Moss *et al*., 2011), and the hydrolysis-defective R48A D-ATL variant failed to catalyze fusion even when GTP was provided (Pendin *et al*., 2011; Byrnes *et al*., 2013). Second, x-ray crystal structure determinations of the ATL1 soluble domain initially revealed two distinct dimer configurations (Bian *et al*., 2011; Byrnes and Sondermann, 2011). Both configurations had the GTPases interacting in a head-to-head manner with bound nucleotides near the dimer interface. However, the conformers also differed from one another markedly. In one (form 2), the three-helix bundle (3HB) comprising the middle domain of each subunit was bent back away from the dimer interface axis, packing against a helix (α6) within the GTPase head of the same subunit (Bian *et al*., 2011; Byrnes and Sondermann, 2011). By contrast, the other conformer (form 1) lacked the intramolecular 3HB-head interactions observed in the form 2 conformer, due to the release of the 3HB from the head and a subsequent rigid body rotation about a conserved proline within the linker connecting the 3HB to the head. The rotation of the 3HB causes the middle domains to cross over one another, bringing the 3HBs, pointing away from

one another initially in an extended configuration, into close parallel alignment (Bian *et al*., 2011; Byrnes and Sondermann, 2011; Byrnes *et al*., 2013). Additionally, crossover buries a much larger surface area (>3.5-fold) between subunits, creating a more stable configuration (Bian *et al*., 2011; Byrnes and Sondermann, 2011; Byrnes *et al*., 2013).

In addition to conformational changes within the GTPase and 3HB domains, a requirement for the cytoplasmic tail of ATL was also demonstrated (Moss *et al*., 2011; Liu *et al*., 2012). Though the tail primary sequence is not well conserved, it is characterized by a predicted amphipathic helix just proximal to the second membrane-spanning segment. A peptide derived from this helix in D-ATL penetrated into the lipid bilayer, and this ability correlated with fusion activity in vitro (Liu *et al*., 2012). Thus tail insertion was proposed to contribute a key lipid-destabilizing force necessary for fusion.

Based on the above findings, a consensus model for the ATL mechanism has emerged: GTP binding and hydrolysis, with help from the C-terminal tail, drives fusion by drawing opposing membrane-anchored ATL soluble domains together in *trans* and inducing crossover formation. Yet there is still little agreement on the details of the fusion mechanism. At first, the lack of consensus was attributed to the uncertainty of the nucleotide-bound state for each of the initial crystal structure dimer conformers. Irrespective of the nucleotide analogue used during crystallization, only GDP was observed in the active site (Bian *et al*., 2011; Byrnes and Sondermann, 2011). Despite this, dimers were suggested to form in the GTP-bound state independent of nucleotide hydrolysis, because stable dimers were recovered after incubation with the nonhydrolyzable GTP analogue GMPPNP, even though they were also recovered with the transition-state analogue GDP-AlF_4^- (Byrnes and Sondermann, 2011; Morin-Leisk *et al*., 2011; Moss *et al*., 2011). Subsequent chemical cross-linking and cryo-electron microscopy (cryo-EM) analysis revealed that the GMPPNP dimers were in the crossover configuration (Morin-Leisk *et al*., 2011). This observation was confirmed by more recent x-ray crystal structure determinations revealing an additional form 3 crossover dimer conformer resembling the previously observed form 1 conformer, though with clear differences in the active site and also exhibiting more tightly packed interactions overall (Byrnes *et al*., 2013). The form 3 dimer, produced upon crystallization with either GMPPNP or GDP-AlF_4^-, retained the respective analogues in the active site, indicating

that ATL1 is capable of adopting the tightly packed crossover configuration in at least two distinct nucleotide-bound states. Collectively the observations failed to resolve whether dimer formation and/or crossover require nucleotide hydrolysis.

Fortunately, recent kinetic measurements revealed that both dimer formation and crossover, at least in the soluble phase, are catalyzed by nucleotide hydrolysis. Using fluorescence resonance energy transfer–based probes to independently monitor head-to-head contact and crossover formation within the truncated ATL1 soluble domain, Sondermann and colleagues observed relatively efficient head contact and crossover with GMPPNP, as predicted from earlier studies. Remarkably, however, both head contact and crossover were accelerated two orders of magnitude (from $t_{1/2}$ ~100 s to $t_{1/2}$ ~1 s) in the presence of hydrolyzable GTP (Byrnes *et al*., 2013).

Of significance, previous studies probing the conformational coupling of ATL to its GTP hydrolysis cycle have largely been carried out in the soluble phase, using molecules lacking a membrane anchor (Bian *et al*., 2011; Byrnes and Sondermann, 2011; Byrnes *et al*., 2013; Morin-Leisk *et al*., 2011; Moss *et al*., 2011). This might present a serious caveat if the soluble domain were to behave differently from its membrane-anchored counterpart, possibly due to greater flexibility in the absence of membrane anchoring. To address this issue, we used membrane-anchored ATL to analyze the requirement for both GTP hydrolysis and for crossover in the context of both membrane tethering and membrane fusion reactions. Similar to the recent model put forth by Sondermann and colleagues, in which energy input is required at the earliest *trans* pairing step of the fusion reaction (Byrnes *et al*., 2013), our results revealed a clear requirement for nucleotide hydrolysis in the stable *trans* pairing of ATL molecules during vesicle tethering. However, unlike the recently proposed model, our findings also revealed that crossover can be uncoupled from tethering by mutation. Thus crossover formation, though possibly catalyzed in concert with tethering by nucleotide hydrolysis as put forth recently (Byrnes *et al*., 2013), nevertheless plays a more pivotal role in driving membrane fusion than in membrane tethering.

MATERIALS AND METHODS

Cells, constructs, and reagents

Cell expression studies were conducted on Cos-7 cells maintained at 37°C in a 5% CO2 incubator in DMEM (Sigma-Aldrich) and 10% FBS (Atlanta Biologicals) with 1% penicillin/streptomycin (Thermo Fisher Scientific). N-terminally eYFP tagged D-ATL was kindly provided by James McNew (Rice University, TX). The 6xHis-tagged *Drosophila melanogaster* atlastin (D-ATL) was constructed for protein production using PCR amplification of nucleotides encoding amino acids 1–541 of D-ATL from eYFP-DATL and cloned into the pRSETB vector at NheI and EcoRI sites. Mutations specific to this study were generated using QuikChange mutagenesis (QIAGEN) and fully verified by sequencing (Genewiz). With the exception of Fig 3-6, all variants used for protein production in this study, including the wild type, had the following additional amino acid changes G343C, C350A, C429L, C452L, C501A. These substitutions were introduced at the outset for the express purpose of restricting the reactivity of the sulfhydryl-reactive cross-linker BMOE to the G343 position. Notably, a D-ATL version containing all of the indicated substitutions had fusion activity similar to that of the unaltered D-ATL (Fig S3-4). The variants used in Fig 3-6 had none of the above cysteine substitutions. The Myc-REEP5 construct was previously described (Morin-Leisk et al., 2011). All lipids were purchased from Avanti Polar Lipids. GTP, GDP, GMPPNP and GTPγS were purchased (Sigma-Aldrich), reconstituted to 100 mM stocks in 10 mM Tris, 1 mM EDTA pH 8.0, and stored at -80°C.

Protein expression and purification

Protein expression was induced with 0.2 mM IPTG in BL21(DE3)pLysS cells at 16°C for 2.5 hrs. Cells were lysed in 4% Triton-X 100 (Roche) in a standard lysis buffer and 6xHis-tagged proteins purified using standard protocols on Ni^{+2} agarose beads (QIAGEN). Bound protein was eluted in 50 mM Tris, pH 8.0, 250 mM imidazole, 100 mM NaCl, 5 mM $MgCl_2$, 10% glycerol, 2 mM β-mercaptoethanol, 0.1% Anapoe-X 100 (Affymetrix), 1mM EDTA. Protein yields were typically 4–8 mg/ml (~1 mg per liter of

culture), >85% pure, flash frozen in liquid N_2, and stored at -80°C.

Proteoliposome production

Lipids in chloroform dried down by rotary evaporation were hydrated by resuspension in A100 Buffer (25 mM HEPES pH 7.4, 100 mM KCl, 10% glycerol, 2 mM β-mercaptoethanol, 1 mM EDTA) (Moss et al., 2011), final lipid concentration ~10 mM, and subjected to 12 freeze thaw cycles in liquid N2 and room temperature water. 100-300 nm diameter liposomes were formed by extrusion through 100 nm polycarbonate filters using the LipoFast LF-50 extruder (Avestin) and checked for size by DLS (as described below and Fig S3-1). Unlabeled liposomes consisted of POPC:DOPS (85:15) and labeled liposomes had POPC:DOPS:NBD-DPPE:rhodamine-DPPE (82:15: 1.5:1.5). D-ATL in 0.1% Anapoe-X 100 was reconstituted into pre-formed 100 nm liposomes as previously described (Moss et al., 2011; Orso et al., 2009). In brief, all reconstitutions were carried out at a protein to lipid ratio of 1:300 at an effective detergent-to-lipid ratio of ~0.7 as previously described (Moss et al., 2011). Protein and lipid were incubated at 4°C for 1 h. Detergent was removed by SM-2 Bio-Beads (BioRad) at 70 mg Triton-X 100 per 1 g of beads. Insoluble protein aggregates were pelleted by centrifugation of the samples in a microcentrifuge for 10 min at 16,000 x g. Thereafter, reconstituted D-ATL proteoliposomes were adjusted to 50% Nycodenz and separated from unincorporated protein by flotation of proteoliposomes through a (50%/45%/0%) Nycodenz (Axis-Shield) 5 ml step gradient. All Nycodenz solutions were made in A100 Buffer without glycerol. After centrifugation at 40 k rpm for 16 h at 4°C in a SW-50.1 rotor, the gradient was fractionated and analyzed by SDS-PAGE stained with Coomassie Blue to assess insertion efficiency. The proteoliposomes typically migrated to the 45%/0% Nycodenz interface. Finally, the floated fraction was desalted over a 2.4 ml Sephadex A (GE Healthcare) column into A100 Buffer, stored at 4°C and used within 72 hr.

Fusion Assay

Fusion assays were performed as previously described (Moss et al., 2011), except that donor and acceptor proteoliposomes were mixed at a molar ratio of 1:2. In brief, labeled donor proteoliposomes (0.2mM) were mixed with unlabeled acceptor proteoliposomes (0.4mM) in A100 Buffer in the presence of 5 mM $MgCl_2$ in a total

volume of 200 µl per reaction. The reaction mixture was transferred into a clear, flat-bottomed polystyrene 96- well plate (Corning) and incubated at 37°C for 10 min. The fusion reaction was started by addition either of 2 mM GTP, 2 mM GMPPNP (final concentration), or buffer. NBD fluorescence (excitation 460 nm, emission 538 nm) was measured at 1-min intervals with a 1 sec shaking after every read. After 60 min, 10 µl of 10% Anapoe-X 100 was added to determine the total fluorescence in the sample. All measurements, reported as the percent of total fluorescence after solubilization in Anope-X 100, were acquired on a Tecan Safire II fluorescence plate reader using Microsoft Excel.

Dynamic light scattering (DLS)

Proteoliposomes (1 mM total lipid) in A100 Buffer were incubated in the absence or presence of 2 mM GTP, GDP, or GMPPNP all in the presence of 5 mM $MgCl_2$. Incubations were for 10 min at 37°C unless indicated otherwise. Only for P319G,K320E D-ATL, the $MgCl_2$ concentration was lowered to 3 mM to reduce a low level of size shift seen in the absence of nucleotide. Thereafter, the reaction was diluted tenfold (0.1 mM total lipid) into A100 Buffer + 5 mM MgCl2 in a disposable polystyrene cuvette (Thermo Fisher Scientific). Measurements were acquired on a Malvern ZetaSizer Nano Series (Model#Zen3600) instrument. Parameters were set automatically by the instrument software (Dispersion Technology Software version 5). Where indicated, EDTA was added to samples after the initial measurement to a final concentration of 40 mM and the measurements repeated after 10 min. The average of three measurements per sample was used to represent the z-average of the vesicles.

Cryo-EM

Proteoliposomes in A100 Buffer + 5 mM MgCl2 were incubated in the absence or presence of 2 mM GTP for 20 min at RT. Reaction solutions (4 µl) were applied onto R 2/1 Quantifoil® R2/1 holey carbon EM grids (Quantfoil Micro Tools GmbH, Jena, Germany), blotted from the backside of the grid for 3-4 sec and manually plunge-frozen into liquid ethane. The frozen grids were loaded onto a Gatan 626 single tilt liquid N2 cryo-holder (Gatan Inc., Warrendale, PA) and imaged at 200 kV with an FEI TF20

microscope (FEI Corp., OR). Low-dose (~20 electron/Å2) projection images were recorded on a 4k x 4k UltraScan 4000 CCD camera (Gatan, Inc., Warrendale, PA) at under focus of ~2 μm and nominal magnifications of 50,000x. A total of 70-100 images were recorded from randomly selected areas in each cryo-specimen. The width of the zipper-like structures was determined by measuring the distance between the two outer dark density peaks from opposing membranes using the line profile function in the Digital Micrograph software (Gatan Inc., Warrendale, PA). Only the images recorded under similar defocus values were used for the analysis. The average width was calculated from 10-15 straight "zipper" profiles.

Fluorescence microscopy

Cos-7 cells on 12 mm glass coverslips (24-well plate) were transfected with 100 ng of the indicated eYFP-D-ATL plasmids and 1.5 μl Lipofectamine 2000 transfection reagent (Life Technologies) according to manufacturer's instructions. 48 hrs following transfection, cells were fixed in 3% paraformaldehyde in PBS, washed, and mounted directly. For REEP5 co-localization, cells were co-transfected with 50 ng eYFP-D-ATL and 50 ng Myc-REEP5, fixed in ice cold MEOH and stained as previously described (Morin-Leisk et al., 2011) with the 9E10 monoclonal antibody against the Myc epitope followed by Alexa 568-conjugated goat anti-mouse secondary antibody (Life Technologies). Images were obtained using a spinning-disk confocal scanhead (Yokagawa; PerkinElmer) mounted on an Axiovert 200 microscope (Zeiss) with a 100x 1.4 NA objective (Zeiss) and acquired using a 12-bit ORCA-ER camera (Hamamatsu Photonics). Maximal value projections of sections at 0.2-μm spacing were acquired using Micro-manager open source software (UCSF).

Cross-linking

Purified 6xHis-tagged D-ATL (residues 1 to 415) and variant proteins were dialyzed into SEC buffer (25 mM Tris-HCl pH 7.0, 100 mM NaCl, 5 mM MgCl2, 2 mM EGTA) at 4°C and pre-cleared by centrifugation at 100,000 rpm for 15 min (TLA100). 5μM of each protein was incubated at RT in SEC buffer, pH 7.0, in the absence or presence of 2 mM GMPPNP, GDP, GTP, GDP-AlF_4^- (2 mM GDP/2 mM AlCl3/20 mM

NaF) or $AlF4^-$ only (2 mM AlCl3/20 mM NaF). After 30 min at RT, the reaction was diluted 2.5-fold into SEC (to 2 μM D-ATL) in the absence or presence of 6 μM BMOE (Thermo Fisher Scientific) and incubated for 1 h at RT. Samples were then quenched with 20 mM DTT for 15 min, mixed with reducing sample buffer, resolved by SDS-PAGE and stained with Coomassie Blue.

GTPase Assay

Purified 6xHis-tagged D-ATL (residues 1 to 415) and variant proteins were dialyzed into 50 mM Tris-HCl, pH 7.5, 100 mM NaCl, 1 mM MgCl2 at 4°C and pre-cleared by centrifugation at 100,000 rpm (TLA100) at 4°C for 15 min. GTPase activity was measured using the Enzchek Phosphate Assay kit (Life Technologies). A standard reaction for GTPase measurements involved mixing 1 U/ml purine nucleoside phosphorylase (PNP), 0.2 mM 2-amino-6-mercapto-7-methylpurine riboside (MESG) in the provided buffer (50 mM Tris–HCl, pH 7.5, 1 mM $MgCl_2$, 0.1 mM sodium azide) supplemented with 100 mM NaCl and 0.5 mM GTP in a total volume of 200 ml. After 10 min at 37°C, reactions were transferred to a 96-well plate (Costar) and started by addition of either buffer or 6xHis-tagged D-ATL variants at a final concentration of 1 or 2 mM. Absorbance at 360 nm was monitored at 30 s intervals for 30 min at 37°C in a plate reader (Tecan, Safire 2). Data were normalized to a phosphate standard and initial velocities calculated using the early linear portion of each curve.

RESULTS

Membrane-tethering assay

To clarify the energetics of *trans* dimer formation in the context of membranes, we set out to establish an assay that would independently evaluate the requirements for ATL-mediated membrane tethering, apart from fusion. For the tethering assay, we wanted to adhere closely to fusion conditions to maximize the relevance of our findings. However, because fusion could complicate the evaluation of tethering, we expressly prevented fusion, at least at the outset, by using membrane-anchored versions of ATL with small C-terminal truncations removing the cytoplasmic tail and/or the second transmembrane (TM) helix. Truncation had previously been reported to block fusion (Moss *et al*., 2011; Liu *et al*., 2012), but we reasoned that it might not adversely impact tethering, because *trans* interactions between TM helices or the tail had not been reported. Furthermore, because human ATL had not yet been reported to catalyze fusion, we used D-ATL, which catalyzes fusion robustly in a GTP hydrolysis–dependent manner and is ~50% identical to ATL1/2/3 (Orso *et al*., 2009; Bian *et al*., 2011). To first confirm that the truncated constructs were fusion incompetent under our assay conditions, we assessed their fusion kinetics relative to the full-length (FL) protein. As expected, fusion by FL D-ATL was strictly dependent on GTP hydrolysis, with no fusion signal either in the absence of nucleotide or in the presence of GMPPNP (Figure 3-1). Also as anticipated (Moss *et al*., 2011; Liu *et al*., 2012), both the tailless protein and a further truncated protein, containing just the first TM helix (single TM D-ATL; Liu *et al*., 2012), were entirely defective for fusion (Figure 3-1).

Membrane tethering assessed by dynamic light scattering

On the basis of our expectation that tethering of individual proteoliposomes in the absence of fusion should generate larger proteoliposome clusters, we used dynamic light scattering (DLS), which is well-suited to detecting such size changes (Arac *et al*., 2006). Proteoliposomes for the tethering assay were prepared in the same manner as for the fusion assay. Single TM D-ATL proteoliposomes, confirmed to be fusion incompetent (Figure 3-1), were incubated with GTP-Mg^{+2} at 37°C for varying times, and the mean

hydrodynamic diameters of both the starting and resulting liposome populations were monitored. The starting proteoliposomes were relatively monodisperse with a 200- to 300-nm mean hydrodynamic diameter (*z*-average; Supplemental Figure S3-1 and Figure 3-2A). On addition of GTP-Mg^{+2}, the samples became polydisperse and the *z*-average increased rapidly, reaching values on the order of several microns by 10 min (Figure 3-2A). The observed size shift was temperature dependent and reversed by EDTA treatment, consistent with GTP-Mg^{+2} dependence (Figure 3-2B). Notably, even without EDTA treatment, the GTP-Mg^{+2}–induced size shift was reversed after prolonged incubation, driven possibly by dimer disassembly after GTP depletion (Figure 3-2C; Morin-Leisk *et al*., 2011; Byrnes *et al*., 2013).

GTP-dependent membrane tethering visualized by cryo-EM

To complement the DLS assay, we also performed cryo-EM analysis, which revealed the morphology of a putative GTP-dependent ATL-tethered intermediate (Figure 3-3). After brief incubation with or without GTP, samples were deposited onto EM grids and immediately subjected to plunge freezing. Overview images taken at low magnification showed large clusters of vesicles in the GTP sample, often 1 to 2 μm in length, compared with a more dispersed arrangement in the absence of GTP (Figure 3-3A). D-ATL–mediated vesicle tethering was directly visualized as zipper-like parallel-aligned membrane interfaces within each cluster in the GTP sample (Figure 3-3B, with a further enlarged image shown in Figure 3-3C, left panel). These structures were likely formed through extended interactions between single TM D-ATL in opposing proteoliposomes. Importantly, the zipper-like structures were seen more frequently with GTP than without, consistent with the DLS results (Figure 3-3D, WT, black vs. gray bars).

Tethering depends on GTP hydrolysis

Next we assessed the dependence of tethering on GTP hydrolysis. The nonhydrolyzable analogue GMPPNP was used, because it promoted stable dimer formation of the truncated ATL1/2 soluble domain (Byrnes and Sondermann, 2011; Byrnes *et al*., 2013; Morin-Leisk *et al*., 2011), albeit more slowly than GTP (Byrnes *et*

al., 2013). Moreover, the form 3 ATL1 dimer structure was crystallized with GMPPNP and clearly retained the analogue within the active site (Byrnes *et al*., 2013). Based on prior soluble-phase data, including our own (Morin-Leisk *et al*., 2011), our expectation was that tethering would occur readily with GMPPNP but possibly more slowly than with GTP. Strikingly, there was robust tethering of single TM D-ATL proteoliposomes only in the presence of GTP. Neither GDP nor GMPPNP could promote it, indicating a strict dependence on nucleotide hydrolysis (Figure 3-4). Similar results were obtained using a version of D-ATL lacking the tail but retaining the second TM helix (Figure 3-4). Additionally, another nonhydrolyzable analogue (GTPγS) also failed to support tethering (Supplemental Figure S3-2).

We were struck by the apparent lack of tethering in the absence of nucleotide hydrolysis. Unfortunately, AlF_4^- by itself caused membranes to aggregate, rendering a test of the transition-state analogue GDP-AlF_4^- unfeasible in this assay. Instead, we sought an independent means of confirming the nucleotide hydrolysis requirement. For this, we took advantage of D-ATL variants with mutations in a key conserved catalytic residue R48, which when mutated to R48E or R48A, abolishes GTPase activity (Bian *et al*., 2011; Byrnes and Sondermann, 2011; Pendin *et al*., 2011). In the form 3 dimer conformer, the R48 side chain was observed to point in toward each respective active site, functioning as an intramolecular arginine finger to stabilize the negatively charged hydrolytic transition state (Byrnes *et al*., 2013). However, in the form 1 and 2 dimer conformers, the same side chain was observed to point out toward the dimer interface (Bian *et al*., 2011; Byrnes and Sondermann, 2011). Thus R48 may swing away from the dimer interface en route to hydrolysis, moving in toward the active site to perform its catalytic function. A similar dimer-dependent rearrangement of the same R48 catalytic residue occurs in the closely related human guanylate-binding protein 1 (Ghosh *et al*., 2006). Accordingly, charge reversal to R48E (R77E in ATL1) blocked GTP hydrolysis as well as stable dimer formation with either GMPPNP or GDP-AlF_4^-, presumably by introducing charge repulsion at the dimer interface (Byrnes and Sondermann, 2011). In contrast, charge removal to alanine (R48A) did not impair GMPPNP-dependent stable dimer formation in the soluble phase, likely because the remaining head contacts were sufficient for dimerization (Pendin *et al*., 2011; Byrnes *et al*., 2013). However,

elimination of the positive charge within the active site, normally provided by the arginine finger, nearly eliminated hydrolytic activity (Pendin *et al*., 2011; Byrnes *et al*., 2013). Confirming our results with GMPPNP (Figure 3-4) and GTPγS (Supplemental Figure S3-2), neither the R48A nor R48E variant was capable of tethering vesicles (Figure 3-4). It is worth mentioning that ATL is consistently monomeric in the absence of nucleotide or in the presence of GDP (Byrnes and Sondermann, 2011; Morin-Leisk *et al*., 2011; Moss *et al*., 2011), and because our membrane-anchored D-ATL was prepared in the absence of nucleotide, it was unlikely that hydrolysis was serving to break up preexisting ATL crossover dimers. Altogether these results established, for the first time, that tethering by membrane-anchored D-ATL requires energy input from GTP hydrolysis. Notably, the lack of any detectable vesicle tethering with GMPPNP contrasted with previously observed formation of GMPPNP-induced stable, truncated, soluble-domain dimers (Byrnes and Sondermann, 2011; Morin-Leisk *et al*., 2011). The difference, though it remains to be demonstrated, may reflect further slowing of hydrolysis-independent crossover (observed with truncated ATL) by the conformational constraints imposed by membrane anchoring.

Tethering does not depend on a salt bridge required for fusion

On the basis of the hydrolysis requirement for tethering (Figure 3-4) combined with the prior observation that hydrolysis catalyzed concerted head contact and crossover in the soluble phase (Byrnes *et al*., 2013), we anticipated that crossover formation would also be required for tethering (Byrnes *et al*., 2013). Work from our lab had previously shown that the crossover dimer configuration of soluble ATL2 depends on an intramolecular salt bridge between two oppositely charged residues at the heart of the crossover in the ATL1 crystal structures (Morin-Leisk *et al*., 2011). One residue, K372, is in the linker connecting the GTPase head to the 3HB; and the other residue, E380, is nearby at the start of the 3HB (Figure 3-5A). Though the K372-E380 salt bridge is intramolecular, it likely stabilizes a kinked conformation of the linker in each monomer; the kink in turn promotes crossover dimer formation by facilitating intermolecular packing interactions. Supporting this hypothesis, charge reversal of either of the residues (K372E or E380R) impaired formation of a cross-linked product predicted to depend on

crossover (Morin-Leisk *et al*., 2011). These mutations also had functional consequences, blocking the ability of ATL2 to support ER network formation in cells (Morin-Leisk *et al*., 2011). Attesting to the specificity of the charge-reversal mutations, the inhibitory effects of each single charge-reversal mutation were fully rescued in the compensatory double mutant (K372E,E380R; Morin-Leisk *et al*., 2011). Of relevance to this work, K372 and E380 are conserved not only between ATL1 and ATL2, but also in D-ATL. Moreover, charge reversal of either of the corresponding residues in D-ATL (K320E and E328R) had previously been reported to block fusion (Bian *et al*., 2011). Consequently we reasoned that the corresponding salt bridge in D-ATL would be essential for fusion and that mutations perturbing it might prove useful for testing the dependence of membrane tethering on crossover.

To assess whether K320 and E328 form a required salt bridge for D-ATL, we first expressed each charge-reversal mutation in the context of FL D-ATL. Like ATL2, wild-type D-ATL expression did not adversely affect the branched ER network morphology in Cos-7 cells (Figure 3-5B, quantified in 3-5C). In contrast, and as previously observed for ATL2 (Morin-Leisk *et al*., 2011), expression of either the K320E or E328R D-ATL variant led to dominant-negative perturbations of the ER, including loss of the tubular network in the periphery and collapse into bundles or aggregates of ER membrane (Figure 3-5B, quantified in 3-5C). Although the perturbations were stronger for K320E than for E328R (Figure 3-5C), the dominant-negative effects of either mutation were fully rescued in the double-mutant variant (Figure 3-5B, quantified in 3-5C), again attesting to the importance of the salt bridge for in vivo functionality. Up to this point, the analogous mutations in D-ATL seemed to behave similarly to those in ATL2, consistent with conservation of the salt bridge as a stabilizing force for forming the crossover dimer. That these and other D-ATL variants were correctly ER targeted was confirmed by counterstaining for cotransfected REEP5, a tubular ER marker (Hashimoto *et al*., 2014; Supplemental Figure S3-3).

For confirming the importance of the K320-E328 salt bridge for fusion, both single- and double-mutant variants were constructed in the context of FL D-ATL and incorporated into liposomes for the fusion assay. Neither the K320E nor the E328R variant had fusion activity, as anticipated (Figure 3-5D; Bian *et al*., 2011). Remarkably,

the double-mutant variant catalyzed fusion to a similar extent as wild-type, though with slowed kinetics (Figure 3-5D). This result confirmed the importance of the K320-E328 salt bridge for fusion. Whether the compensatory mutation restored full lipid bilayer fusion, rather than selectively restoring outer leaflet mixing, remains to be determined, requiring additional assays that measure inner leaflet and content mixing (Orso *et al*., 2009; Liu *et al*., 2012).

Having established the importance of the K320-E328 salt bridge for fusion, we asked whether tethering would also depend on the salt bridge. The single TM D-ATL variants containing either the K320E or E328R mutation were assessed for tethering by DLS. To our surprise, both variants tethered membranes robustly and in a manner that depended on hydrolyzable GTP, contrasting with the nucleotide binding–defective R48E variant, which failed to tether under any condition (Figure 3-5E). Similar results were obtained with FL versions of the K320E and E328R mutant variants retaining the second TM helix and tail (Figure 3-5E). Thus, although membrane fusion depended considerably on the K320-E328 salt bridge, tethering did not.

Disruption of the D-ATL K320-E328 salt bridge does not abolish crossover

Our results thus far suggested that tethering might be crossover independent. Notably, though, our earlier work demonstrating the dependence of crossover on the identified salt bridge had been carried out exclusively on ATL2. Consequently we needed to confirm the effect of the corresponding mutations on D-ATL crossover. We therefore subjected the K320E variant of the D-ATL soluble domain to the same cross-linking analysis used previously to monitor ATL2 crossover (Morin-Leisk *et al*., 2011).

The 8Å homobifunctional sulfhydryl cross-linker BMOE, is ideal for capturing ATL2 crossover dimers, because two sulfhydryl 3HB residues (C395) come to within ~8 Å of one another uniquely in the crossover dimer configuration (Bian *et al*., 2011; Byrnes and Sondermann, 2011; Byrnes *et al*., 2013; Morin-Leisk *et al*., 2011). D-ATL has a glycine at the same position, and replacing it with cysteine to generate G343C D-ATL did not at all impair fusion activity (Supplemental Figure S3-4). As anticipated (Morin-Leisk *et al*., 2011), cross-linked D-ATL soluble-domain dimers were captured in the presence of GMPPNP and also with GTP (albeit less so), but not with either GDP or in

the absence of nucleotide (Figure 3-6A). Presumably, a lower level of crossover dimers were captured after incubation with GTP, because the dimers form rapidly ($t_{1/2}$~1 s) but also undergo disassembly upon GTP consumption (Byrnes *et al*., 2013), rendering them harder to capture in the subsequent cross-linking step. A higher percentage of crossover dimer capture was seen with D-ATL (~66%) than was previously seen with ATL2 (~32%), possibly because the D-ATL crossover dimer is more stable than its ATL2 counterpart. Finally, crossover dimers were also captured efficiently with GDP-AlF_4^-. This was anticipated, based on the idea that crossover is catalyzed by GTP hydrolysis, as well as the observation that ATL1 crystals formed with the transition-state analogue produced the crossover dimer configuration (Byrnes *et al*., 2013).

We next tested the ability of the salt bridge variant K320E D-ATL (with G343C) to undergo crossover. As anticipated (Morin-Leisk *et al*., 2011), GMPPNP-dependent cross-linking was inhibited for this variant. But to our surprise, GDP-AlF_4^--dependent cross-linking was not (Figure 3-6A). GDP-AlF_4^- was not tested in our previous analysis (Morin-Leisk *et al*., 2011); therefore it remains to be clarified whether the same lack of sensitivity would also be observed for ATL2. Regardless, it was clear that the K320E mutation may impair but does not altogether block D-ATL crossover.

Identifying new D-ATL mutations that abolish crossover

The ability of the K320E variant to undergo crossover, albeit reduced, raised an obvious concern that this variant retained activity in the tethering assay (Figure 3-5E), not because of a lack of requirement for crossover in tethering, but because the K320E mutation only partially impaired crossover. To address this concern, we searched for a second mutation in a nearby residue that might eliminate crossover altogether. Two proline residues in the linker connecting the 3HB to the GTPase head (P317 and P319) at or near the pivot point of the 3HB rotation (Figure 3-6B) seemed good candidates for mediating this rotation (Bian *et al*., 2011; Byrnes and Sondermann, 2011). When expressed in Cos-7 cells, both P317G and P319G D-ATL variants, like the K320E variant, perturbed the ER network, indicating a loss of ER network–forming functionality (Figure 3-6C, quantified in 3-6D). As before, ER targeting was confirmed by counterstaining for cotransfected REEP5 (Supplemental Figure S3-3). In the cross-

linking assay, the P317G mutation only slightly affected crossover, whereas the P319G mutation had an inhibitory effect on par with the K320E mutation, inhibiting GMPPNP-dependent but not GDP-AlF_4^-–dependent crossover (Figure 3-6A). Encouraged by the partial inhibition of crossover caused by the P319G mutation, we tested whether it might result in a more potent block when combined with the K320E mutation. As expected, the double-mutant P319G,K320E variant in Cos-7 cells also perturbed ER network morphology (Figure 3-6C, quantified in 3-6D). Strikingly, and in contrast to the single-mutant variants, the double-mutant variant displayed a complete block in our cross-linking assay, even in the presence of GDP-AlF_4^- (Figure 3-6A). The cross-linking assay was also attempted on membrane-anchored molecules, but technical issues hindered the analysis. Still, given the complete block exhibited by the double-mutant soluble domain, it was difficult to envision any crossover capability on the part of the more constrained membrane-anchored counterpart. In sum, the combined P319G,K320E mutations were likely to provide an effective means of blocking crossover.

One final concern was that the double P319G,K320E mutations might not only block crossover but also impair GTP hydrolysis. Recent work had revealed a sensitivity of GTP loading to mutations in 3HB residues outside the GTPase domain, presumably because the mutations impeded packing of the 3HB against the α6 helix within the head (Byrnes *et al*., 2013). Therefore it was imperative that any effect of the P319G,K320E mutation on GTP loading or GTP hydrolysis be ruled out. GTPase assays revealed that all variants, including P319G,K320E, were as active as the wild-type protein in their ability to hydrolyze GTP, confirming that the mutations selectively impaired crossover (Figure 3-6E).

Tethering does not depend on crossover

Finally, we tested for the ability of the hydrolysis-active, but crossover–defective, P319G,K320E variant to mediate tethering. As with either the single TM or FL versions of the K320E variant (Figure 3-5E), the double-mutant P319G,K320E FL variant still tethered membranes robustly and in a manner dependent on hydrolyzable GTP (Figure 3-6F). As also seen for the K320E FL variant, the P319G,K320E FL variant lacked any detectable fusion activity (Figure 3-6G). On the basis of the lack of impairment of

tethering by either the K320E or P319G,K320E mutations, we were compelled to conclude that membrane tethering by D-ATL depends strictly on GTP hydrolysis but not on forming the crossover configuration. Importantly, tethering by either the K320E or P319,K320E mutant variants, both of which retained the second TM helix and tail, was morphologically similar to that seen with single TM D-ATL, with zipper-like parallel-aligned membrane interfaces (Figure 3-3C) that were seen more frequently with GTP than without (Figure 3-3D). In addition, although further structural work will be required to fully resolve the difference, "zippers" formed with the crossover–defective P319G,K320E variant appeared slightly wider than those formed with either the partially crossover–defective (K320E) or crossover–competent (single TM) variants, suggestive of a more extended tether in the absence of crossover (Figure 3-3D).

FIGURES

Figure 3-1: Tail less and single TM D-ATL are fusion incompetent.

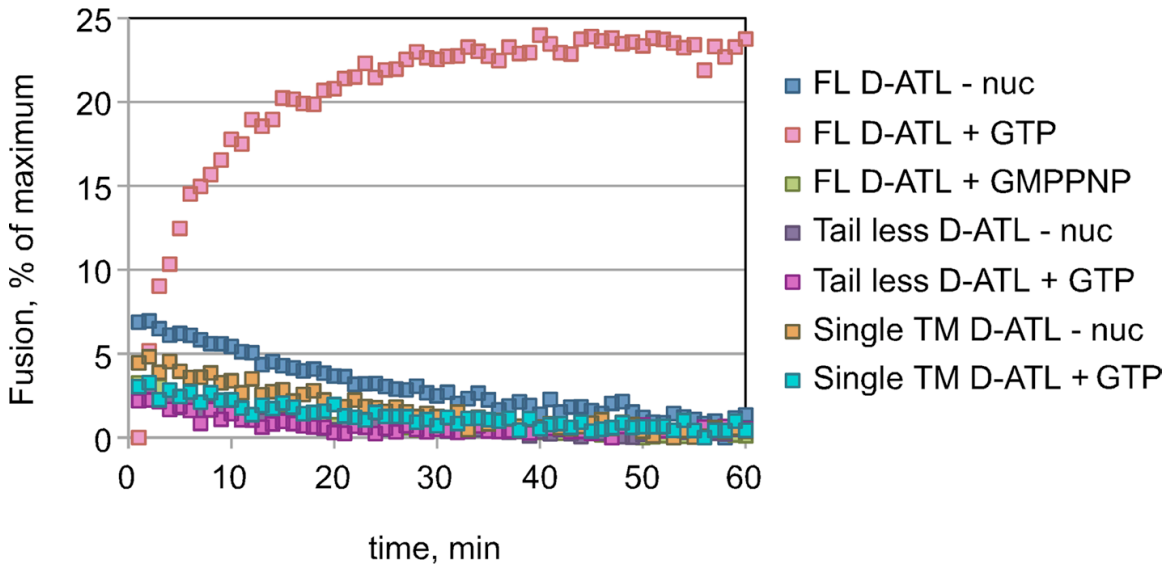

Full length (FL), tail less (residues 1–471), or single TM (residues 1–447) D-ATL was reconstituted into donor and acceptor vesicles. Fusion was monitored by the de-quenching of NBD-labeled lipid present in the donor vesicles after addition of GTP or GMPPNP or in the absence of nucleotide.

Figure 3-2: Fusion-incompetent D-ATL is capable of tethering membranes.

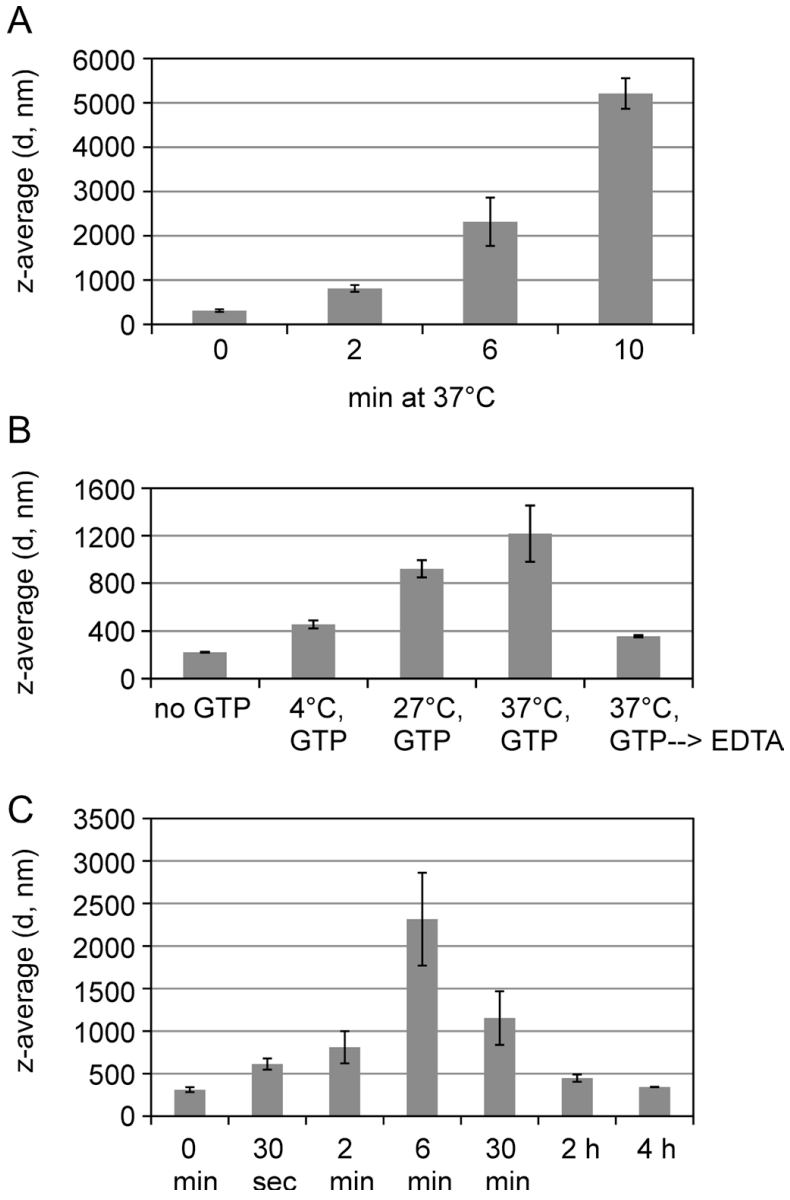

(A) Tethering is time dependent. Single TM D-ATL was reconstituted into vesicles and incubated with GTP at 37°C for the indicated times before DLS measurements. (B) Tethering is temperature dependent. Vesicles were incubated at the indicated temperatures in the absence of GTP (37°C) or presence of GTP at the indicated temperatures for 10 min; this was followed by DLS. The 37°C GTP samples were further treated with EDTA and re-measured by DLS. (C) Tethering is reversible. Prolonged incubation at 37°C led to reversal of tethering as indicated by DLS. In each case, the average of three independent measurements ± SD is shown.

Figure 3-3: Cryo-EM visualization of vesicle tethering by D-ATL.

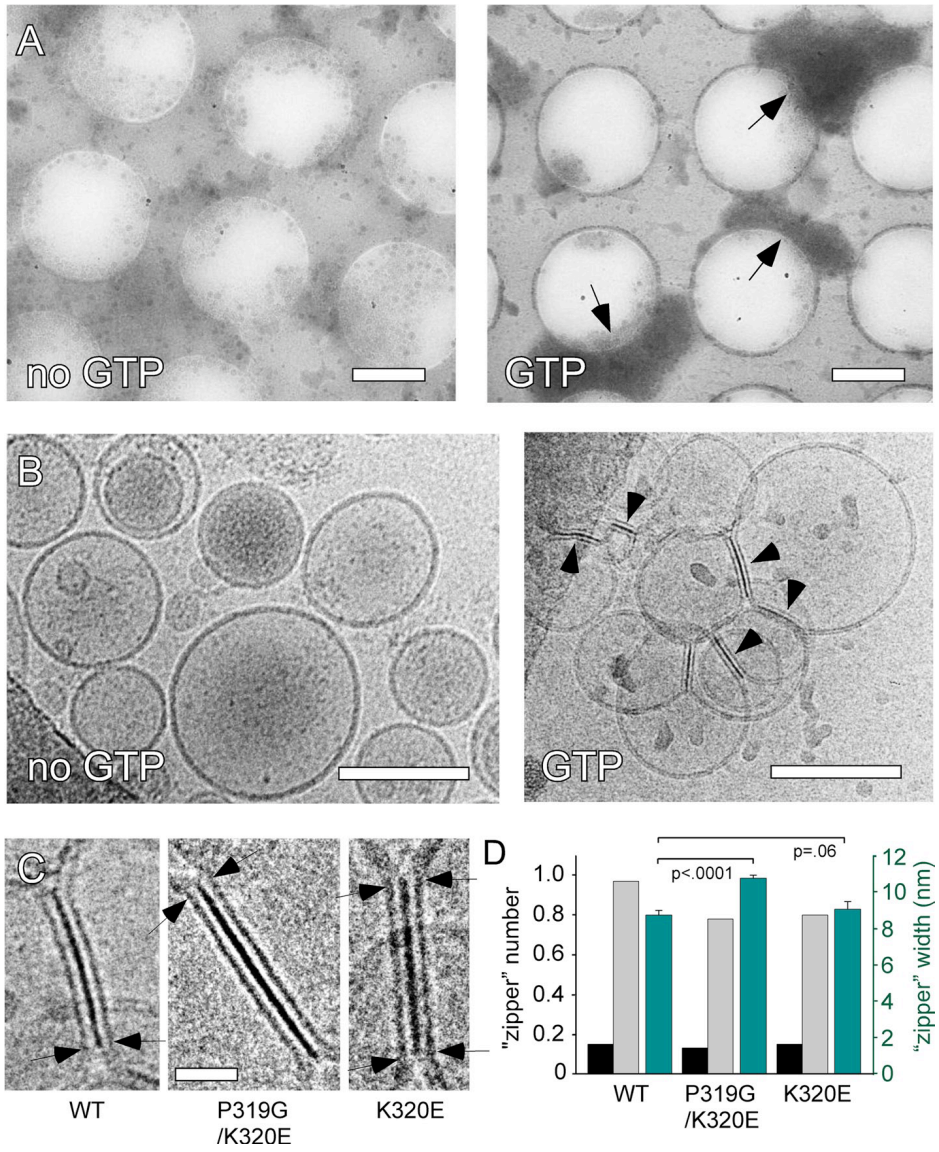

(A and B) Single TM D-ATL reconstituted into vesicles was incubated at RT for 20 min in the absence or presence of GTP and imaged with cryo-EM at low (A) and high (B) magnification. Scale bars: (A) 1 μm; (B) 100 nm. Arrowheads (B) mark zipper-like structures formed between opposing membranes. (C) Enlarged views of the zipper-like structures from wild-type single TM (left), P319G,K320E FL (middle), and K320E FL (right) D-ATL. Arrows indicate where two membranes are "zippered" together. Scale bar: 20 nm. (D) Comparison of the average number of tethered structures per micrograph, in the absence (black) and presence (gray) of GTP. Data shown are from 70–100 micrographs per sample. Also shown is a comparison of the average width of the "zippers" (green) in the presence of GTP from wild-type single TM, P319G,K320E FL and K320E FL D-ATL samples. Measurements are derived from >10 "zippers" for each, ± SD. The indicated *p* values were determined using an unpaired Student's *t* test.

Figure 3-4: Tethering depends on GTP hydrolysis.

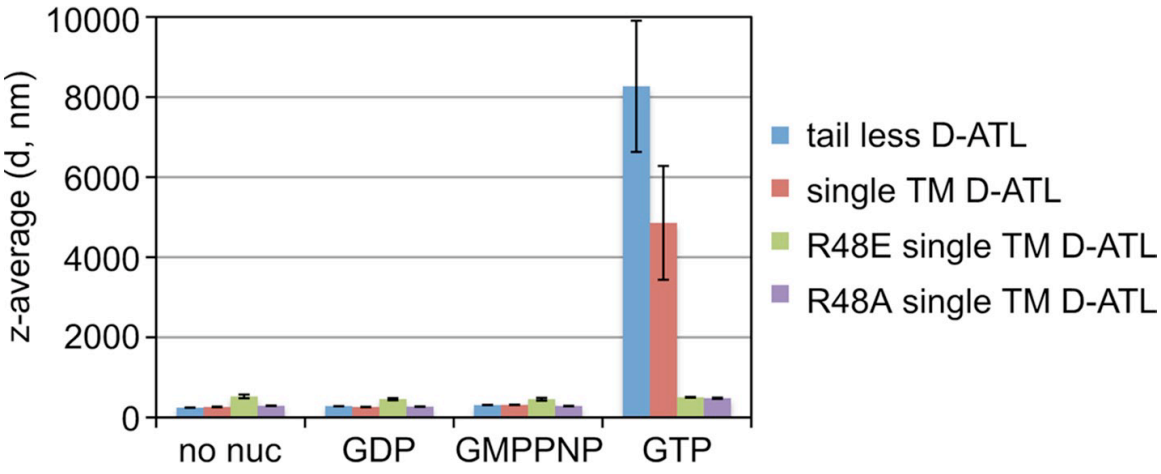

Wild-type, R48E (both dimerization incompetent and hydrolysis defective), or R48A (dimerization competent but hydrolysis defective) mutant variants of single TM D-ATL were reconstituted into vesicles and incubated at 37°C for 10 min in the presence or absence of the indicated nucleotides and subjected to DLS. A tail less version of wild-type D-ATL is also shown. The average of three independent measurements ± SD is shown for each condition.

Figure 3-5: Fusion but not tethering depends on a K320-E328 salt bridge.

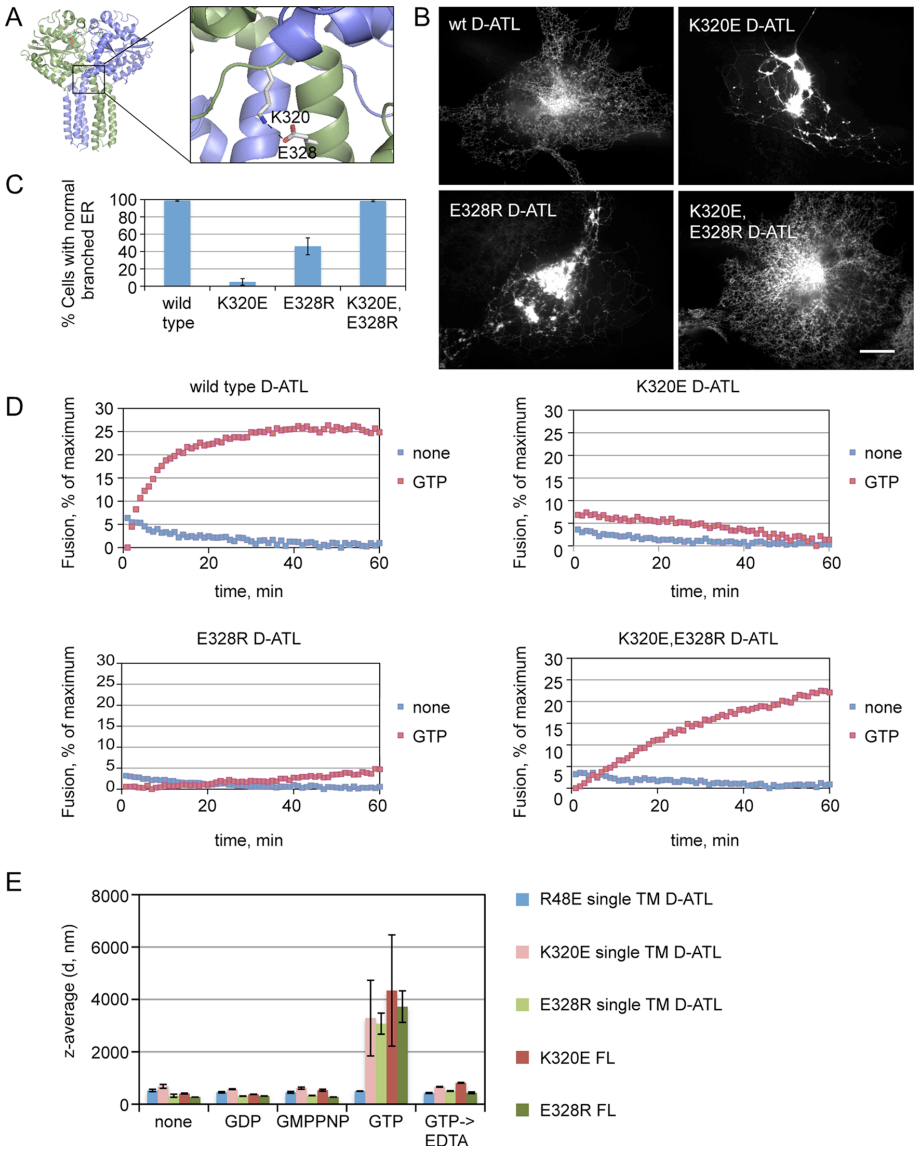

(A) The position of the K320-E328 salt bridge is superimposed onto a PyMOL rendering of the ATL1 crossover dimer PDB 3QNU. (B) Expression of the individual K320E and E328R FL D-ATL variants but not the compensatory double-mutant (K320E,E328R) variant leads to abnormal ER network structure in Cos-7 cells. Cells transfected with the indicated eYFP-tagged variants were imaged 48 h later by confocal microscopy. Scale bar: 10 µm. (C) Quantification of the percent of expressing cells displaying a normal branched ER, >100 cells per measurement, average of three independent measurements ± SD. (D) The K320-E328 salt bridge is required for fusion. Wild-type, K320E, E328R, or the double-mutant (K320E,E328R) variant of FL D-ATL were reconstituted into donor and acceptor vesicles. Fusion was monitored by the dequenching of NBD-labeled lipid present in the donor vesicles in the presence or absence of GTP. (E) The K320-E328 salt bridge is not required for tethering. Either single TM or FL versions of either K320E or E328R D-ATL were incorporated into vesicles and incubated at 37°C for 5 min with the indicated nucleotides. Thereafter samples were subjected to DLS. For comparison, tethering by the single TM R48E D-ATL variant is also shown. The average of three independent measurements ± SD is shown for each condition.

Figure 3-6: Tethering does not require crossover.

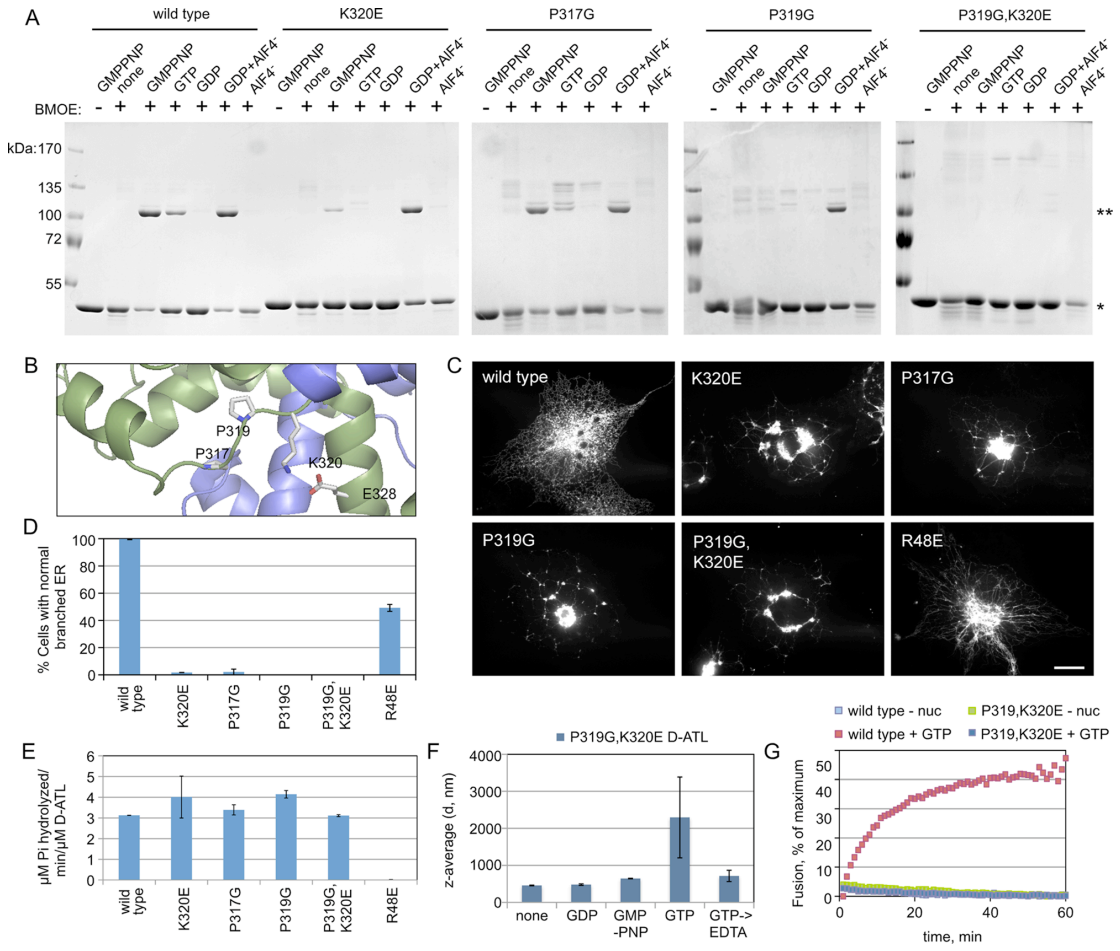

(A) The K320E mutation partially inhibits crossover, but the double mutation P319G,K320E abolishes it. The soluble domain of wild-type, K320E, P317G, P319G, or P319G,K320E D-ATL was incubated at RT for 20 min in the presence or absence of the indicated nucleotides and then subjected to BMOE cross-linking. The single asterisk marks the soluble-domain monomer and the double asterisk marks the cross-linked dimer. All variants had the G343C substitution. (B) The positions of linker mutations made to block D-ATL crossover superimposed onto a PyMOL rendering of the ATL1 crossover dimer PDB 3QNU. (C) Expression of linker mutant variants in Cos-7 cells perturbs ER network morphology. Cells transfected with the indicated FL eYFP-tagged D-ATL mutant variants were visualized 48 h later by confocal microscopy. Scale bar: 10 µm. (D) The percent of cells expressing each variant and showing a normal branched ER, >100 cells per measurement, average of three independent measurements ± SD are quantified. The dimerization- and hydrolysis-defective R48E D-ATL is also shown for comparison. (E) Mutations that block crossover do not impair GTPase activity. The soluble domain of each crossover–defective variant was assayed for GTPase activity. The average of three independent measurements ± SD is shown. R48E is shown for comparison. (F) Crossover–defective P319G,K320E D-ATL can tether. Vesicles containing P319G,K320E FL D-ATL were assessed for tethering by DLS after incubation at 37°C for 10 min in the presence or absence of the indicated nucleotides. The average of three independent measurements ± SD is shown for each condition. (G) The P319G,K320E mutations block fusion. Wild-type or P319G,K320E D-ATL was reconstituted into donor and acceptor vesicles. Fusion was monitored by the dequenching of NBD-labeled lipid present in the donor vesicles in the presence or absence of GTP.

Figure 3-7: Working model for D-ATL–catalyzed membrane tethering and fusion.

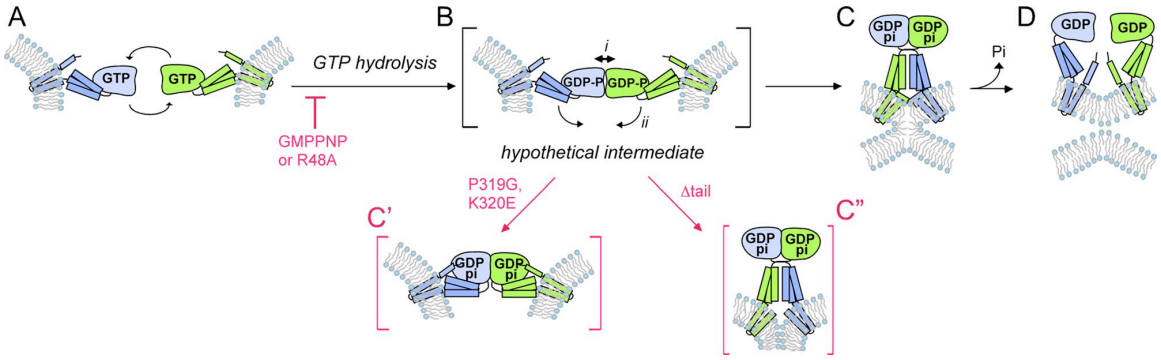

(A) GAP-like intermolecular interactions between GTP-bound subunits on opposing membranes triggers GTP hydrolysis. (B) Hydrolysis initiates conformational changes in the GTPase head (a short-lived hypothetical intermediate is shown in brackets) to simultaneously stabilize head-to-head contact for stable *trans* pairing (i) and release the 3HB for crossover (ii). Stable *trans* pairing tethers opposing membranes to one another, while crossover, with assistance from the tail, powers fusion (C). After fusion, P_i release may trigger dimer disassembly for subunit recycling (D). Both tethering and fusion are inhibited when hydrolysis is blocked by either GMPPNP or the catalytic R48A mutation. C′ and C″ depict tethered intermediates (bracketed in red) that accumulate either when crossover is blocked by P319G,K320E mutation (C′) or when the absence of the tail permits crossover but not lipid mixing (C″).

SUPPLEMENTARY FIGURES

Figure S3-1: DLS analysis of single TM D-ATL vesicles.

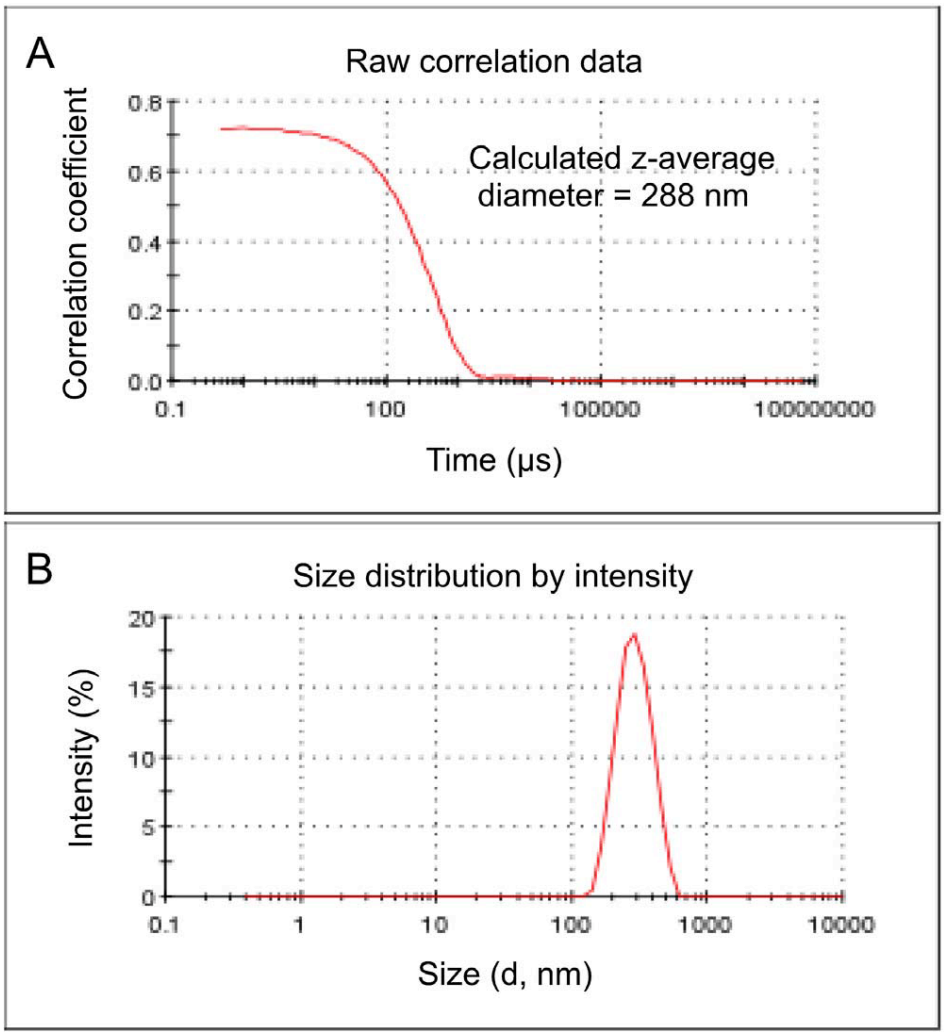

(A) Representative raw data showing the decay of the autocorrelation function with delay time for a sample containing single TM D-ATL vesicles prior to any treatment. (B) Intensity size distribution of the starting vesicles based on the correlation data.

Figure S3-2: The non-hydrolysable GTP analogue GTPγS fails to support vesicle tethering.

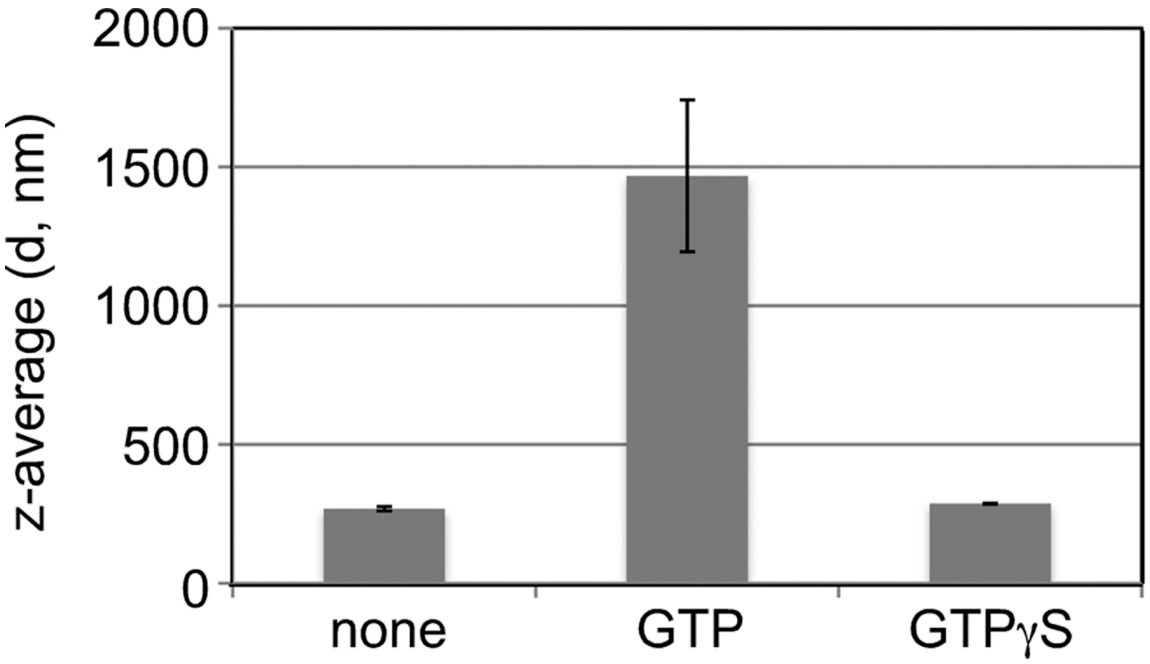

Tail less D-ATL (residues 1-471) reconstituted into vesicles was incubated at 37°C for 10 min in the presence or absence of GTP or GTPγS and subjected to DLS. The average of 3 independent measurements ± S.D. is shown for each condition.

Figure S3-3: Crossover defective D-ATL mutant variants co-localize with the ER marker REEP5 and perturb ER morphology.

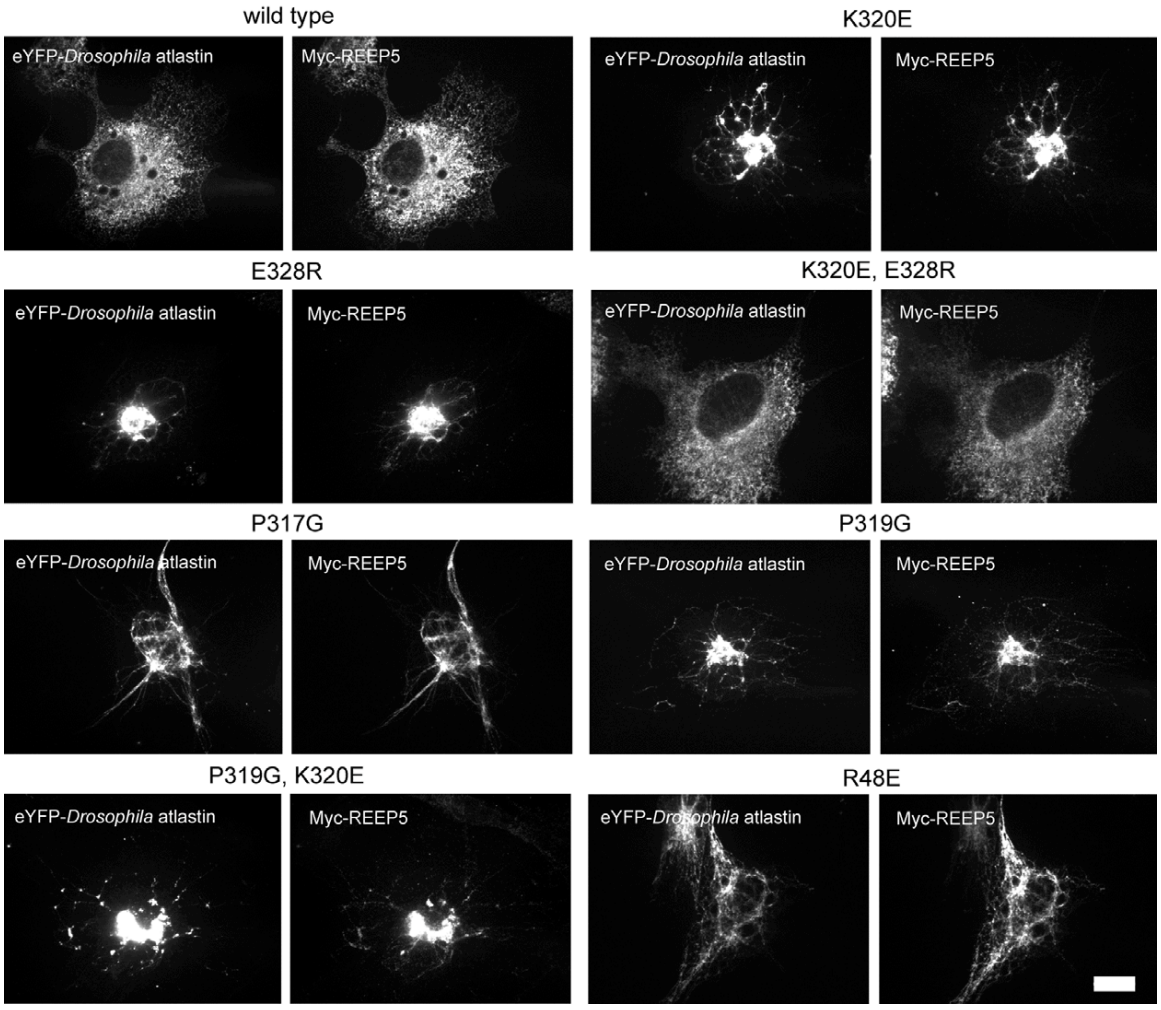

Cells co-transfected with the indicated eYFP-tagged full-length D-ATL variants and the Myc-tagged ER marker REEP5 were fixed and stained 48 hrs later using antibodies against the Myc epitope and viewed by confocal microscopy. The nucleotide-binding mutant variant R48E is also shown for comparison. Scale bar, 10μM.

Figure S3-4: Cysteine substitutions do not impair D-ATL fusion activity.

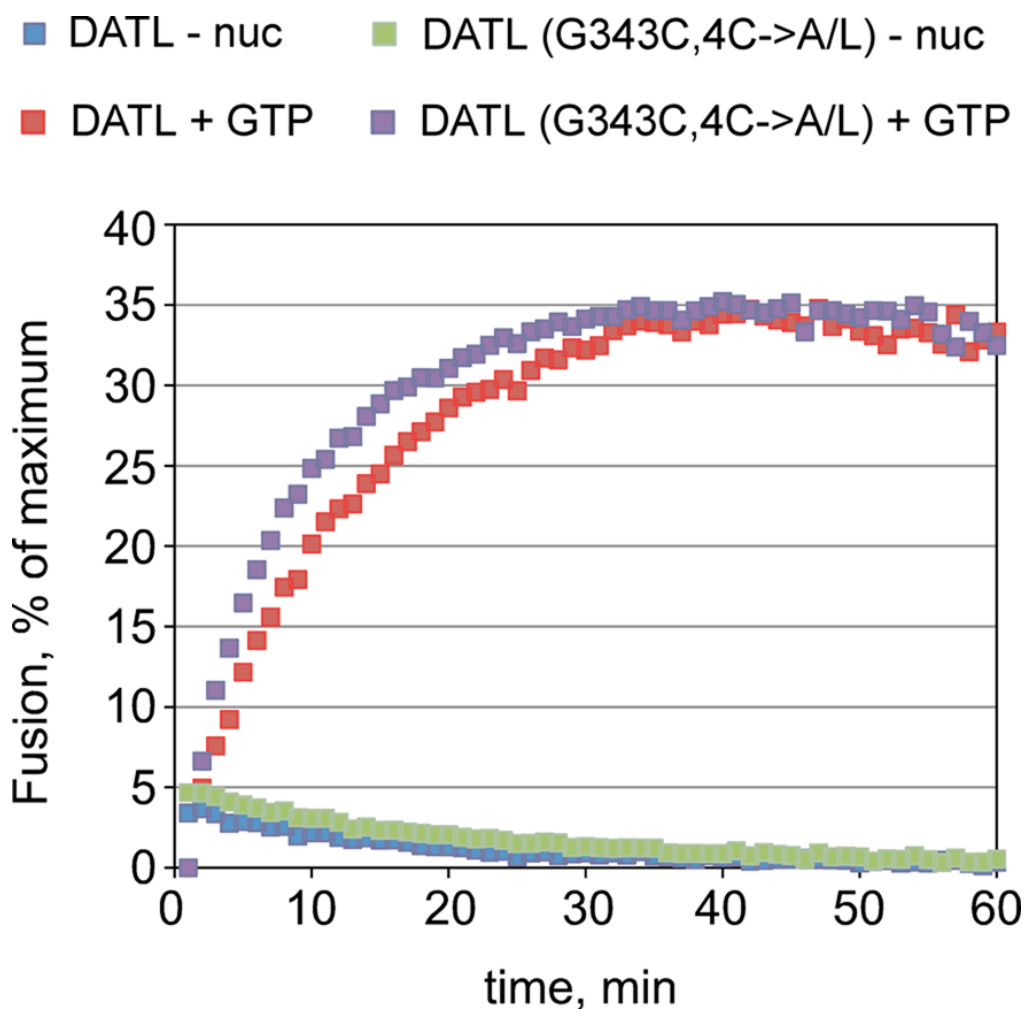

For technical reasons a G343C, as well as four additional substitutions (cysteine to alanine/leucine), were made in D-ATL proteins used throughout this study (see Materials and methods for details). None of these substitutions impaired D-ATL fusion activity. To illustrate this point, the fusion kinetics of unaltered D-ATL is compared to that of D-ATL with all of the substitutions used.

DISCUSSION

GTP hydrolysis catalyzes stable *trans* pairing for tethering

We observed *trans* pairing between opposing membrane-anchored D-ATL, as defined by vesicle tethering, to be GTP dependent under a variety of conditions: either when D-ATL was anchored by a single TM helix (Figure 3-4), two TM helices (Figures 3-4 and 3-5E), or both TM helices and the C-terminal tail (Figures 3-5E and 3-6F). Furthermore, under no condition did the nonhydrolyzable analogue GMPPNP (or GTPγS, Supplemental Figure S3-2) substitute for GTP. Also consistent with a requirement for hydrolyzable GTP, the R48A variant, defective specifically for nucleotide hydrolysis (Pendin *et al*., 2011; Byrnes *et al*., 2013), failed to tether (Figure 3-4).

The implication that nucleotide hydrolysis might be a prerequisite for, rather than a consequence of, stable *trans* pairing may seem counterintuitive, especially because stable truncated ATL dimers were readily captured with the nonhydrolyzable GTP analogue GMPPNP (Byrnes and Sondermann, 2011; Morin-Leisk *et al*., 2011; also Figure 3-6A). However, given the recent observation that dimer formation and crossover were both 100-fold faster with hydrolysis than without (Byrnes *et al*., 2013), it is now evident that the ready accumulation of truncated stable dimers in the absence of hydrolysis was likely a reflection of the stability of the crossover dimer configuration rather than a reflection of the GTP-bound state triggering crossover. Indeed, the form 1 crossover dimer was initially crystallized in the presence of GDP (Bian *et al*., 2011), which generally fails to induce dimer formation in solution (Byrnes and Sondermann, 2011; Morin-Leisk *et al*., 2011; Moss *et al*., 2011). Thus the physiological trigger for stable dimer formation is likely not the binding but rather the hydrolysis of GTP. As alluded to in the *Results* section, we speculate that hydrolysis may be triggered by an initial low-affinity *trans* interaction between GTP-bound heads, which may stimulate hydrolysis in a GAP-like manner through rearrangement of an arginine finger within each head, with hydrolysis in turn generating the high-affinity head-to-head contacts necessary for a productive fusion event.

Collectively our findings are most consistent with the role of GTP hydrolysis in the model put forth recently by Sondermann and colleagues, in which GTP catalyzes the

formation of head contacts required to tether opposing membranes in preparation for fusion (Byrnes *et al*., 2013). This aspect of their model, based solely on conformational analysis of the ATL1 soluble domain, is now well supported for membrane-anchored D-ATL in the context of the fusion reaction. However, in contrast to another aspect of their model, in which crossover serves primarily to tether opposing membranes in *trans* (Byrnes *et al*., 2013), our findings indicate that crossover is dispensable for tethering in the context of the fusion reaction.

Crossover formation is not required to tether membranes

We concluded that *trans* pairing is independent of crossover configuration formation, because robust tethering was observed by D-ATL variants that were essentially crossover defective (Figure 3-6, A and F). Two potential caveats to this interpretation are worth consideration, however. First, because our assay for crossover competency is a soluble-phase assay, there is a formal possibility that the membrane-anchored P319G,K320E variant is able to achieve the crossover configuration, even though the truncated molecule cannot. We consider this possibility unlikely, because membrane anchoring would be more likely to impede rather than promote crossover. The absence of any detectable cross-linked product, even under the relatively permissive conditions of our soluble-phase assay, which captures both slow and fast crossover events (Byrnes *et al*., 2013), likely reflects complete or near-complete loss of crossover capability on the part of the P319G,K320E variant. A second caveat pertains to the definition of crossover. Dimer capture with BMOE, with its 8Å spacer arm, is expected to depend on close parallel 3HB alignment. A hybrid conformation, with the 3HBs neither fully extended nor fully parallel aligned, could form and yet escape capture by BMOE cross-linking. Therefore our conclusions are necessarily limited to assessing the requirement for the fully parallel-aligned crossover conformation. Regardless, our results provide compelling evidence that the ability of D-ATL to undergo full crossover is not a prerequisite for tethering.

Crossover formation may power lipid mixing

Even though full crossover formation was not essential to tethering, it is likely necessary for membrane fusion. The K320E D-ATL variant, only partially defective for crossover (Figure 3-6A), was nevertheless fusion incompetent (Figure 3-5D; Bian *et al*., 2011). Similarly, the P317G and P319G mutations each only mildly or partially impairing crossover (Figure 3-6A), respectively, exerted dominant-negative effects on ER morphology consistent with a fusion defect (Figure 3-6, C and D). These observations suggest that membrane fusion may require formation of most or all of the contacts observed in the form 3 conformer, with loss of even a subset of stabilizing contacts impairing fusion activity. We speculate that the binding energy of crossover therefore contributes substantially to catalyzing lipid mixing for fusion.

A working model for ATL-catalyzed fusion

On the basis of the information at hand, we suggest the following working model for the ATL fusion reaction cycle (Figure 3-7). The model starts with ATL molecules on opposing membranes encountering one another in the GTP-bound state (Figure 3-7A), followed by GAP-like interactions between heads in *trans*. Because tethering was not observed with nonhydrolyzable GTP or with the R48A hydrolysis-defective variant, we speculate that these GAP-like interactions are weak head contacts that nevertheless are sufficient to induce rearrangement of catalytic residues required for hydrolysis (Figure 3-7B). We suggest that GTP hydrolysis in turn catalyzes conformational changes within the head that 1) strengthen the initial head contact, resulting in a stably engaged *trans* dimer for tethering; and 2) simultaneously release the 3HBs from the heads to enable crossover for fusion (Figure 3-7C). Though our results are also compatible with tethering occurring upstream of crossover formation, the concerted tethering and crossover depicted in the model are more consistent with the recent observation that head contact and crossover are both triggered near simultaneously in the soluble phase (Byrnes *et al*., 2013). Once fusion has occurred, we further speculate that P_i release induces disassembly of the crossover dimer for subunit recycling (Figure 3-7D). Many of the details of our working model remain to be clarified, particularly with regard to the upstream *trans* interactions that lead to hydrolysis and the downstream steps that drive dimer disassembly. Yet the model provides a framework that is largely consistent with observations made within this study

and previous observations by others. For instance, inhibition of nucleotide hydrolysis blocks the reaction cycle before tether formation (Figure 3-4). In contrast, inhibition of crossover formation does not impede tether formation, though it does block fusion (Figure 3-6, F and G). Finally, truncation of the molecule to remove the lipid-destabilizing effects of the tail blocks fusion (Moss *et al*., 2011; Liu *et al*., 2012) but still enables tethering (Figures 3-1 and 3-2). In the latter two cases, the putative tethered intermediates that accumulate as a consequence of mutation have been visualized directly by cryo-EM (Figure 3-3). In the case of the single TM variant lacking the tail, the tethered bilayers were tightly opposed, as would be predicted by stable *trans* interaction involving crossover. Remarkably, the presumptive tethered membrane interfaces formed without crossover (P319G,K320E) were slightly wider, corresponding to a somewhat longer distance between inner leaflet densities. This would be consistent with the formation of a more extended tether in the absence of crossover formation. However, further analysis will be required to fully resolve these structural differences.

In summary, our findings provide new insights into the conformational coupling of membrane-bound ATL to its GTP hydrolysis cycle and begin to reveal the role of the crossover conformation change in the fusion mechanism. Future work should enable continued refinement of our understanding of how the ATL mechanochemical cycle powers the fusion of ER membranes.

REFERENCES

Allan, V.J. and R.D. Vale. 1991. Cell cycle control of microtubule-based membrane transport and tubule formation in vitro. J. Cell Biol. 113:346-359.

Anwar, K., R.W. Klemm, A. Condon, K.N. Severin, M. Zhang, R. Ghirlando, J. Hu, T.A. Rapoport, and W.A. Prinz. 2012. The dynamin-like GTPase Sey1p mediates homotypic ER fusion in S. cerevisiae. J Cell Biol. 197:209-217.

Arac, D., X. Chen, H.A. Khant, J. Ubach, S.J. Ludtke, M. Kikkawa, A.E. Johnson, W. Chiu, T.C. Sudhof, and J. Rizo. 2006. Close membrane-membrane proximity induced by Ca(2+)-dependent multivalent binding of synaptotagmin-1 to phospholipids. Nat Struct Mol Biol. 13:209-217.

Bian, X., R.W. Klemm, T.Y. Liu, M. Zhang, S. Sun, X. Sui, X. Liu, T.A. Rapoport, and J. Hu. 2011. Structures of the atlastin GTPase provide insight into homotypic fusion of endoplasmic reticulum membranes. Proc Natl Acad Sci U S A. 108:3976-3981.

Byrnes, L.J., A. Singh, K. Szeto, N.M. Benvin, J.P. O'Donnell, W.R. Zipfel, and H. Sondermann. 2013. Structural basis for conformational switching and GTP loading of the large G protein atlastin. EMBO J. 32:369-384.

Byrnes, L.J., and H. Sondermann. 2011. Structural basis for the nucleotide-dependent dimerization of the large G protein atlastin-1/SPG3A. Proc Natl Acad Sci U S A. 108:2216-2221.

Friedman, J.R., B.M. Webster, D.N. Mastronarde, K.J. Verhey, and G.K. Voeltz. 2010. ER sliding dynamics and ER-mitochondrial contacts occur on acetylated microtubules. J Cell Biol. 190:363-375.

Ghosh, A., G.J. Praefcke, L. Renault, A. Wittinghofer, and C. Herrmann. 2006. How guanylate-binding proteins achieve assembly-stimulated processive cleavage of GTP to GMP. Nature. 440:101-104.

Hashimoto, Y., M. Shirane, F. Matsuzaki, S. Saita, T. Ohnishi, and K.I. Nakayama. 2014. Protrudin regulates endoplasmic reticulum morphology and function associated with the pathogenesis of hereditary spastic paraplegia. J Biol Chem. 289:12946-12961.

Lee, C., and L.B. Chen. 1988. Dynamic behavior of endoplasmic reticulum in living cells. Cell. 54:37-46.

Lee, C., M. Ferguson, and L.B. Chen. 1989. Construction of the endoplasmic reticulum. J Cell Biol. 109:2045-2055.

Liu, T.Y., X. Bian, S. Sun, X. Hu, R.W. Klemm, W.A. Prinz, T.A. Rapoport, and J. Hu. 2012. Lipid interaction of the C terminus and association of the transmembrane segments

facilitate atlastin-mediated homotypic endoplasmic reticulum fusion. Proc Natl Acad Sci U S A. 109:E2146-2154.

McNew, J.A., H. Sondermann, T. Lee, M. Stern, and F. Brandizzi. 2013. GTP-Dependent Membrane Fusion. Annu Rev Cell Dev Biol.

Morin-Leisk, J., S.G. Saini, X. Meng, A.M. Makhov, P. Zhang, and T.H. Lee. 2011. An intramolecular salt bridge drives the soluble domain of GTP-bound atlastin into the post-fusion conformation. J Cell Biol. 195:605-615.

Moss, T.J., C. Andreazza, A. Verma, A. Daga, and J.A. McNew. 2011. Membrane fusion by the GTPase atlastin requires a conserved C-terminal cytoplasmic tail and dimerization through the middle domain. Proc Natl Acad Sci U S A. 108:11133-11138.

Orso, G., D. Pendin, S. Liu, J. Tosetto, T.J. Moss, J.E. Faust, M. Micaroni, A. Egorova, A. Martinuzzi, J.A. McNew, and A. Daga. 2009. Homotypic fusion of ER membranes requires the dynamin-like GTPase atlastin. Nature. 460:978-983.

Park, S.H., and C. Blackstone. 2010. Further assembly required: construction and dynamics of the endoplasmic reticulum network. EMBO Rep. 11:515-521.

Pendin, D., J. Tosetto, T.J. Moss, C. Andreazza, S. Moro, J.A. McNew, and A. Daga. 2011. GTP-dependent packing of a three-helix bundle is required for atlastin mediated fusion. Proc Natl Acad Sci U S A. 108:16283-16288.

Shibata, Y., T. Shemesh, W.A. Prinz, A.F. Palazzo, M.M. Kozlov, and T.A. Rapoport. 2010. Mechanisms determining the morphology of the peripheral ER. Cell. 143:774-788.

Waterman-Storer, C.M.a.S.E.D. 1998. Endoplasmic reticulum membrane tubules are distributed by microtubules in living cells using three distinct mechanisms. Curr. Biol. 8:798-806.

Zhang, M., F. Wu, J. Shi, Y. Zhu, Z. Zhu, Q. Gong, and J. Hu. 2013. ROOT HAIR DEFECTIVE3 family of dynamin-like GTPases mediates homotypic endoplasmic reticulum fusion and is essential for Arabidopsis development. Plant Physiol. 163:713-720.

CHAPTER 4

CONCLUSION AND FUTURE DIRECTIONS

Despite our advancement in understanding the role of ATL in structuring the ER, the actual mechanism of ATL-mediated fusion still remains to be clarified. For instance, while our work has clarified the upstream steps within the ATL fusion cycle by revealing that GTP-hydrolysis facilitates stable engagement of GTP-bound ATL head groups in opposing membranes and that this initial trans-pairing could be uncoupled from crossover by mutation, suggesting that crossover is not required for membrane tethering, we were not able to resolve whether crossover occurred in concert with or subsequent to this initial membrane-tethering step. Therefore, further refinement of our model could be achieved through kinetic-based experiments, such as FRET-based stop-flow analysis on membrane-anchored, full-length ATL molecules by measuring and comparing the rates of initial trans pairing, crossover and GTP-hydrolysis. Similar rates between initial trans pairing, crossover and GTP-hydrolysis would suggest a more concerted reaction mechanism; whereas, a delay between trans-pairing and crossover might be suggestive of a more sequential reaction mechanism.

Separately, many of the downstream steps within the ATL fusion cycle, including the actual lipid-mixing step and disassembly remain to be explored. Although, we speculate that Pi release might catalyze disassembly, this has yet to be demonstrated for membrane-anchored, full-length ATL molecules. Blocking Pi release either chemically or through the identification of ATL variants would be informative in elucidating the role of Pi release in the ATL-mediated fusion reaction, either in the context of disassembly or some other discrete step within the ATL-fusion cycle.

Another important component in understanding the ATL fusion cycle is through the characterization of identified ATL-interacting proteins. Although various ATL isoforms have been reported to bind to a number of other ER-localized proteins including reticulons, DP1, spastin, REEP1, and protrudin (Blackstone *et al*., 2011, Chang *et al*., 2013); the functional significance of these putative interactions remains unknown. Moreover, mutations in ATL and several of these ATL-interacting proteins are associated

with the disease hereditary spastic paraplegia (HSP), a motor neurological disorder that is characterized by weakness and spasticity in the lower limbs of affected individuals (Fink, 2006), highlighting the need to understand the physiological significance of these putative interactions not only for ER biogenesis, but also in the context of human health.

Lastly, because HSP is associated with mutations in ATL1, one of the human isoforms, it will be vital to understand why the human isoforms of ATL are incapable of fusing synthetic liposomes. While it is possible that the human isoforms require an interacting partner, whereas D-ATL does not, it is equally possible that the human isoforms possess a yet unidentified auto-inhibitory domain or some other form of modification that inhibits its fusion capability *in vitro*. Identification of either the interacting partner or the structural elements/modifications would be highly informative in understanding the regulation of ATL and might lead to the establishment of an ideal assay system for understanding and treating patients suffering from HSP as a result of mutations in ATL1.

I am certain that many of these unexplored areas will be addressed in the near future, leading to a more comprehensive understanding of the ATL fusion mechanism and its role in ER biogenesis.

REFERENCES:

Blackstone, C. 2012. Cellular pathways of hereditary spastic paraplegia. Annu Rev Neurosci. 35:25-47.

Chang J, Lee S, Blackstone C. Protrudin binds atlastins and endoplasmic reticulum shaping proteins and regulates network formation. 2013. Proc Natl Acad Sci U S A. 110:14954–14959.

Fink, J.K. 2006. Hereditary spastic paraplegia. Curr Neurol Neurosci Rep. 6:65-76.